ROLE OF MICRORNA 214 IN CYCLIC STRETCH INDUCED AORTIC VALVE PATHOGENESIS

A Dissertation
Presented to
The Academic Faculty

by

Md Tausif Salim

In Partial Fulfillment
of the Requirements for the Degree
Master of Science in Chemical Engineering in the
School of Chemical and Biomolecular Engineering

Georgia Institute of Technology
May 2018

COPYRIGHT © 2018 BY MD TAUSIF SALIM

ROLE OF MICRORNA 214 IN CYCLIC STRETCH INDUCED AORTIC VALVE PATHOGENESIS

Approved by:

Dr. Ajit P. Yoganathan, Advisor
School of Chemical and Biomolecular Engineering
Georgia Institute of Technology

Dr. Robert M. Nerem
School of Chemical and Biomolecular Engineering
Georgia Institute of Technology

Dr. Hanjoong Jo
The Wallace H. Coulter Department of Biomedical Engineering
Georgia Institute of Technology

Date Approved: [Month dd, yyyy]

To my parents and my wife

ACKNOWLEDGEMENTS

First, I would like to express my gratitude to Dr. Y for giving me the opportunity to conduct research in CFM lab. I would like to convey my gratitude to Shiva for helping me in sorting out problems (professional or personal) in an objective fashion. Thanks to Joan for being my mentor and helping me sort out all my research problems. Special thanks to Swetha for always finding time to answer any of my stupid research questions. Thanks to Tim for teaching me all the preliminary techniques needed to work in the mechanobiology area. I am extremely grateful to Dr. Jo for allowing me to work in his lab. I am also very grateful to Dr. Nerem for giving me helpful tips in terms of career planning. Last but not the least, I am grateful to all CFM lab members and all my family members. I wouldn't be here without my parents whose hardwork and sacrifices enabled me to stand here. Thanks a lot, Tisha for being always there for me.

TABLE OF CONTENTS

LIST OF TABLES

LIST OF FIGURES

LIST OF SYMBOLS AND ABBREVIATIONS

ATF4	Activating Transcription Factor 4
AV	Aortic Valve
BCL11B	B-Cell Lymphoma/Leukemia 11B
BCL2L1	BCL2 Like 1
BGLAP	Bone Gamma-Carboxyglutamate Protein
CHOP	C/EBP Homologous Protein
ER	Endoplasmic Reticulum
MMP-2	Matrix Metalloproteinase 2
MMP-9	Matrix Metalloproteinase 9
TRB3	Tribbles Homolog 3
TWIST1	TWIST Family BHLH Transcription Factor 1
VEC	Valvular Endothelial Cell
VIC	Valvular Interstitial Cell

SUMMARY

Aortic valve (AV) is a dynamic structure that experiences different types of cyclic mechanical forces, such as stretch, shear, etc. These mechanical stimuli regulate the cellular phenotypes of the valve. Adverse alteration in any of these mechanical stimuli can initiate a cascade of pathological events, ultimately leading to AV disease. Since the discovery of microRNAs and their regulatory function in modulating gene expression, numerous studies have identified several microRNAs with therapeutic potential to treat different diseases. Similar studies have also identified many microRNAs related to cardiovascular diseases. Among those, miR-214 is a major microRNA that has been found to be significantly associated with AV calcification, as well as other cardiovascular diseases.

The objective of the current thesis work was to investigate the functional relation between cyclic stretch and miR-214 in promoting AV disease. Elevated cyclic stretch has been shown to induce adverse extracellular matrix remodeling and higher calcification in AV. An *ex vivo* stretch bioreactor was used to apply uniaxial cyclic stretch on freshly collected porcine AV tissues. The first specific aim sought to understand the effect of physiological and pathological levels of cyclic stretch on miR-214 expression in AV. It was found that pathological cyclic stretch downregulates miR-214 expression during stretch-induced AV calcification. This, in turn, indicates a potentially protective role of miR-214 in stretch-induced AV disease. The second specific aim investigated the effect of cyclic stretch on the expression of miR-214's target gene, ATF4 and two other downstream genes (CHOP and BCL2L1). It was found that pathological cyclic stretch upregulates

ATF4 and downregulated pro-survival BCL2L1 expression, which is in line with the high ATF4 expression and increased cell apoptosis in calcified human AVs. Pathological cyclic stretch didn't change the expression of CHOP in AV. Since the results of first specific aim pointed toward a protective role of miR-214, the effect of miR-214 mimic on ATF4, CHOP, BCL2L1 and osteocalcin (calcification related gene) expression was studied in the third specific aim. It was found that miR-214 overexpression considerably suppressed the expression of ATF4 gene, with lesser effects on the other genes. Together, these results may have identified a protective role of miR-214 in stretch-induced AV disease via its functional relation with ATF4 and other downstream genes (CHOP and BCL2L1).

CHAPTER 1. INTRODUCTION

1.1 The Heart and The Cardiac Cycle

The heart is a major organ of the human body. It pumps oxygenated blood returning from the lungs to the rest of the body and deoxygenated blood from the right side of the heart to the lungs. A normal heart has four chambers – the left and right atria, and the left and right ventricles (Figure 1.1a).

The right (deoxygenated) and left (oxygenated) sides of the heart are separated by a muscular wall called the septum. The right atrium collects deoxygenated blood from the vena cavae and pumps it via the right ventricle and the pulmonary arteries to the lungs, where the blood is oxygenated. The oxygenated blood returns to the left atrium via the pulmonary veins and is pumped to the systemic circulation when the left ventricle contracts during systole.

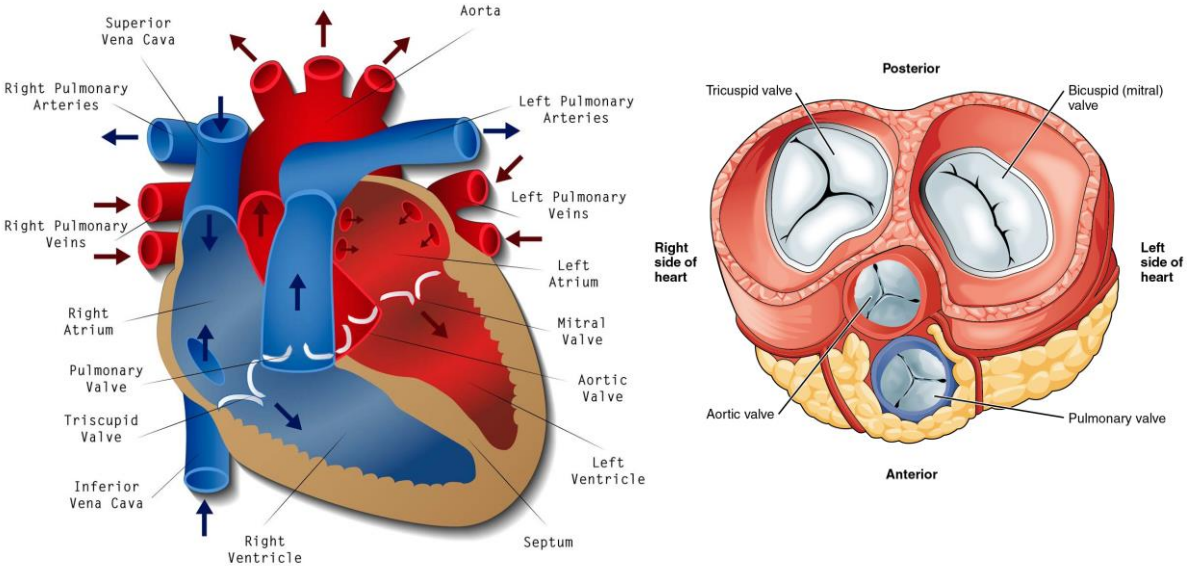

(a) Four chambers (b) Heart valves

Figure 1.1 – Anatomy of the heart.

The heart has four valves (Figure 1.1b): two on each side to maintain unidirectional flow of blood through the heart. These valves can be classified into two types based on their anatomical location: atrioventricular valves (mitral and tricuspid valve) and semilunar or outflow tract valves (aortic and pulmonary valve). The atrioventricular valves have chordae tendinae that attach to papillary muscles on the ventricular walls. This structural feature is absent in the outflow tract valves.

A normal cardiac cycle can be divided into several distinct phases. During atrial contraction, blood is ejected from the atria into the ventricles resulting in a rise in ventricular pressure. A fourth heart sound may be heard at this juncture. At the onset of systole, ventricular isovolumic contraction occurs with the closing of the atrioventricular

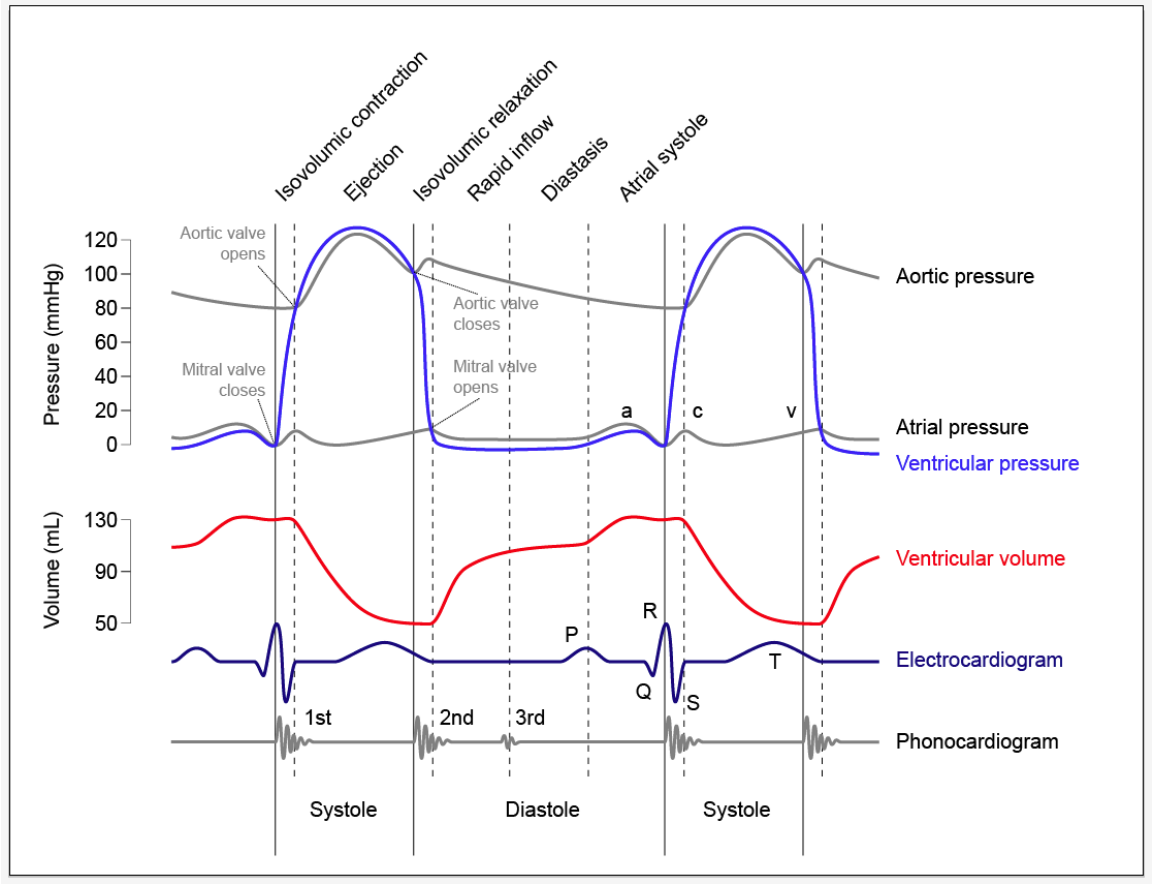

Figure 1.2 – Cardiac cycle.

valves first followed by all the valves. During this stage, the ventricular volume remains constant. In the rapid ejection phase, as soon as the pressure in the left ventricle exceeded the pressure in the aorta, the aortic valve opens and blood flows rapidly from the ventricle into the aorta. Following rapid ejection, the rate of outflow from the ventricle decreases, and the ventricular and aortic pressures start to decrease in the reduced ejection phase.

At the end of systole, during the isovolumic relaxation phase, the ventricular ejection decreases to zero. The left ventricle pressure falls below the pressures in the aorta and pulmonary artery, which causes the aortic and pulmonary valves to close (beginning of diastolic phase). Once the ventricular pressure falls below the atrial pressure the atrioventricular valves open and rapid ventricular filling begins. During this period, the flow of blood from the aorta to the peripheral arteries continues, and the aortic pressure slowly decreases. This rapid ventricular filling phase is followed by the reduced ventricular filling phase in which a large portion of filling occurs.

1.2 The Aortic Valve (AV)

The aortic valve (AV) is situated at the aortic root and regulates blood flow from the left ventricle into the aorta. As shown in Figure 1.3, it consists of three semilunar cusps or leaflets, which are attached to a fibrous annulus embedded within the left ventricle and the septum. Two adjacent leaflets are attached at the commissures and there is an elliptical depression behind each leaflet called the sinus of Valsalva. The left and right sinuses contain ostia that lead into the left and right main coronary arteries. The third sinus does

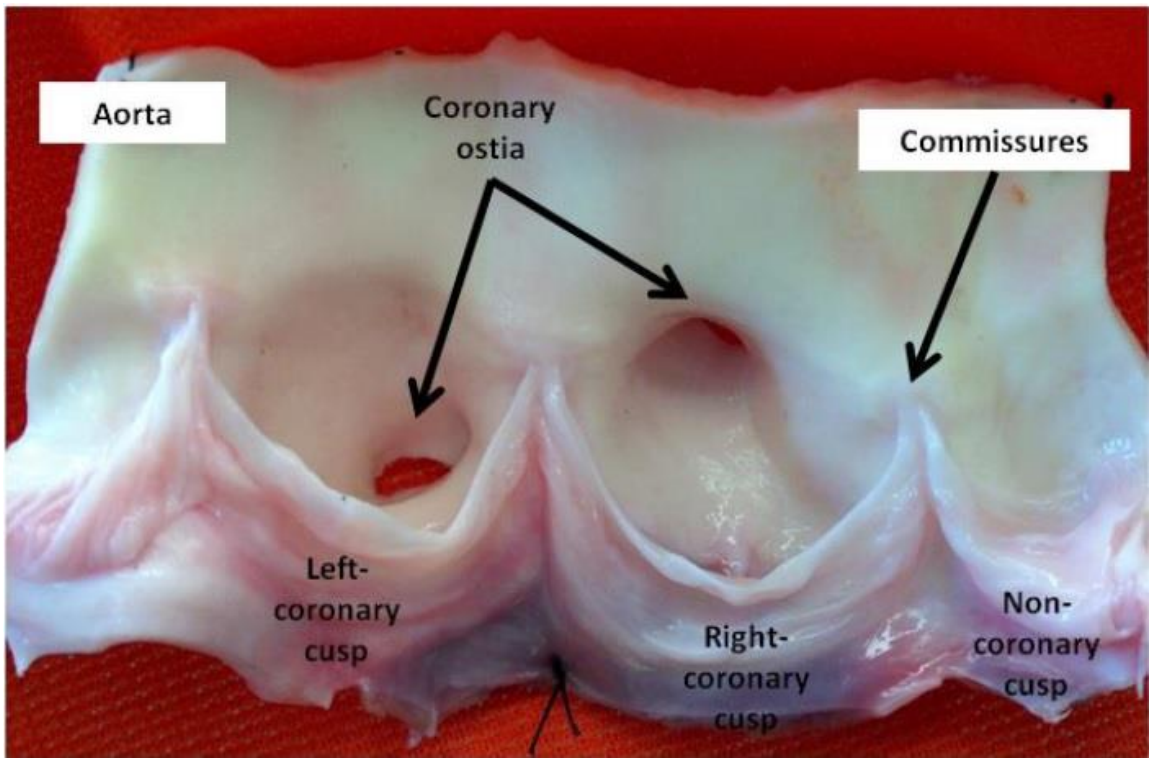

Figure 1.3 – Excised porcine AV (Balachandran, 2010).

not feed a coronary artery and is called a non-coronary sinus. Based on their respective anatomical positions, the three AV leaflets are thereby named the left coronary cusp (LCC), the right coronary cusp (RCC) and the non-coronary cusp (NCC). The basal regions of the leaflets are attached to the sinuses of Valsalva, whereas the sinotubular junction (STJ)

connects the sinuses to the aorta (Figure 1.4). Hence, the three leaflets, in combination with the sinuses of Valsalva, form the functional unit of the aortic valve.

1.3 Structure of the AV Leaflet

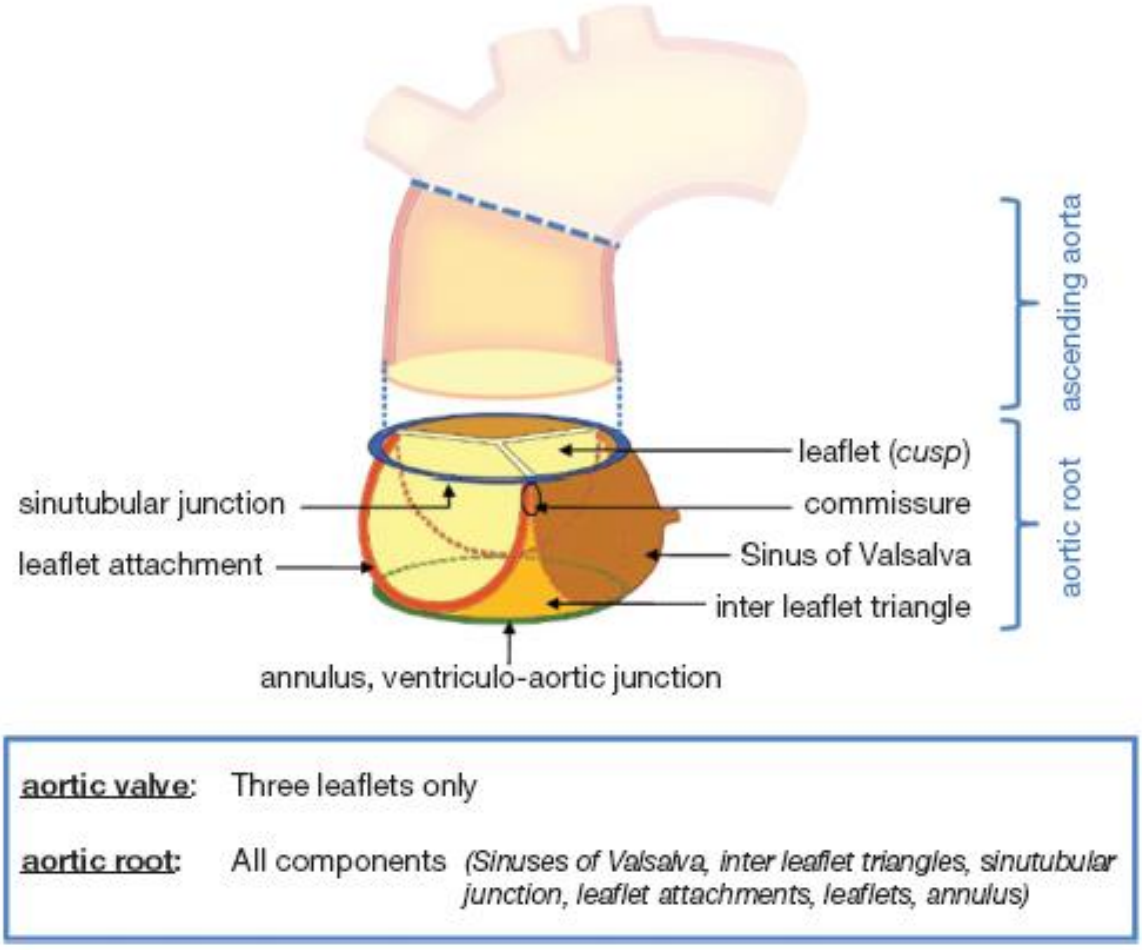

Figure 1.4 – Aortic root anatomy (Charitos et al., 2013).

The AV leaflets are lined with one layer of endothelial cells (ECs) on both the aortic (leaflet surface facing the aorta) and ventricular (leaflet surface facing the left ventricle) sides. In the interior region, the leaflets are populated with interstitial cells (ICs), which represent the most abundant cell type in AV. Each leaflet consists of three distinct layers, namely, the fibrosa, the spongiosa and the ventricularis. The fibrosa and the ventricularis are located immediately below the endothelial layer on the aortic and ventricular surfaces

of the leaflet, respectively. The spongiosa lies between the fibrosa and the ventricularis (Figure 1.5).

The fibrosa provides the major load-bearing capacity of the valve leaflet (Wiltz et

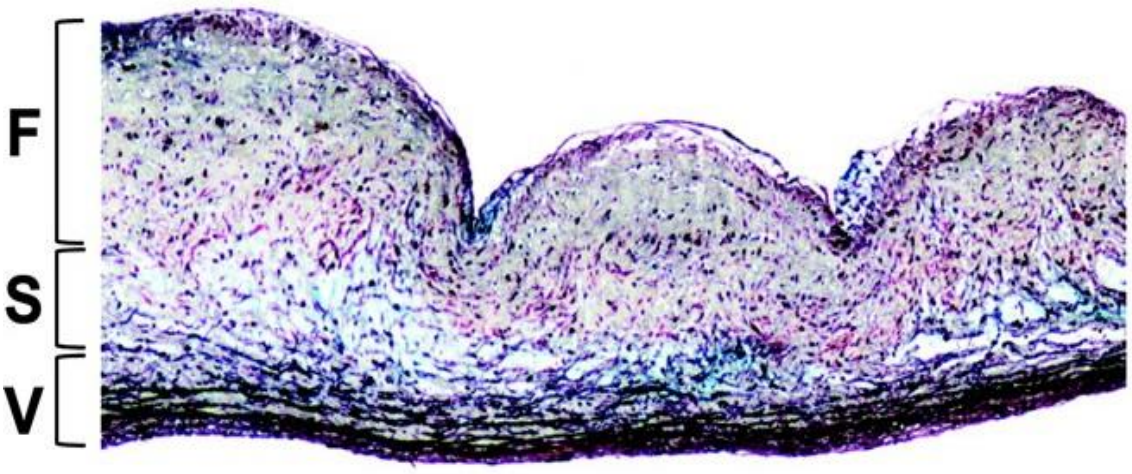

Figure 1.5 – Normal porcine AV leaflet stained with Movat pentachrome, demonstrating the trilaminar structure [F = Fiborsa, S = Spongiosa, and V = Ventricularis] (Chen et al., 2011).

al., 2013). It is mainly composed of circumferentially oriented collagen fibers, which are interconnected with radially aligned elastin fibers. The ventricularis, on the other hand, primarily consists of elastin fibers. Elastin helps with restoring the crimped state of collagen fibers via its recoil action. The spongiosa is mainly composed of glycosaminoglycans and proteoglycans. It works as a lubricating layer between the fibrosa and the ventricularis to promote flexibility. It also dampens the vibrations arising from a closing valve and prevents delamination.

1.4 AV Cell Biology

The cells of the aortic valve can be broadly categorized into two classes:

(i) Endothelial cells (ECs): Cells that line the surface of AV leaflets, and

(ii) Interstitial cells (ICs): Cells that populate the interior region of AV leaflets.

Homeostasis of both cell types is required to maintain physiological functioning of AV. Pathological alteration in one cell type can induce similar adverse alteration in the other cell type, which would eventually lead to AV disease (Figure 1.6).

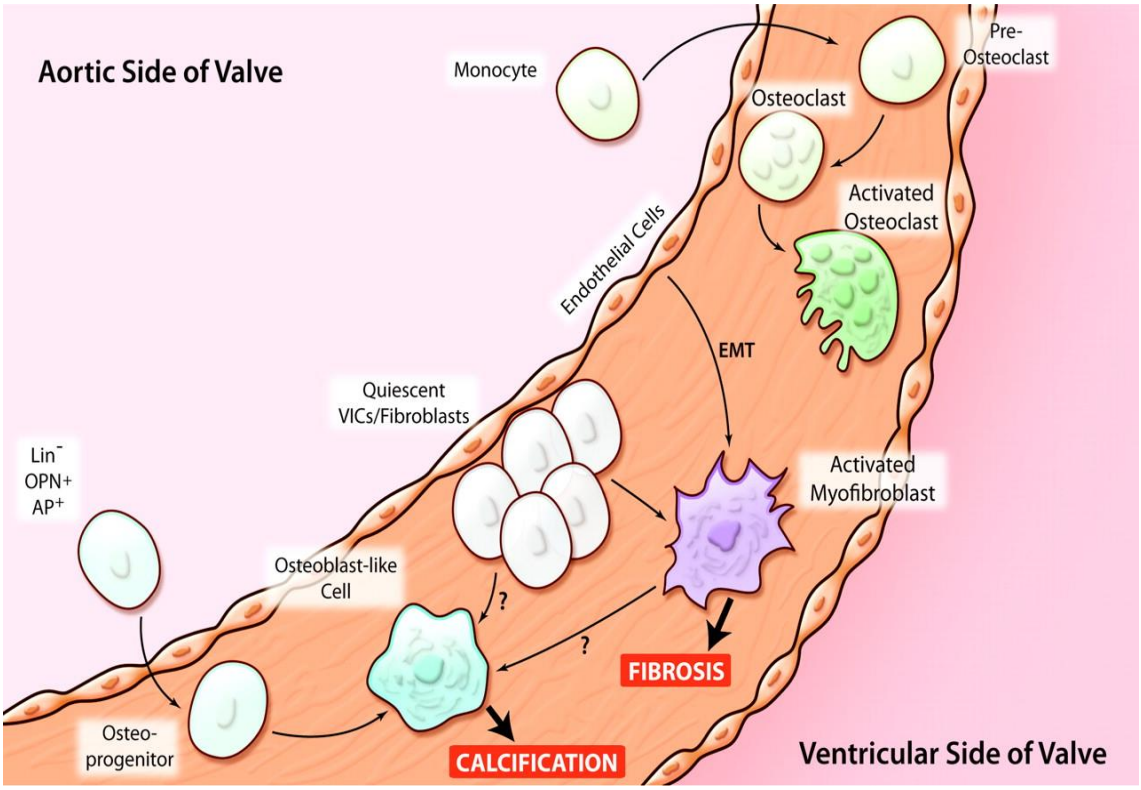

Figure 1.6 – Pathological alteration in either cell type (endothelial or interstitial) can lead to AV disease (Miller et al., 2011).

1.4.1 Endothelial Cells

Valvular endothelial cells (VECs) form a monolayer on the aortic and ventricular surfaces of the aortic valve. Interestingly, the preferential orientation of these cells is perpendicular to the direction of blood flow (Deck et al., 1986), which contrasts with the parallel alignment of vascular endothelial cells (Langille et al., 1981). These imply a significant difference in the mechanical stresses experienced by the valvular and vascular endothelial cells (Butcher et al., 2004), which is further emphasized by their distinct transcriptional profiles (Butcher et al., 2006).

In a co-culture model, VECs have been shown to promote a more quiescent phenotype of valvular interstitial cells (VICs) (Butcher et al., 2006). Pathological alteration in extracellular matrix (ECM) composition prompts VECs to undergo endothelial-to-mesenchymal transformation (EndMT) (Dahal et al., 2017), leading to AV disease. Additionally, endothelial nitric oxide synthase (eNOS) has been shown to protect against aortic valve fibrosis (El Accaoui et al., 2014).

Oscillatory shear stress, as experienced by VECs on the fibrosa side, causes upregulation of EndMT genes (Mahler et al., 2014). While EndMT represents an essential process during embryogenesis, it is believed that dysregulated EndMT contributes to the initiation and progression of AV disease (Chakraborty et al., 2010). Interestingly, Rathan et al. (2011) showed that exposure of fibrosa to low oscillatory shear stress results in much higher AV calcification compared to the physiological level.

VECs have been also found to exhibit side-specificity in gene expression under shear stress conditions (Holliday et al., 2011), emphasizing the significantly different shear

stress profiles on the fibrosa and ventricularis sides of AV in vivo (Kvitting et al., 2004; Markl et al., 2005). These side-specific and shear-dependent transcriptional profiles may underlie the observed preferential AV calcification on the fibrosa side (Chen et al., 2011).

1.4.2 Interstitial Cells

Valvular interstitial cells (VICs) represent the majority of cell population in aortic valve. These cells are heterogeneous in nature, comprising of specific cell phenotypes (such as smooth muscle cell, fibroblast and myofibroblast). Interstitial cells (ICs) play a crucial role in maintaining the physiological function of aortic valve through the regulation of extracellular matrix (ECM) protein synthesis and extracellular matrix remodeling (Taylor et al., 2003). However, under pathological conditions (such as hemodynamic stress), these cells transform into an abnormally activated state from the regular quiescent state and promote the initiation and progression of aortic valve disease (Liu et al., 2007).

Interestingly, VICs have been shown to suppress endothelial-to-mesenchymal transformation (EndoMT) (Shapero et al., 2015) and calcification (Hjortnaes et al., 2015) of valvular endothelial cells (VECs). Hence, it is evident that VICs regulate the physiological function of VECs via cell-cell interactions.

VICs exhibit significantly different gene expression profiles under different pressure conditions (Warnock et al., 2011), matrix elasticity (Ma et al., 2017), stiffness (Mabry et al., 2015), etc., representing varying degree of myofibroblastic activation. Therefore, mechanical forces have a predominant role in modulating the phenotypic switch of interstitial cells.

Several genes have been reported to suppress calcification of VICs, such as IL-37 (Zeng et al., 2017), Klotho (Li et al., 2017), ATG7 (Deng et al., 2017), etc. On the other hand, genes like NTF3 (Yao et al., 2017), DPP4 (Choi et al., 2017), HMGB1 (Shen et al., 2017), etc. promote VIC calcification. So, these highlight the complex nature of VIC function and its pathological activation and progression toward aortic valve calcification.

1.5 AV Tissue Mechanics and Hemodynamics

AV tissues exhibit viscoelasticity and highly non-linear stress-strain behavior (Billiar et al, 2000; Billiar et al, 2000). The internal configuration of the fiber network in AV continuously undergoes strain-induced changes, which involve straightening of highly crimped collagen fibers and rotation of these fibers toward the axis of stretch (Sacks et al., 2007). The AV leaflets experience tensile and bending stresses during the cardiac cycle (Figure 1.7). Interestingly, majority of the stresses and strains occur during diastole and

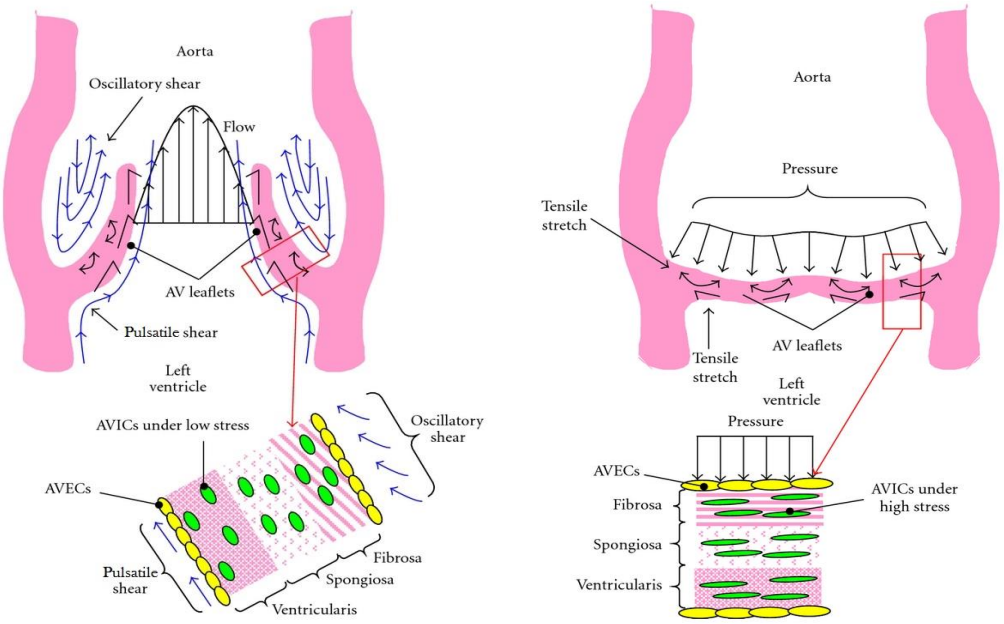

(a) Peak Systole (b) Peak Diastole

Figure 1.7 – Mechanical forces experienced by AV (Balachandran et al., 2011).

early systole. The total stresses, as a combination of bending and membrane stretching, were found to be in the order of 50 kPa during systole and 500 kPa during diastole. These result into a 10% leaflet stretching in the circumferential direction from peak systole to peak diastole (Thubrikar et al., 1986; Thubrikar et al., 1986; Thubrikar et al., 1979).

Additionally, the fibrosa and ventricularis sides of AV experience bidirectional oscillatory shear stress and unidirectional pulsatile shear stress, respectively (Balachandran et al., 2011) (Figure 1.7). The peak value of the unidirectional pulsatile shear stress was found to be around 80 dyne/cm2, whereas the one for the bidirectional oscillatory shear stress was ± 10 dyne/cm2 (Rathan et al., 2016; Yap et al., 2012; Yap et al., 2012; Rathan et al., 2011; Ge et al., 2009; Cao et al., 2016).

To ensure healthy functioning of AV, it is highly important that all mechanical forces lie within respective physiological ranges. Any significant deviation from the physiological range may initiate sustained pathological responses at the cellular and tissue levels, ultimately leading to AV disease.

1.6 Effect of Mechanical Stretch on AV

Elevated cyclic stretch (15%) was found to induce increased extracellular matrix (ECM) remodeling in AV by upregulating the expression of Matrix Metalloproteinase 2 and 9 (MMP-2 and -9), Cathepsin S, Cathepsin K, etc. (Balachandran et al., 2009). In addition to that, cellular proliferation and apoptosis in AV was significantly higher under 15% stretch (Balachandran et al., 2009). Interestingly, higher cyclic stretch (15%) also resulted in increased AV calcification compared to the physiological level (10%), including upregulation of calcification-related genes, such as Bone Morphogenetic Protein-4 (BMP-

4), Runt related Transcription Factor 2 (RUNX2), Osteocalcin, etc. (Balachandran et al., 2010). Hence, pathologically high cyclic stretch (15%) contributes to AV pathogenesis by promoting adverse ECM remodeling and calcification, as opposed to the maintenance of AV homeostasis by physiological stretch (10%).

1.7 AV Stenosis and Treatment Options

Aortic valve (AV) stenosis or aortic stenosis (AS) is characterized by narrowing of the valve opening during systole (Figure 1.8, top row), resulting in a larger pressure gradient between the left ventricle and the aorta. Under this situation, the left ventricle must work harder to overcome the increased afterload caused by the stenotic AV. This is like attaching smaller and smaller nozzles to the end of a garden hose. The narrowing from the

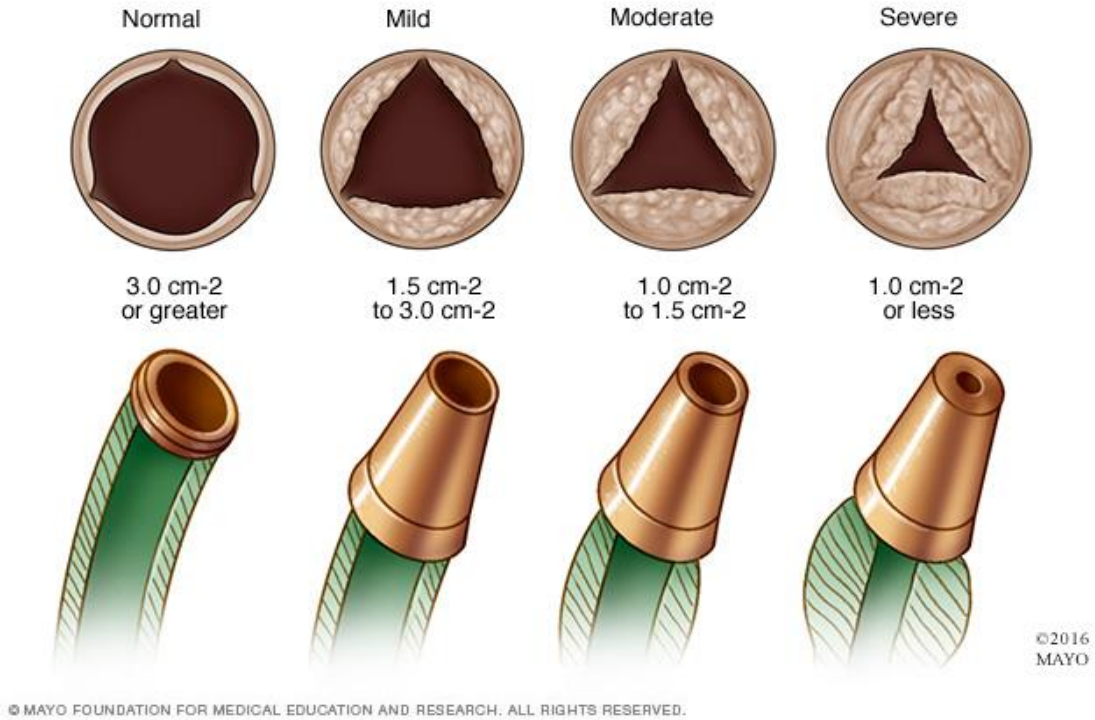

© MAYO FOUNDATION FOR MEDICAL EDUCATION AND RESEARCH. ALL RIGHTS RESERVED.

Figure 1.8 – AV stenosis (Mayo Clinic).

nozzle slows the forward flow of water and results in progressive pressure buildup within the garden hose (Figure 1.8, bottom row).

The main reason behind the occurrence of AS is thickening and calcification of AV leaflets, preferentially on the fibrosa side (Figure 1.9). Normally, the pressure gradient

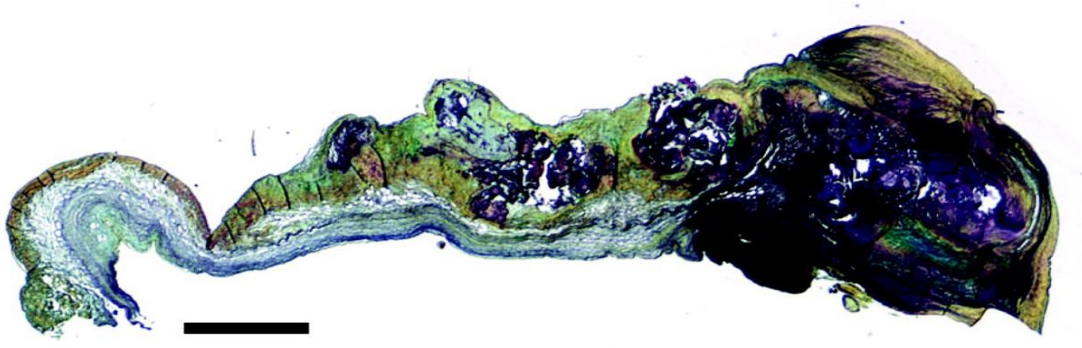

Figure 1.9 – Movat pentachrome stain of a calcified human AV, demonstrating maladaptive ECM remodeling and calcification (purple). Scale bar is 1 mm. (Chen et al., 2011).

across a healthy aortic valve is only a few mm Hg. However, with progressive narrowing of AV opening, the pressure gradient increases gradually. A mild stenosis is characterized by a pressure gradient of around 20 mm Hg. When the pressure gradient ranges between 20 and 40 mm Hg, it is indicated as moderate stenosis. A case of severe stenosis happens when the pressure gradient is higher than 40 mm Hg (Cleveland Clinic).

In a recent study, Osnabrugge et al. (2013) found that more than 12% of the elderly population (age ≥ 75 years) are diagnosed with AS, with more than 3% representing the severe case. In addition to that, severe AS has a worse prognosis than many metastatic cancers (New Heart Valve). Hence, this disease poses a significant burden on the elderly population. At present, there is no therapeutic drug available to treat AS. The only available treatment options are either surgical aortic valve replacement (SAVR) or transcatheter aortic valve replacement (TAVR). SAVR is the gold standard for treating severe AS in

(a) Carpentier-Edwards PERIMOUNT Magna Ease Bioprosthetic Aortic Valve

(b) St. Jude Medical Regent Mechanical Heart Valve

Figure 1.10 – Prosthetic heart valves.

operable patients, whereas TAVR offers a minimally invasive, catheter-based treatment option for inoperable AS patients (Leon et al., 2016; Kodali et al., 2012; Smith et al., 2011). There are two different types of prosthetic heart valves available for SAVR (Figure 1.10): (i) mechanical (generally used in younger AS patients) and (ii) bioprosthetic (generally used in older AS patients). On the other hand, there are a few FDA-approved transcatheter

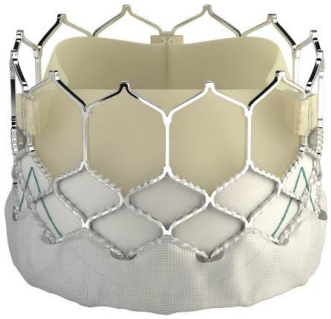

(a) Edwards SAPIEN 3

(b) Medtronic CoreValve

Figure 1.11 – Transcatheter heart valves.

heart valves used in TAVR, such as the Edwards SAPIEN 3 valve and Medtronic CoreValve (Figure 1.11).

1.8 Endoplasmic Reticulum (ER) Stress

Endoplasmic reticulum (ER) facilitates proper folding and maturation of proteins before these are delivered to other cellular compartments. ER stress occurs when there is an accumulation of unfolded proteins in the ER lumen, leading to the activation of unfolded protein response (UPR) signaling pathways. In the case of prolonged activity of the UPR signaling pathways, mitigation of ER stress becomes impossible and cellular apoptosis takes place (Walter et al., 2011; Xu et al., 2005).

There are three main branches of the UPR signaling pathways (Figure 1.12). These are: (i) Activating Transcription Factor 6 (ATF6) mediated pathway, (ii) PRKR-Like Endoplasmic Reticulum Kinase (PERK)/Eukaryotic Translation Initiation Factor-2α (eIF2α) mediated pathway, and (iii) Inositol-Requiring Enzyme 1 (IRE1) mediated

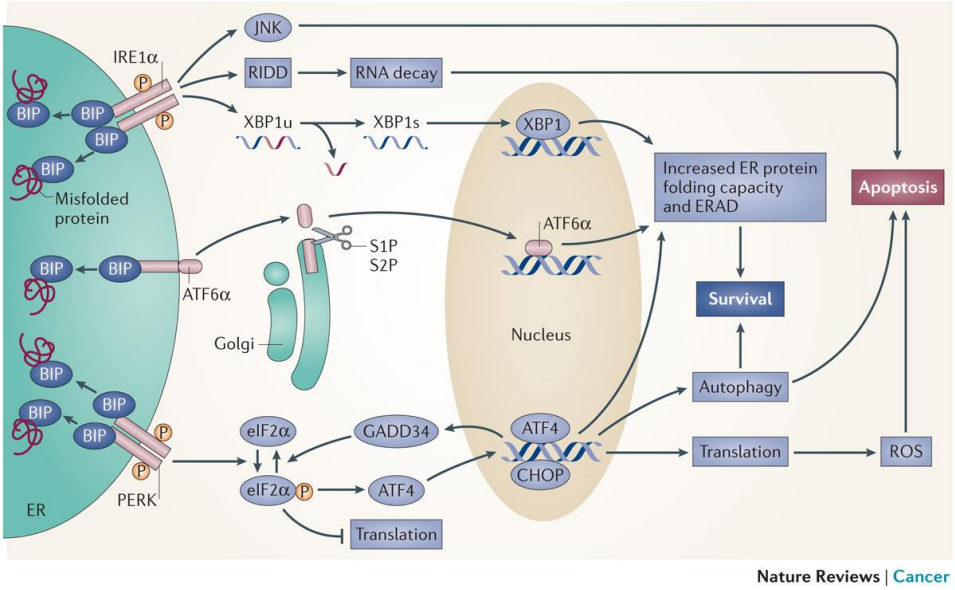

Figure 1.12 – ER stress pathways (Wang et al., 2014).

pathway.

Since part of this thesis focuses on the PERK/eIF2α mediated ER stress pathway, the following sections present a detailed description of this signaling branch and its associations with cardiovascular disease:

1.8.1 PERK/eIF2α mediated ER Stress Pathway

PERK is a type I transmembrane protein of ER. Under non-stress conditions, Heat Shock Protein 90 (HSP90) and Binding Immunoglobulin Protein (BIP) bind to the cytoplasmic and ER luminal domains of PERK, respectively, and prevents its activation. However, under ER stress conditions, BIP binds to unfolded and misfolded proteins. This, in turn, releases PERK and activates it via homodimerization and autophosphorylation. PERK activation is followed by phosphorylation of eIF2α, which results in attenuation of translation initiation and shutdown of protein synthesis (Wang et al., 2014; Walter et al., 2011).

Paradoxically, PERK-eIF2α activation increases the translation of a select group of mRNAs, such as that encoding Activating Transcription Factor 4 (ATF4). ATF4 then enters the nucleus and activates the transcription of several ER stress response genes, including C/EBP Homologous Protein (CHOP). CHOP expression promotes protein synthesis to induce protein misfolding and oxidative stress, eventually leading to cell death. It also downregulates the expression of pro-survival genes (such as BCL2L1) (Noh et al., 2015). However, chronic activation of PERK is required to induce a significant increase in the steady state levels of CHOP expression (Wang et al., 2014; Walter et al., 2011).

1.8.2 PERK/eIF2α Pathway in Cardiovascular Diseases

ATF4 and CHOP expression was found to be significantly upregulated in the myocardium of heart failure patients (Fu et al., 2010). Similar upregulation was also observed in calcified human AV samples compared to healthy control (Wang et al., 2017; Cai et al., 2013). In atherosclerosis, ruptured plaques were found to exhibit significantly increased CHOP expression (Myoishi et al., 2007). These imply that PERK/eIF2α pathway is significantly upregulated in cardiovascular diseases and can be a potential target for therapeutic applications (Minamino et al., 2010).

1.9 miR-214 in Cardiovascular Diseases

microRNAs are small (~ 22 nucleotides in length) non-coding RNAs that modulate gene expression by silencing their targets (Ha et al., 2014). Since discovery of the first microRNA (lin-4) in 1993 (Lee et al., 1993), these have been implicated in nearly all developmental and pathological processes (Sun et al., 2010). Due to their role in modulating gene expression, microRNAs have been widely considered as a potential therapeutic option for different diseases, such as cancer (Rupaimoole et al., 2017; Shah et al., 2016).

Many microRNAs have been found to be involved with cardiovascular diseases (McManus et al., 2015; Romaine et al., 2013; Quiat et al., 2013). Among these, miR-214 is of paramount importance due to its regulatory role in physiological and pathological processes of the cardiovascular system (Figure 1.13).

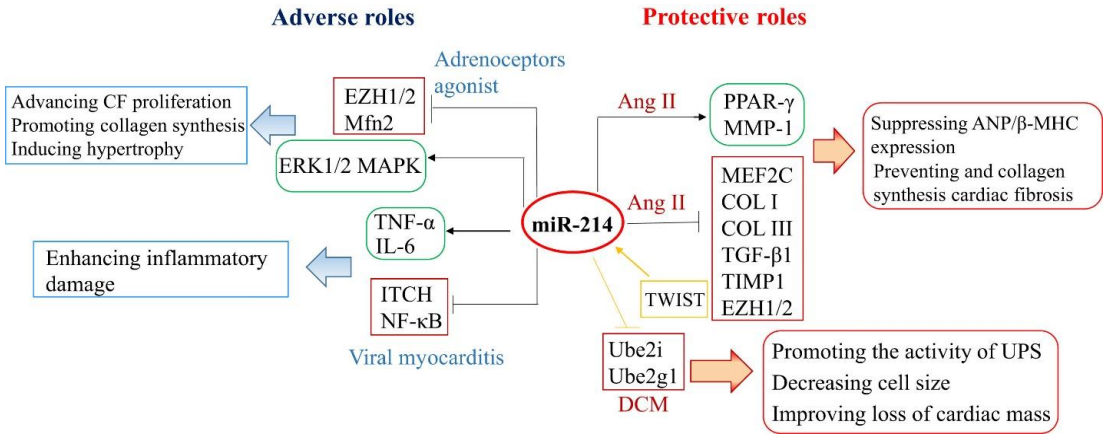

Figure 1.13 – miR-214 in cardiovascular diseases (Zhang et al., 2017).

The expression of miR-214 is upregulated during myocardial infarction (Van Rooij et al., 2008) and inhibits left ventricular remodeling by targeting Phosphatase and Tensin Homolog (PTEN) (Yang et al., 2016). Upregulated expression of miR-214 plays a protective role against ischemic injury by suppressing the expression of Sodium/Calcium Exchanger 1 (NCX1) (Aurora et al., 2012). This protective role is associated with its inhibitory effect on cardiac fibrosis (Dong et al., 2016). Additionally, circulating miR-214 expression was found to be correlated with the severity of coronary artery disease (CAD) (Jin et al., 2015; Lu et al., 2013).

miR-214 expression is upregulated during cardiac hypertrophy (Van Rooij et al., 2006) and overexpression of miR-214 promotes hypertrophy by suppressing Enhancer of Zeste Homolog 2 (EZH2) expression (Yang et al., 2014). Similar upregulation of miR-214 expression is observed in heart failure patients (Duan et al., 2015). On the other hand, the expression of miR-214 is downregulated during dilated cardiomyopathy (Baumgarten et al., 2013).

Interestingly, hypoxia induces upregulation of miR-214 expression in a model of pulmonary arterial hypertension (PAH) and loss of miR-214 leads to right ventricle hypertrophy (RVH) (Stevens et al., 2016). Similar upregulation of left ventricular miR-214 expression was observed in an Angiotensin II (AngII) infusion model of hypertension (McGinnigle et al., 2017). On the contrary, Liu et al. (2016) reported that miR-214 promotes hypoxia-induced pulmonary hypertension by suppressing the expression of Cyclin L2 (CCNL2).

miR-214 exerts a proliferative effect on vascular smooth muscle by targeting PTEN (Zhong et al., 2016), whereas inhibition of miR-214 restores their contractile phenotype by upregulating the expression of Myocyte Enhancer Factor 2C (MEF2C) and Leiomodin 1(LMOD1) (Sahoo et al., 2016).

In AV disease, the functional role of miR-214 is not clear yet. Song et al. (2017) and Wang et al. (2017) reported that calcified human AVs exhibit a decreased expression of miR-214 compared to normal control, whereas Li et al. (2016) and Xu et al. (2017) found the opposite. In a recent study, Rathan et al. (2016) showed that miR-214 is a side-specific microRNA in AV and its expression is upregulated when fibrosa is exposed to low oscillatory shear stress. However, this increased expression was found to provide a protective effect against AV fibrosis by downregulating the expression of Transforming Growth Factor-β1 (TGF-β1).

Therefore, it is evident that miR-214 has a diversified role in cardiovascular diseases. Fundamental understanding of its functional role will be necessary to elucidate the underlying mechanisms behind its association with different pathological conditions.

1.10 Rationale for Thesis Research

miR-214 has been shown to be a side-specific and shear-dependent microRNA in porcine AVs (Rathan et al., 2016). In addition to that, ATF4 and CHOP (downstream genes in the PERK/eIF2α mediated ER stress pathway) expression was found to be upregulated during AV calcification (Wang et al., 2017; Cai et al., 2013). Interestingly, ATF4 has been reported to be a target of miR-214 (Wang et al., 2013).

Since stretch is one of the major mechanical forces experienced by AV (Balachandran et al., 2011) and elevated stretch induces significantly higher AV calcification (Balachandran et al., 2010), it will be interesting to explore the effect of cyclic stretch on the expression of miR-214 and its target ER stress response genes (such as ATF4). Hence, this dissertation will focus on investigating the role of miR-214 in stretch-induced AV disease. An ex vivo approach using whole porcine AV tissues was adopted since it retains both the cells and the native extracellular matrix. Three specific aims have been designed to study the role of miR-214 in stretch-induced AV disease.

The first specific aim will elucidate the effect of cyclic stretch on miR-214 expression in AV. The second specific aim will evaluate the effect of cyclic stretch on ATF4 (miR-214 target) and its downstream genes, CHOP and BCL2L1. The third specific aim will explore the effect of miR-214 mimic on ATF4, CHOP, BCL2L1 and osteocalcin (calcification gene) expression in AV. In combination, this information will provide a better understanding of the functional role of miR-214 in AV disease.

CHAPTER 2. HYPOTHESIS AND SPECIFIC AIMS

Cyclic stretch is one of the major mechanical forces as experienced by AV (Balachandran et al., 2011). Previously, elevated cyclic stretch (15%) was shown to promote adverse extracellular matrix (ECM) remodeling and calcification in AV (Balachandran et al., 2009; Balachandran et al., 2010). In a recent study, Rathan et al. (2016) reported that increased expression of side-specific and shear-dependent miR-214 can suppress AV fibrosis by downregulating TGF-β1 expression. In addition to that, miR-214 expression was found to be downregulated in calcified human AVs compared to healthy control (Song et al., 2017; Wang et al., 2017).

Interestingly, the expression of ATF4 (a target of miR-214) and CHOP (transcriptional target of ATF4) are significantly upregulated in calcified human AVs compared to normal control (Wang et al., 2017; Cai et al., 2013). CHOP also downregulates the expression of pro-survival gene BCL2L1 under apoptotic conditions (Noh et al., 2015). It should be noted here that both ATF4 and CHOP are major components of the ER stress pathways (Ron et al., 2007). Therefore, it will be interesting to see the effect of cyclic stretch on the expression of miR-214 and its target ER stress response genes (such as ATF4).

The hypothesis of this dissertation is that pathological cyclic stretch dysregulates the expression of miR-214 as well as those of its target ATF4 and subsequent downstream genes, CHOP and BCL2L1 in AV. Additionally, it is hypothesized that miR-214 overexpression reverses the above-mentioned changes in gene expression and suppresses osteocalcin expression in AV.

The hypotheses will be tested via three specific aims as follows:

1) Effect of cyclic stretch on miR-214 expression in AV
2) Effect of cyclic stretch on ATF4, CHOP and BCL2L1 expression in AV
3) Effect of miR-214 mimic on ATF4, CHOP, BCL2L1 and osteocalcin expression in AV

The overall organization of the three specific aims is depicted in the following diagram:

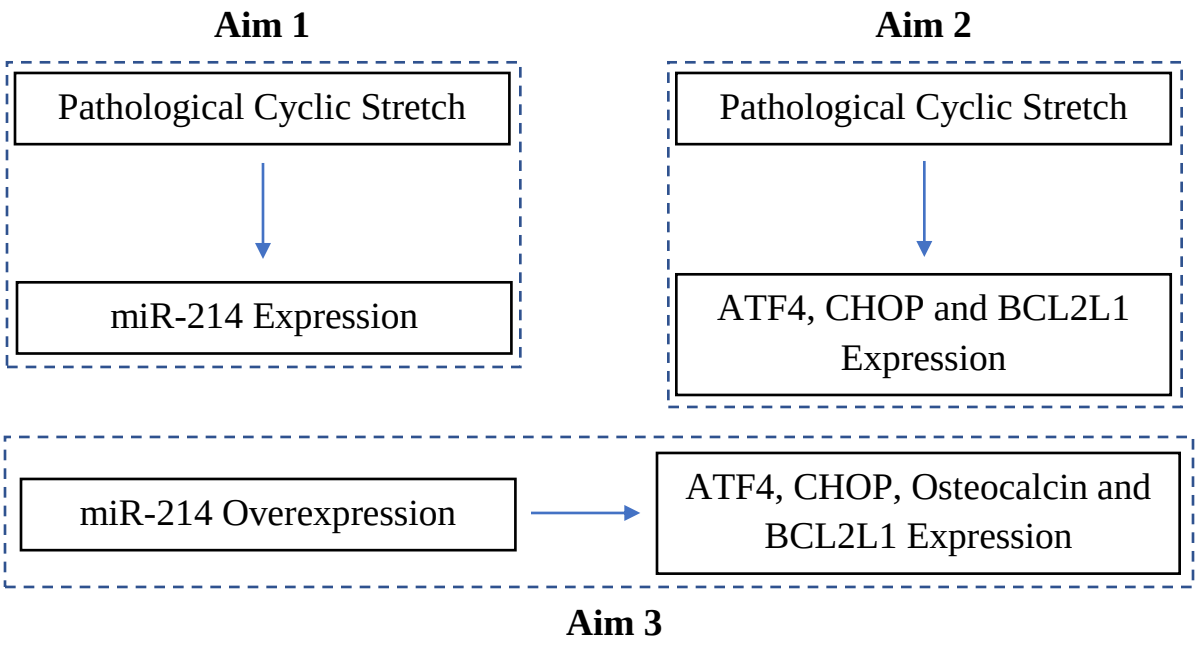

Figure 2.1 – Overall organization of specific aims.

2.1 Effect of Cyclic Stretch on miR-214 Expression in AV

This specific aim will focus on elucidating the effect of cyclic stretch on miR-214 expression in AV. miR-214 has been recently identified as one of the side-specific and shear-dependent miRNAs in porcine AVs (Rathan et al., 2016), emphasizing its potential role in AV pathogenesis. Since stretch is a major mechanical force that is experienced by AV during each cardiac cycle, it will be interesting to see its effect on miR-214 expression. The hypothesis of this specific aim is that pathological cyclic stretch can dysregulate the expression of miR-214 in AV.

Porcine AV tissues will be cyclically stretched at the physiological (10%) and pathological (15%) level for 2 days in regular medium and for 7 days in osteogenic medium. Cyclic stretching at 15% for 2 days in regular medium and for 7 days in osteogenic medium will represent the stretch-induced early remodeling and late calcification stages of AV disease, respectively. For both cases, 10% cyclic stretch will serve as the physiological counterpart (2-day 10% stretch in regular medium and 7-day 10% stretch in osteogenic medium, respectively). Subsequently, the expression of miR-214 will be evaluated in the stretched AV tissue samples using RT-qPCR.

2.2 Effect of Cyclic Stretch on ATF4, CHOP and BCL2L1 Expression in AV

This specific aim will focus on elucidating the effect of cyclic stretch on the mRNA expression of ATF4, CHOP and BCL2L1 genes in AV. ATF4 and CHOP are major components of the ER stress pathways and pro-survival gene BCL2L1 can be downregulated by CHOP under apoptotic conditions (Ron et al., 2007; Noh et al., 2015). It has been shown that both ATF4 and CHOP are significantly upregulated in calcified human AVs compared to healthy control (Cai et al., 2013; Wang et al., 2017). Therefore, it will be interesting to see the effect of cyclic stretch on the mRNA expression of ATF4, CHOP and BCL2L1 genes in AV. The hypothesis of this specific aim is that pathological cyclic stretch can dysregulate the expression of ATF4, CHOP and BCL2L1 genes in AV.

Porcine AV tissues will be cyclically stretched at the physiological (10%) and pathological (15%) level for 2 days in regular medium and for 7 days in osteogenic medium. Cyclic stretching at 15% for 2 days in regular medium and for 7 days in osteogenic medium will represent the stretch-induced early remodeling and late calcification stages of AV disease, respectively. For both cases, 10% cyclic stretch will serve as the physiological counterpart (2-day 10% stretch in regular medium and 7-day 10% stretch in osteogenic medium, respectively). Subsequently, the mRNA expression of ATF4, CHOP and BCL2L1 genes will be evaluated in the stretched AV tissue samples using RT-qPCR.

2.3 Effect of miR-214 Mimic on ATF4, CHOP, BCL2L1 and Osteocalcin Expression in AV

This specific aim will focus on elucidating the effect of miR-214 overexpression on the mRNA expression of ATF4, CHOP, BCL2L1 and osteocalcin (BGLAP) genes in AV. ATF4 has been reported to be a target of miR-214 (Wang et al., 2013). Interestingly, both CHOP and BGLAP are transcriptional targets of ATF4 (Ron et al., 2007; Lian et al., 2009). As mentioned previously, increased CHOP expression may downregulate the expression of pro-survival gene BCL2L1 under apoptotic conditions (Noh et al., 2015). Therefore, it will be interesting to see the effect of miR-214 mimic on the mRNA expression of ATF4, CHOP, BCL2L1 and BGLAP genes in AV. The hypothesis of this specific aim is that miR-214 overexpression can downregulate the expression of ATF4, CHOP and BGLAP genes and upregulate the expression of BCL2L1 gene in AV tissues.

Porcine AV tissues will be statically cultured with either negative control mimic or miR-214 mimic for 2 days in osteogenic medium. Use of osteogenic medium will promote a calcific environment. Subsequently, miR-214 expression as well as the mRNA expression of ATF4, CHOP, BCL2L1 and BGLAP genes will be evaluated in the resulting AV tissue samples using RT-qPCR.

CHAPTER 3. METHODS

3.1 Stretch Bioreactor System

The stretch bioreactor system used in this dissertation was previously designed and validated in the Cardiovascular Fluid Mechanics Laboratory (Balachandran, 2010). The following figure indicates the main features of the stretch bioreactor.

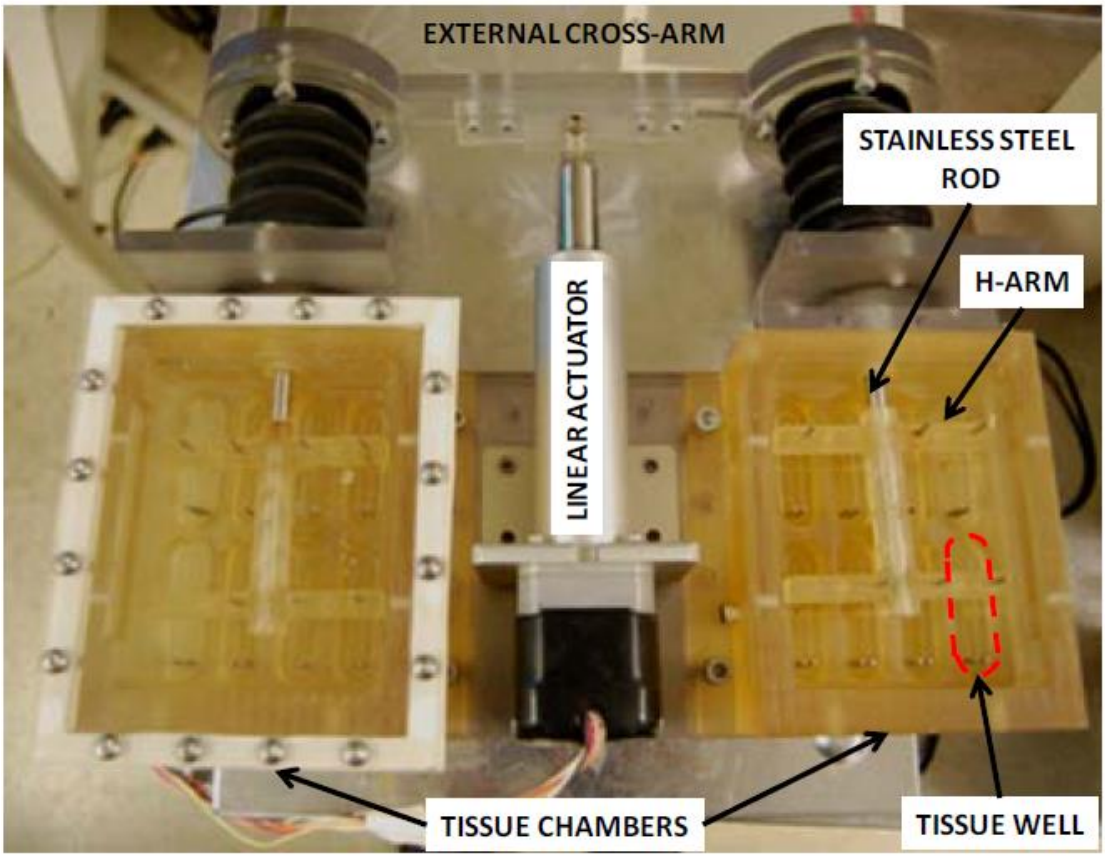

Figure 3.1 – Stretch bioreactor.

Briefly, the bioreactor has two identical chambers, each containing 8 wells for culturing 16 tissues at the same time (one tissue sample per well). Each well can contain approximately 5 mL of culture medium. There are two stainless steel posts in each well – one stationary and the other mobile. The stationary post is fixed to the bottom surface of

each well, whereas the moving post is mounted from an H-shaped arm that is coupled to a rigid, stainless steel rod. This stainless-steel rod is further coupled to a cross-arm and a linear actuator (ULTRA MOTION part no. D-A.083-HT17-2-2NO-ES-BR/RC4). The motion of the linear actuator is controlled by a ST5-Si stepper motor drive (APPLIED MOTION), which is connected to a laptop. Appropriate stretch program (10% or 15% stretch, Si Programmer^{TM}, APPLIED MOTION) is downloaded from the laptop to the motor drive to initiate a cyclic stretch experiment. This whole setup is depicted in the following diagram:

Figure 3.2 – Setup of stretch bioreactor system.

Additionally, each chamber of the bioreactor is always covered with a transparent lid, while the stainless-steel rods are covered with rubber bellows on the outside of the bioreactor. These provide the necessary environmental sealing to ensure sterile operation.

The stretch bioreactor system is made of polysulfone (most of the parts) and polycarbonate (chamber lids) for biocompatibility. Prior to each stretch experiment, the bioreactor is ethylene-oxide sterilized in a 12-hour (or 24-hour) cycle to prevent contamination.

3.2 Workflow of *Ex vivo* Stretch Experiment

The following diagram outlines the workflow for setting up and running an *ex vivo* stretch experiment:

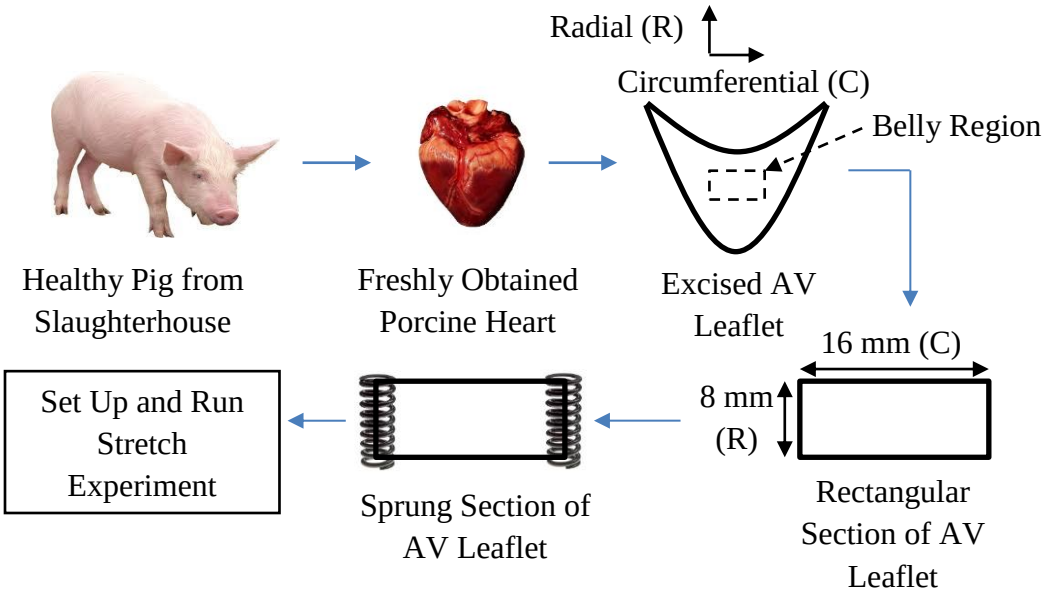

Figure 3.3 – Workflow for setting up a stretch experiment

Each of the above steps is detailed described below:

3.2.1 Harvesting of Porcine Aortic Valve (AV) Tissue

Healthy porcine hearts are obtained immediately (within 10 – 15 minutes) after slaughter from a local abattoir (HOLIFIELD FARMS, COVINGTON, GA). The three AV leaflets from each heart are excised using a surgical scissor and stored in a 50-mL tube (VWR catalogue no. 89004-364) containing sterile, DNase/RNase-free ice-cold Dulbecco's Phosphate-Buffered Saline (DPBS; THERMO FISHER SCIENTIFIC catalogue no. 21600044) solution on-site. After excising the required number of AV leaflets, these are transported back to the laboratory (transportation time does not exceed 1

hour). All tools (metallic tray, forceps, surgical scissors) used in the harvesting process are sterile.

3.2.2 Stretch Experiment Setup

Upon arriving in the laboratory, excised AV leaflets are transferred to petri dishes (VWR catalogue no. 25373-085) containing sterile, DNase/RNase-free ice-cold DPBS solution inside a Class II Biological Safety Cabinet. From thereon, all the following steps are carried out inside the safety cabinet. A rectangular section of 16 mm (in the circumferential direction) by 8 mm (in the radial direction) is cut from the belly region of each AV leaflet tissue using a surgical blade (VWR catalogue no. 2976#10) and stored in sterile, DNase/RNase-free ice-cold DPBS solution. Next, two stainless steel springs (MCMASTER CARR part no. 9663K16) are manually inserted (an optimum of four turns or insertions) on either side (circumferential direction) of each tissue section so that the tissue section covers at least half the inner diameter of the spring.

After completion of the springing step, the tissue sections are statically kept in sterile regular culture medium. Next, 5 mL of regular or osteogenic culture medium (depending on the type of experiment) is added to each well of the stretch bioreactor. Then, each sprung tissue section is mounted between the stationary and moving posts of one of the bioreactor wells. Once all the sprung tissue sections are mounted inside the wells of the bioreactor, the moving post is incrementally moved away from the stationary post to a final position where the distance between two posts is 18.7–19 mm (as measured by slide callipers). This distance approximately corresponds to an unstretched initial condition for each tissue section.

After that, the appropriate stretch program is downloaded from the laptop to the ST5-Si stepper motor drive that controls the linear actuator of the bioreactor and the program is thereby executed to start the cyclic stretch experiment at 60 cycles/minute.

Next, it is quickly checked (both visually and quantitatively by slide callipers) whether all the tissue sections are being cyclically stretched in an appropriate manner. Finally, the stretch bioreactor system is carefully transferred from the biological safety cabinet to a humid CO_2 incubator. Throughout the duration of the stretch experiment, the following operating conditions are maintained inside the incubator:

Table 3.1 – Operating conditions inside the incubator

Operating Variable	Operating Condition
Chamber Temperature	37°C
CO_2 Concentration	5%

It is ensured that all tools (tweezers, scalpel handle, surgical blades, springs, allen key) and the stretch bioreactor system (including the moving posts and assembly screws) are sterilized by ethylene oxide (Anprolene AN74j Sterilizer, ANDERSEN PRODUCTS) beforehand. Additionally, aseptic techniques are strictly followed and 70% ethanol (VWR catalogue no. 71002-398) and RNase AWAY decontaminant solution (VWR catalogue no. 53225-514) are used to maintain sterile RNase-free conditions.

3.2.3 Replacing Culture Medium

Over the course of a stretch experiment, the culture medium is replaced every 48 hours. It is ensured that the 2 – 200 µL (VWR catalogue no. 47745-170) and 50 – 1000 µL (VWR catalogue no. 47745-174) pipet tips are autoclaved beforehand. Additionally, aseptic techniques are strictly followed and 70% ethanol and RNase AWAY decontaminant solution are used to maintain sterile RNase-free conditions.

3.2.4 Tissue Sample Collection After Completion of Stretch Experiment

After completion of the experiment, the stretch bioreactor system is carefully transferred from the CO_2 incubator to the biological safety cabinet. Next, AV tissue samples are taken out of the bioreactor and washed three times in sterile DNase/RNase-free ice-cold DPBS solution to remove the residual culture medium adhering to the tissues. Then, the portions of each tissue section connected to the springs are discarded and only the middle portion is kept for further analyses.

If the tissue samples are to be used for qPCR, then each of these samples is transferred to an autoclaved RNase/DNase-free 2 mL microcentrifuge tube (VWR catalogue no. 87003-298), followed by snap-freezing using liquid nitrogen and storage in –80°C freezer. On the other hand, if the tissue samples are to be used for qualitative (Von Kossa and Alizarin Red stains) and quantitative (Arsenazo assay) assessment of calcification, one-third of each tissue sample (in the radial direction) is excised along the circumferential direction, embedded in Optimum Cutting Temperature (OCT) compound and stored in –80°C freezer. The remaining portion of the tissue sample is transferred to an autoclaved RNase/DNase-free 2 mL microcentrifuge tube, snap-frozen in liquid nitrogen

and stored in –80°C freezer. However, for immunostaining, the whole tissue sample is embedded in OCT compound and stored in –80°C freezer.

All tools (tweezers, scalpel handle, surgical blades) and microcentrifuge tubes are autoclaved beforehand. Additionally, aseptic techniques are strictly followed and 70% ethanol and RNase AWAY decontaminant solution are used to maintain sterile RNase-free conditions.

3.3 Formulations of Different Tissue Culture Media

Two types of culture medium are used in static or stretch experiments: regular and osteogenic medium. The regular medium is used to maintain normal cell viability of porcine AV tissues over the course of an experiment, whereas the osteogenic medium is used to accelerate the process of AV calcification by adding specific chemicals that promote osteogenesis. Both media formulations were previously developed and validated in the Cardiovascular Fluid Mechanics Laboratory (Balachandran, 2010).

3.3.1 Formulation of Regular Culture Medium

The formulation of regular medium is outlined in the following table:

Table 3.2 – Regular culture medium

Component	Stock Concentration	Required Concentration	Required Amount or Volume in 1L Medium
Dulbecco's Modified Eagle's Medium (DMEM)	–	13.36 g/L	13.36 g

Table 3.2 Continued

[THERMO FISHER SCIENTIFIC catalogue no. 12100061]			
Bovine Calf Serum [FISHER SCIENTIFIC catalogue no. SH3007203]	–	10% (volume by volume %)	100 mL
Sodium Bicarbonate [SIGMA ALDRICH catalogue no. S5761]	–	3.7 g/L	3.7 g
Ascorbic Acid [SIGMA ALDRICH catalogue no. A7631]	10 mg/mL of ultrapure water	50 mg/L	5 mL
HEPES Buffer [FISHER SCIENTIFIC catalogue no. BP299-1]	–	2.5% (volume by volume %)	25 mL
Non-essential Amino Acid Solution [SIGMA ALDRICH catalogue no. M7145]	100x	1% (volume by volume %)	10 mL
Antibiotics [FISHER SCIENTIFIC catalogue no. SV3007901]	100x	1% (volume by volume %)	10 mL
Ultrapure Water [Synergy System, EMD MILLIPORE]	–	–	As needed for 1 L final volume

The final pH of the medium is adjusted between 7.2 and 7.4 using 1N NaOH (SIGMA ALDRICH catalogue no. S2770) or 1N HCl (SIGMA ALDRICH catalogue no. H9892) while thoroughly mixing by a NuovaTM stirring hotplate (THERMO FISHER SCIENTIFIC). Eventually, the medium is sterile-filtered using a 0.2 µm vacuum filter unit (VWR catalogue no. 89216-298) and stored in 4°C fridge. It is ensured that the 1 L glass bottle into which the above listed components are added is autoclaved. Additionally, aseptic techniques are strictly followed and 70% ethanol and RNase AWAY decontaminant solution are used to maintain sterile RNase-free conditions.

3.3.2 Formulation of Osteogenic Culture Medium

The osteogenic medium is simply the regular medium supplemented with specific chemicals that induce osteogenic differentiation. These additional reagents, as outlined below, are separately added to a petri dish or each bioreactor well during setting up a static or stretch experiment, respectively.

Table 3.3 – Osteogenic culture medium

Component	Stock Concentration	Required Concentration	Required Volume in 5 mL (or 20 mL) Medium
Sodium Phosphate Monobasic Monohydrate [FISHER SCIENTIFIC catalogue no. S369-500]	100 mM (in ultrapure water)	3.8 mM	190 µL (760 µL)
β-Glycerophosphate [SIGMA ALDRICH catalogue no. G9422]	100 mM (in ultrapure water)	1 mM	50 µL (200 µL)

Table 3.3 Continued

Dexamethasone [SIGMA ALDRICH catalogue no. D4902]	2.5 mM (in 100% ethanol)	10 µM	20 µL (80 µL)
Transforming Growth Factor-β1 (TGF-β1) [SIGMA ALDRICH catalogue no. T5050]	1 µg/mL (in 4 mM HCl containing 1 mg/mL BSA)	1 ng/mL	5 µL (20 µL)

All components are sterile-filtered using a 0.2 µm syringe filter (FISHER SCIENTIFIC catalogue no. 09-719C). The stock solution of sodium phosphate is stored in 4°C fridge, whereas β-glycerophosphate and dexamethasone solutions are stored in –20°C freezer and TGF-β1 solution in –80°C freezer.

3.4 Workflow for Real-Time Quantitative Polymerase Chain Reaction (RT-qPCR)

The detection and relative quantification of miRNA or mRNA in tissue samples is accomplished using RT-qPCR. The entire process is comprised of several steps, as outlined in the following diagram:

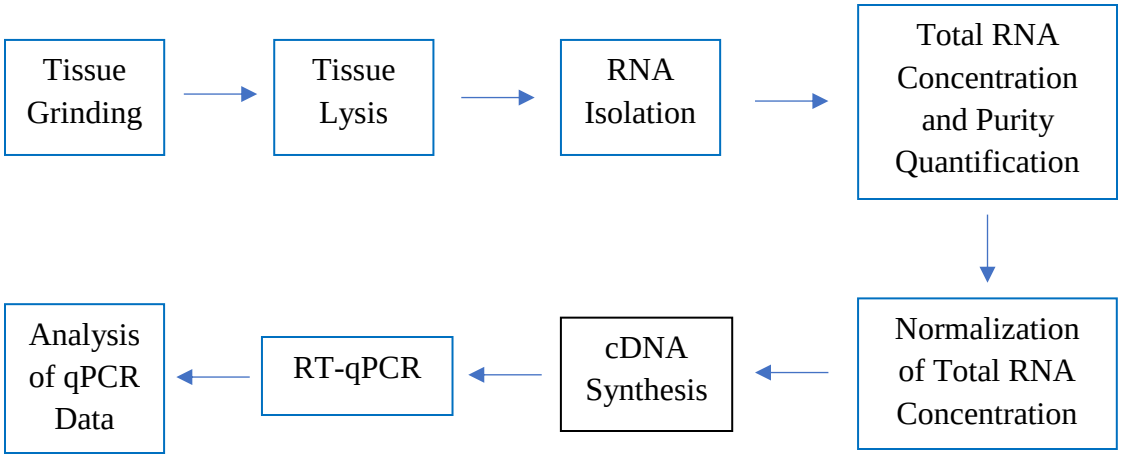

Figure 3.4 – Workflow diagram for RT-qPCR

Each of the above steps is described in detail in the following sections:

3.4.1 Tissue Grinding

Before starting the tissue grinding process, the countertop area and all the material surfaces that come in contact with the tissue sample are thoroughly wiped by RNase AWAY decontaminant solution (VWR catalogue no. 53225-514). First, porcine aortic valve (AV) tissue sample from static or stretch experiments is placed in a mortar (VWR catalogue no. 470148-960). Then, liquid nitrogen is added from a dewar flask (VWR catalogue no. 63415-000) to completely immerse the tissue sample inside the mortar. After that, a pestle (VWR catalogue no. 470148-960) is used to gradually apply a twisting downward motion on the tissue sample, thereby slowly grinding it to a fine powder form.

Throughout the entire process, it is ensured that the tissue sample is always immersed in liquid nitrogen.

3.4.2 Tissue Lysis

Immediately after grinding the tissue sample to a fine powder form, more liquid nitrogen is added to the mortar to form a slurry-like mixture. The mixture is then transferred to an autoclaved RNase-free 2 mL microcentrifuge tube (VWR catalogue no. 87003-298) via a funnel (VWR catalogue no. 414004-269). The remaining liquid nitrogen inside the microcentrifuge tube evaporates within the next 5 – 10 seconds. To lyse the grinded tissue sample, 1500 µL of QIAzol lysis reagent (QIAGEN catalogue no. 79306) is added to the microcentrifuge tube using a 1000 µL pipettor (VWR catalogue no. 89079-974). During this step, it is ensured that the 50 – 1000 µL pipet tips (VWR catalogue no. 47745-174) being used are autoclaved. Subsequently, proper mixing of the powdered tissue sample and the lysis reagent is ensured using a vortex mixer (DADE catalogue no. S8223-1), followed by a static reaction time of 1 minute. Throughout the entire process, the microcentrifuge tube is kept on ice. After this step, the process of RNA isolation can be started right away or the microcentrifuge tube containing the powdered tissue sample/lysis reagent mixture can be stored in –80°C freezer for RNA isolation later.

3.4.3 RNA Isolation

Before starting the process of RNA isolation, it is ensured that the 50 – 1000 µL and 2 – 200 µL pipet tips (VWR catalogue no. 47745-170), and the 2 mL microcentrifuge tubes are autoclaved. RNA isolation is accomplished by using the Direct-zolTM RNA MiniPrep Plus RNA isolation kit from ZYMO RESEARCH (catalogue no. R2072).

First, all microcentrifuge tubes containing the powdered tissue sample/lysis reagent mixtures are centrifuged in a SorvallTM LegendTM Micro 21R microcentrifuge at 13,000xg for 10 minutes. After that, the supernatant tissue lysate (almost 1500 µL) is collected equally into two autoclaved RNase-free 2 mL microcentrifuge tubes. Then, 750 µL of 100% molecular biology-grade ethanol (SIGMA ALDRICH catalogue no. E7023) is added to each of those tubes. After thorough mixing using a vortex mixer, 750 µL of the mixture is transferred into a Zymo-SpinTM IIICG Column (provided in the kit) in a Collection Tube (provided in the kit), which is centrifuged at 13,000xg for 1 minute. The flow-through is subsequently discarded, and the step is repeated three more times using the same Spin Column and Collection Tube to elute the full 3000 µL mixture of tissue lysate and 100% ethanol.

800 µL of RNA Wash Buffer (provided in the kit) is then added to the Spin Column, and the Spin Column-Collection Tube assembly is centrifuged at 13,000xg for 1 minute. After discarding the flow-through, an 80 µL mixture of DNase I and DNA Digestion Buffer (both provided in the kit) is added to the column using a 100 µL pipettor (VWR catalogue no. 89079-974), followed by an incubation period of 15 minutes at room temperature (20 – 25°C). The mixture contains 10 µL DNase I solution and 70 µL DNA Digestion Buffer.

Subsequently, 800 µL of Direct-zolTM RNA PreWash (provided in the kit) is added to the Spin Column, and the Spin Column-Collection Tube assembly is centrifuged at 13,000xg for 1 minute, followed by disposal of the flow-through. This step with Direct-zolTM RNA PreWash is repeated one more time. Then, 800 µL of RNA Wash Buffer is added to the Spin Column, and the Spin Column-Collection Tube assembly is centrifuged at 13,000xg for 3 minutes to ensure complete removal of the wash buffer.

Following this step, the Spin Column is carefully transferred to an autoclaved RNase-free 2 mL microcentrifuge tube. To elute the isolated RNA, 80 µL DNase/RNase-Free Water (provided in the kit) is directly added to the column matrix, and the Spin Column-Microcentrifuge Tube assembly is centrifuged at 13,000xg for 2 minutes. The spin column is subsequently discarded, and the flow-through collected in the microcentrifuge tube contains the RNA isolated from the powdered tissue sample. The total RNA concentration and RNA purity of the sample can be immediately quantified using a NanoDrop 2000/2000c UV-Vis spectrophotometer (THERMO FISHER SCIENTIFIC) or the RNA sample can be stored in –80°C freezer for total RNA concentration and purity quantification later.

3.4.4 Total RNA Concentration and RNA Purity Quantification

The total RNA concentration and purity of the isolated RNA from a porcine AV tissue sample is quantified using a NanoDrop 2000/2000c UV-Vis spectrophotometer. Prior to beginning the quantification process, the pedestals of the spectrophotometer are cleaned. To do that, 2 µL of DNase/RNase-free water is added on the surface of the bottom pedestal using a 2 µL pipettor (VWR catalogue no. 89079-974), and the upper pedestal arm is then lowered to form a liquid column. After letting it sit for approximately 2 – 3 minutes, the water from both the top and bottom pedestal is wiped away using kimwipes (VWR catalogue no. 470224-038).

At first, a reference RNA quantification is made by adding 2 µL of DNase/RNase-free water on the surface of the bottom pedestal, followed by lowering of the upper pedestal arm and clicking the Blank button in the NanoDrop program. Subsequently, the water from

both the top and bottom pedestal is wiped off. Then, 2 µL of RNA sample is added on the surface of the bottom pedestal, followed by lowering of the upper pedestal arm and clicking the Measure button in the NanoDrop program. The NanoDrop program gives values for RNA concentration (in ng/µL), 260/280 ratio (ratio of absorbance at 260 nm and 280 nm) and 260/230 ratio (ratio of absorbance at 260 nm and 230 nm). The 260/280 and 260/230 ratios are primary and secondary measures, respectively, of RNA purity. In the case of handling multiple RNA samples at once, the system is Blanked after every 3 – 4 measurements. Throughout the entire process, the microcentrifuge tubes containing the RNA samples are kept on ice.

3.4.5 Normalization of Total RNA Concentration

After quantification of the total RNA concentration of all samples from same-day static/stretch experiments, required amounts of DNase/RNase-free water are added to the RNA samples to normalize their RNA concentrations to the same value. The post-normalization total RNA concentration is typically equal to that of the RNA sample which has the lowest total RNA concentration (among all the same-day static/stretch experiment samples), obtained immediately after the NanoDrop measurement. Throughout the whole process, the microcentrifuge tubes containing the RNA samples should be kept on ice. After normalization, the process of cDNA synthesis can be started right away or the RNA samples can be stored in –80°C freezer for cDNA synthesis later.

3.4.6 cDNA Synthesis

The cDNA synthesis process is different based on whether the cDNA is to be used for miRNA or mRNA RT-qPCR. The two distinct synthesis methods are as follows:

3.4.6.1 cDNA Synthesis for miRNA RT-qPCR

In the case of miRNA, the cDNA is synthesized using the miScript II Reverse Transcription Kit (QIAGEN catalogue no. 218161). At first, a reverse transcription mixture (for one reaction) is prepared as outlined in the following table. All the necessary components from the kit are thawed at room temperature (20 – 25°C) and then kept on ice throughout the whole process. When dealing with multiple RNA samples/reactions at once, the total volume of the master mixture should account for 1 – 2 more reactions than the required number.

Table 3.4 – Reverse transcription mixture for miRNA

Component	Required Volume [µL]
5x miScript HiSpec Buffer	4
10x miScript Nucleics Mix	2
miScript Reverse Transcriptase Mix	2

After adding all the above components into an autoclaved 2 mL microcentrifuge tube, the tube should be gently vortexed (for thorough mixing) using a vortex mixer (VWR catalogue no. 97043-562) and briefly centrifuged (for retaining residual liquid from the sides of the tube) in a minicentrifuge (VWR catalogue no. 10067-588). From thereon, the master mixture should be kept on ice. Next, 12 µL of each RNA sample is added to an autoclaved 0.2 mL PCR tube (VWR catalogue no. 20170-012) using a 20 µL pipettor (VWR catalogue no. 89079-974), followed by the addition of 8 µL master mixture. Hence,

the total reaction volume is 20 µL in each tube. After this, all the PCR tubes are centrifuged in the minicentrifuge and placed in the 96-well thermal cycler (BIORAD MyCyclerTM). Prior to the thermal cycling step, the PCR tubes are kept on ice all the time. The run method used in the thermal cycler is as follows:

a. 1st stage: Incubation at 37°C for 1 hour
b. 2nd stage: Incubation at 95°C for 5 minutes to inactivate miScript Reverse Transcriptase Mix
c. 3rd stage: Holding stage at 4°C

After completion of the reaction, the prepared cDNA can be used immediately for RT-qPCR of miRNA. Alternatively, it can be stored in 4°C fridge for short term (maximum one week) or in –20°C/–80°C freezer for long term (several months).

3.4.6.2 cDNA Synthesis for mRNA RT-qPCR

For mRNA, the cDNA is synthesized using the High-Capacity cDNA Reverse Transcription Kit (THERMO FISHER SCIENTIFIC catalogue no. 4368814). At first, a reverse transcription mixture (for one reaction) is prepared as outlined in the following table. All the necessary components from the kit are thawed at room temperature (20 – 25°C) and then kept on ice throughout the entire process. When dealing with multiple RNA samples/reactions at once, the total volume of the master mixture should account for 1 – 2 more reactions than the required number.

Table 3.5 – Reverse transcription mixture for mRNA

Component	Required Volume [µL]
10x RT Buffer	2
25x dNTP Mix (100 mM)	0.8
10x RT Random Primers	2
Multiscribe™ Reverse Transcriptase	1

After adding all the above components into an autoclaved 2 mL microcentrifuge tube, the tube is gently vortexed (for thorough mixing) using a vortex mixer and briefly centrifuged (for retaining residual liquid from the sides of the tube) in a minicentrifuge. From thereon, the master mixture is kept on ice. Next, 14.2 µL of each RNA sample is added to an autoclaved 0.2 mL PCR tube using a 20 µL pipettor, followed by the addition of 5.8 µL master mixture. Hence, the total reaction volume is 20 µL in each tube. After this, all the PCR tubes are centrifuged in the minicentrifuge and placed in the 96-well thermal cycler. Prior to the thermal cycling step, the PCR tubes are kept on ice all the time. The run method used in the thermal cycler is as follows:

a. 1st stage: Incubation at 25°C for 10 minutes
b. 2nd stage: Incubation at 37°C for 2 hours
c. 3rd stage: Incubation at 85°C for 5 minutes
d. 4th stage: Holding stage at 4°C

After completion of the reaction, the prepared cDNA can be used immediately for real-time qPCR of mRNA. Alternatively, it can be stored in 4°C fridge for short term (maximum one week) or in –20°C/–80°C freezer for long term (several months).

3.4.7 RT-qPCR

The process of RT-qPCR is different based on whether it is used for miRNA or mRNA detection and relative quantification. The two distinct methods are as follows:

3.4.7.1 RT-qPCR for miRNA

For the real-time quantitative polymerase chain reaction (RT-qPCR) in each well of a 96-well qPCR plate (VWR catalogue no. 82006-636) to detect and relatively quantify miRNA, the following mixture is prepared:

Table 3.6 – RT-qPCR mixture for miRNA

Component	Stock Solution Concentration [µM]	Required Concentration in 20 µL Reaction Volume [µM]	Required Volume of Stock Solution [µL]
miRNA or U6 Primer	5	1	4
miScript Universal Primer	–	–	4
SYBR Green qPCR Master Mix	–	–	10

When dealing with multiple cDNA samples/reactions at once, the total volume of the reagent mixture should account for 1 – 2 more reactions than the required number. All the necessary components are thawed at room temperature (20 – 25°C) and then kept on ice throughout the whole process. Here, U6 small nuclear RNA is used as the housekeeping gene (QIAGEN catalogue no. MS00033740). The primer assay for the specific miRNA (forward primer) and the miScript Universal Primer (reverse primer) are obtained from QIAGEN (product no. 218300 and 218073, respectively). The VeriQuest SYBR Green qPCR Master Mix is obtained from THERMO FISHER SCIENTIFIC (catalogue no. 756001000RXN).

After adding all the above components into an autoclaved 2 mL microcentrifuge tube, the tube is gently vortexed (for thorough mixing) using a vortex mixer and briefly centrifuged (for retaining residual liquid from the sides of the tube) in a minicentrifuge. From thereon, the reagent mixture is kept on ice. In each well of the 96-well qPCR plate, 2 µL of cDNA sample is added using a 2 µL pipettor (VWR catalogue no. 89079-974), followed by the addition of 18 µL of reagent mixture. Hence, the total reaction volume in each well is 20 µL. Each reaction is set up to have three replicates.

After preparing all the reaction wells, the qPCR plate is covered by an optical adhesive film (THERMO FISHER SCIENTIFIC catalogue no. 4360954) to prevent well-to-well contamination and sample evaporation. Then, to collect the liquid content in each well without bubbles, the qPCR plate is spun at 2500 rpm for 1 minute in a PCR plate spinner (VWR catalogue no. 89184-608). After that, the qPCR plate is placed in the StepOnePlus™ Real-Time PCR System (THERMO FISHER SCIENTIFIC catalogue no. 4376600). The run method used in the PCR system is as follows:

a. Holding (initial activation) stage: Incubation at 95°C for 15 minutes

b. Cycling stage (50 cycles):

    1. Denaturation step: Incubation at 95°C for 15 seconds

    2. Annealing step: Incubation at 55°C for 30 seconds

    3. Extension step: Incubation at 70°C for 30 seconds (real-time fluorescence data are acquired during this step)

c. Melt curve stage:

    1. 1st step: Incubation at 95°C for 15 seconds

    2. 2nd step: Incubation at 60°C for 1 minute

    3. 3rd step: Incremental temperature increase (+ 0.3°C) to 95°C with a holding period of 15 seconds at each increment (real-time fluorescence data are acquired during each temperature increment of this step)

After completion of the RT-qPCR run, the qPCR plate is discarded, and the resulting data (Cycle Threshold or C_t value for each reaction well) are exported from the .eds file (StepOnePlus™ program) to an excel file for further analysis.

3.4.7.2 RT-qPCR for mRNA

For the real-time quantitative polymerase chain reaction (RT-qPCR) in each well of a 96-well qPCR plate to detect and relatively quantify mRNA, the following mixture is prepared:

Table 3.7 – RT-qPCR mixture for mRNA

Component	Stock Solution Concentration [µM]	Required Concentration in 20 µL Reaction Volume [µM]	Required Volume of Stock Solution [µL]
Forward Primer	12.5	2.5	4
Reverse Primer	12.5	2.5	4
SYBR Green qPCR Master Mix	–	–	10

When dealing with multiple cDNA samples/reactions at once, the total volume of the reagent mixture should account for 1 – 2 more reactions than the required number. All the necessary components are thawed at room temperature (20 – 25°C) and then kept on ice throughout the whole process. Here, 18S ribosomal RNA is used as the housekeeping gene. The forward and reverse primers for 18S and all mRNAs of interest are obtained from INTEGRATED DNA TECHNOLOGIES.

After adding all the above components in an autoclaved 2 mL microcentrifuge tube, the tube is gently vortexed (for thorough mixing) using a vortex mixer and briefly centrifuged (for retaining residual liquid from the sides of the tube) in a minicentrifuge. From thereon, the reagent mixture is kept on ice. In each well of the 96-well qPCR plate, 2 µL of cDNA sample and 18 of µL reagent mixture are added. Hence, the total reaction volume in each well is 20 µL. Each reaction is set up to have three replicates.

After preparing all the reaction wells, the qPCR plate is covered by an optical adhesive film to prevent well-to-well contamination and sample evaporation. Then, to collect the liquid content in each well without bubbles, the qPCR plate is spun at 2500 rpm for 1 minute in a PCR plate spinner. After that, the qPCR plate is placed in the StepOnePlusTM Real-Time PCR System. The run method used in the PCR system is as follows:

a. Holding stage:
    1. 1st step: Incubation at 50°C for 2 minutes
    2. 2nd step: Incubation at 95°C for 5 minutes
b. Cycling stage (50 cycles):
    1. Denaturation step: Incubation at 95°C for 3 seconds
    2. Annealing/Extension step: Incubation at 60°C for 30 seconds (real-time fluorescence data are acquired during this step)
c. Melt curve stage:
    1. 1st step: Incubation at 95°C for 15 seconds
    2. 2nd step: Incubation at 60°C for 1 minute
    3. 3rd step: Incremental temperature increase (+ 0.3°C) to 95°C with a holding period of 15 seconds at each increment (real-time fluorescence data are acquired during each temperature increment of this step)

After completion of the qPCR run, the qPCR plate is discarded and the resulting data (Cycle Threshold or Ct value for each reaction well) are exported from the .eds file (StepOnePlusTM program) to an excel file for further analysis.

3.4.7.3 Designing RT-qPCR Primers for mRNA

The forward and reverse primers for a specific mRNA are designed using the NCBI Primer-BLAST website (https://www.ncbi.nlm.nih.gov/tools/primer-blast/). The input values for the most important parameters are listed in the following table:

Table 3.8 – Primer designing protocol for mRNA

Parameter	Value	Comment
Reference Sequence (RefSeq)	Depends on the gene and the species of interest	This is obtained from the NCBI Gene website (https://www.ncbi.nlm.nih.gov/gene)
PCR Product Size	Minimum: 100	–
	Maximum: 200	
Primer Melting Temperature (T_m) [°C]	Minimum: 58.0	–
	Optimum: 60.0	
	Maximum: 62.0	
	Maximum Difference: 2.0	
Exon Junction Span	Primer must span an exon-exon junction	This is the preferable option
	No preference	This is only used when the first option doesn't output any primers
Organism	Pig (*sus scrofa*)	–

Primer Size	Minimum: 18.0	These can be found under the *Advanced Parameters* section of the website
	Optimum: 20.0	
	Maximum: 24.0	
Primer GC Content (%)	Minimum: 30.0	
	Maximum: 80.0	

For all the other parameters, the default values are used. In any case, the designed primer pair is ensured to be specific for the mRNA of interest.

3.4.8 Analysis of RT-qPCR Data

The RT-qPCR data are analyzed using the ΔCT method. First, it is determined whether the standard deviation (SD) of the three C_t values of each sample reaction (housekeeping gene and specific miRNA or mRNA) is less than or equal to 0.5. In case it is higher than 0.5, the C_t value (among the three replicates) causing the high standard deviation is not considered for further analysis. After this, the average values of the three (or two) C_t values for each sample's housekeeping gene and specific miRNA or mRNA reactions are calculated. Next, the miRNA or mRNA expression in each sample is determined using one of the following formulae as appropriate:

$$miRNA\ Expression = 2^{[(Average\ C_t)_{U6} - (Average\ C_t)_{miRNA}]} \ldots\ldots (3.1)$$

$$mRNA\ Expression = 2^{[(Average\ C_t)_{18S} - (Average\ C_t)_{mRNA}]} \ldots\ldots (3.2)$$

To calculate the fold change in miRNA or mRNA expression at a specific experimental condition compared to the reference experimental condition (15% vs. 10%

stretch, for example), the miRNA or mRNA expression values for all samples at the specific and reference conditions are normalized by the average value of the miRNA or mRNA expression in all samples at the reference condition. Hence, this makes the average value of miRNA or mRNA expression at the reference condition 1 and that one at the specific condition some number X, representative of the fold change.

3.5 Statistical Analysis

All the statistical analyses are done using the IBM SPSS Statistics software. Statistically significant difference is achieved when the significance (p) value is less than or equal to 0.05. The first step in comparing two different groups is to check for normality of each data group using the Shapiro-Wilk test. If either one or both groups are not normally distributed ($p \leq 0.05$ in the Shapiro-Wilk test), non-parametric Mann-Whitney U test is used for statistical comparison. On the other hand, if both groups are normally distributed ($p > 0.05$ in the Shapiro-Wilk test), independent samples t-test is used for statistical comparison. In this case, equal variance assumption can be made if Levene's test gives a significance value greater than 0.05.

CHAPTER 4. SPECIFIC AIM 1

4.1 Introduction

It is now well established that the initiation and progression of aortic valve (AV) disease, as characterized by adverse remodeling of extracellular matrix (ECM) and calcification, are regulated in part by hemodynamic forces (Arjunon et al., 2013; Balachandran et al., 2011). These mechanical forces (such as hydrostatic pressure, shear stress, etc.) have been shown to regulate a myriad of mechanosensitive genes in AV (Fernández Esmerats et al., 2016; Holliday et al., 2011; Warnock et al., 2011), including miRNAs.

Elevated cyclic stretch was previously found to induce abnormal ECM remodeling and significant calcification (Ku et al., 2006; Balachandran et al., 2009; Balachandran et al., 2010; Lei et al., 2017). In the recent years, a number of studies have been conducted to identify stretch-responsive miRNAs that regulate cellular processes related to AV pathogenesis, such as miR-148a-3p regulating inflammatory gene expression in aortic valve interstitial cells (Patel et al., 2015). As cyclic stretch is a major biomechanical feature of AV function, these stretch-responsive miRNAs, owing to their regulatory role in modulating gene expression, may possess significant therapeutic potential for the treatment of AV disease.

Recent studies have identified miR-214 as one of the fibrosa-specific and oscillatory shear-induced miRNAs pertinent to AV disease (Rathan et al., 2016). In addition to this, miR-214 was found to be significantly dysregulated in calcified human aortic valves

compared to healthy control (Song et al., 2017; Wang et al., 2017). Therefore, it will be interesting to know whether cyclic stretch modulates miR-214 expression in AV at the physiological and pathological levels.

4.2 Hypothesis

The hypothesis of this specific aim is that pathologically high cyclic stretch can dysregulate the expression of miR-214 in AV tissues.

4.3 Experimental Design

The experimental design used to accomplish the goals of the first specific aim is described in the following sections:

4.3.1 Experimental Conditions

The objective of specific aim 1 was to investigate the effects of physiological and pathological cyclic stretch on miR-214 expression in porcine AV tissues ex vivo. In this study, the physiological level of cyclic stretch was 10%, whereas 15% stretch was used as the pathological level (Balachandran et al., 2010). These two stretch levels of 10% and 15% are representative of the normotensive (Thubrikar, 1989) and hypertensive (Yap et al., 2010) conditions, respectively. Under either stretch level, the AV leaflet tissues were stretched at 60 cycles/minute, which is representative of the normal resting heart rate (60 to 100 beats/minute).

4.3.2 Experimental Duration and Choice of Culture Medium

The following combinations of stretch duration and culture medium were used to study the effect of pathological cyclic stretch (15%) on miR-214 expression at the early and late stages of stretch-induced AV disease:

i. Early stage of abnormal AV remodeling → cyclic stretching at 15% in regular medium for 48 hours (in comparison to 10% stretch)
ii. Late stage of AV calcification → cyclic stretching at 15% in osteogenic medium for 1 week (in comparison to 10% stretch)

To simulate the early, abnormal remodeling stage in AV disease compared to the normal counterpart, porcine AV tissue samples were cyclically stretched at 15% (pathological) and 10% (physiological) for 48 hours in regular culture medium. This specific combination of stretch duration (48 hours) and culture medium (regular) was previously shown to induce significant change in ECM remodeling at 15% stretch compared to 10% (Balachandran et al., 2009). However, no significant calcification of AV tissues was observed under these conditions.

On the other hand, the late stage of AV calcification was simulated by cyclically stretching AV leaflet tissues at 15% for one week in osteogenic culture medium. As usual, cyclic stretching at 10% under the same experimental conditions represented the physiological counterpart. The results from these experiments showed that quantitatively, AV calcification is (at least) two-fold higher at 15% stretch compared to 10% in a statistically significant manner (as shown in Figure 4.1).

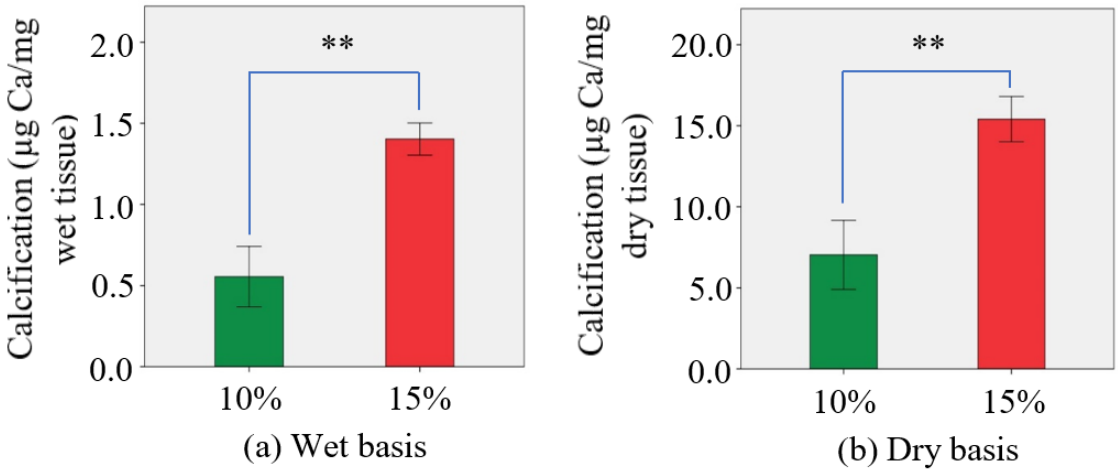

Figure 4.1 – Quantitative assessment of AV calcification resulting from cycling stretching of porcine AV tissues in osteogenic medium for 1 week (n = 6; ** p < 0.01). Data are presented as mean ± standard error of mean.

In addition to these, Alizarin Red and Von Kossa stains (histological stains used for detecting calcification or mineralization) of frozen tissue sections from the above

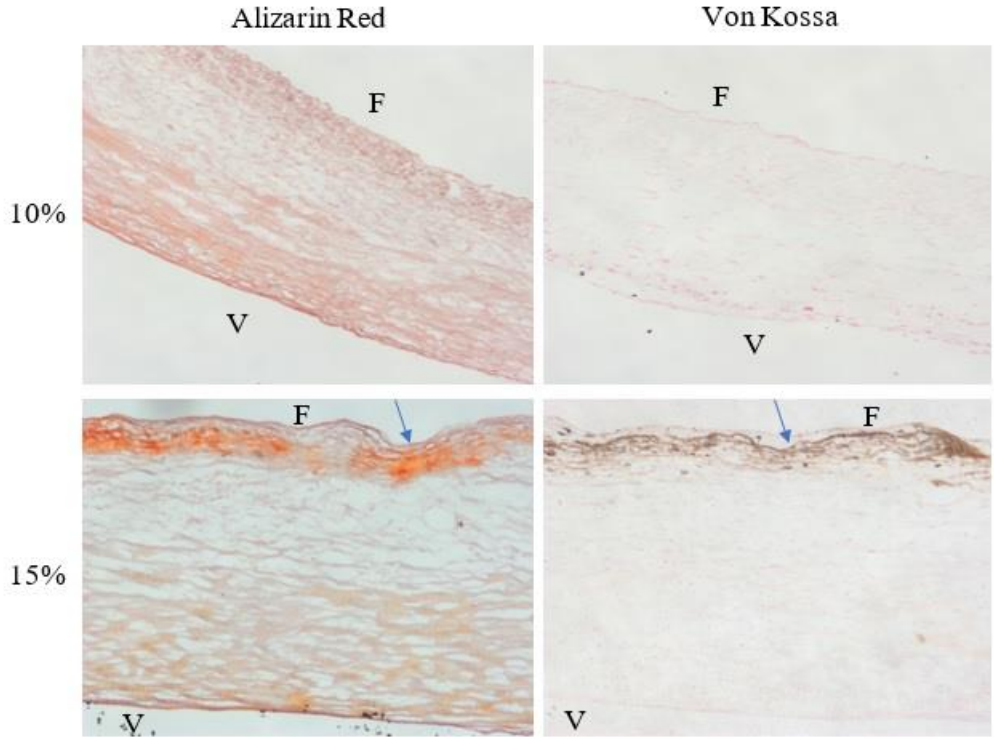

Figure 4.2 – Qualitative assessment of AV calcification resulting from cycling stretching of porcine AV tissues in osteogenic medium for 1 week (F = Fibrosa, V = Ventricularis). Arrows indicate sites of calcification.

experiments showed the same qualitative results, as depicted in Figure 4.2. It should also be noted that under the pathological cyclic stretch (15%), calcification occurred preferentially on the fibrosa side of AV leaflet, which is the scenario in a calcified human aortic valve (Freeman et al., 2005; Chen et al., 2011; Rajamannan et al., 2011).

Previously, it was shown that when porcine AV tissues were cyclically stretched at 15% in osteogenic medium for two weeks, there was an almost six-fold increase in calcification compared to 10% stretch (Balachandran et al., 2010). However, due to the possibility of significant RNA degradation under longer culture duration, stretch experiments with osteogenic medium were kept limited to a culture duration of one week in this study.

4.3.3 Pairing of Stretch Experiments

Two identical stretch bioreactor systems were used to run 10% and 15% stretch experiments in a pairwise fashion using porcine AV tissues harvested on the same day. This ruled out the effect of day-to-day variability in freshly collected tissues on the tissues' biological responses under 10% and 15% stretch.

4.3.4 Sample Pooling

For assessing the mRNA expression of ATF4, CHOP and BCL2L1 genes using real-time quantitative polymerase chain reaction (RT-qPCR), two stretched tissue samples (either 10% or 15%) were randomly pooled into one qPCR sample to increase the resulting total RNA concentration. So, for example, if 16 tissue samples were obtained from each of

the 10% and 15% stretch experiments, the resulting sample size after pooling equaled to 8 for each case.

4.4 Evaluation of miR-214 Expression

The expression of miR-214 in stretched AV tissue samples was evaluated using RT-qPCR. Here, U6 small nuclear RNA (snRNA) was used as the housekeeping gene. The following sections outline the results from RT-qPCR evaluation of miR-214 expression in porcine AV tissue samples from 2-day stretch experiments in regular medium (early stage) and 7-day stretch experiments in osteogenic medium (late stage).

4.4.1 miR-214 Expression in 2-Day Stretch Experiment with Regular Medium

For the first part of specific aim 1, freshly obtained porcine AV leaflet tissues were cyclically stretched at 10% and 15% in regular medium for 48 hours, as described earlier. Higher cyclic stretch (15%) in normal culture environment represented the abnormal

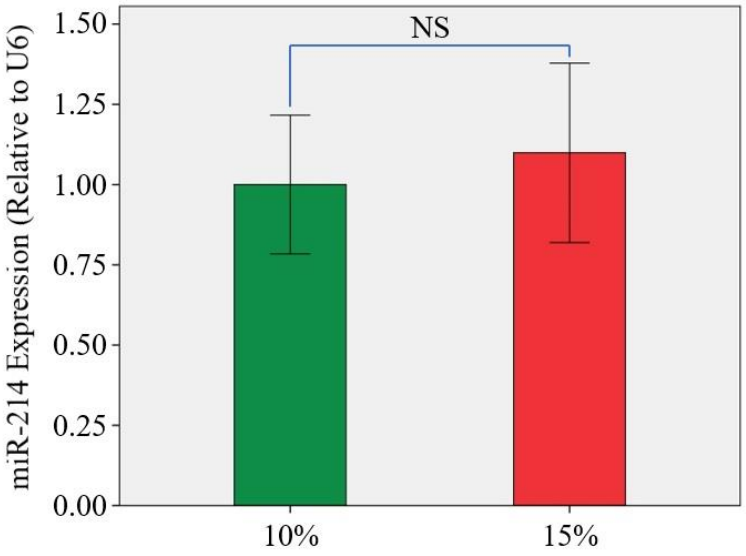

Figure 4.3 – miR-214 expression in porcine AV tissues after cycling stretching in regular medium for 48 hours (n = 8; NS = non-significant). Data are presented as mean ± standard error of mean.

remodeling (early) stage of AV disease, whereas 10% stretch served as the physiological counterpart. After completion of the stretch experiments, the expression of miR-214 (relative to U6) was evaluated in the stretched tissue samples using RT-qPCR. As seen in Figure 4.3, there is no statistically significant difference in miR-214 expression ($p = 0.784$) between 10% and 15% stretch. This may indicate that the early stage of adverse AV remodeling induced by elevated cyclic stretch does not evoke a significant change in miR-214 expression.

4.4.2 miR-214 Expression in 7-Day Stretch Experiment with Osteogenic Medium

For the second part of specific aim 1, freshly obtained porcine AV leaflet tissues were cyclically stretched at 10% and 15% in osteogenic medium for one week, as described earlier. Higher cyclic stretch (15%) in osteogenic culture environment represented the calcification (late) stage of AV disease, whereas 10% stretch served as the physiological counterpart. After completion of the stretch experiments, the expression of miR-214

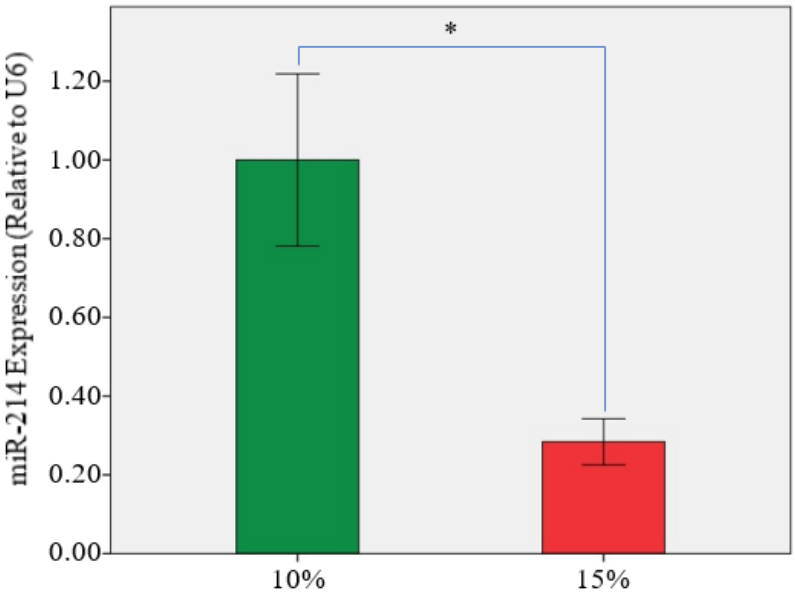

Figure 4.4 – miR-214 expression in porcine AV tissues after cycling stretching in osteogenic medium for 1 week (n = 9 – 10; * $p < 0.05$). Data are presented as mean ± standard error of mean.

(relative to U6) was evaluated in the stretched tissue samples using RT-qPCR. As shown in Figure 4.4, miR-214 expression is significantly downregulated at 15% stretch compared to 10%. This may point toward a potentially negative correlation between miR-214 expression and stretch-induced calcification in the late stage of AV disease.

4.5 Summary of miR-214 RT-qPCR Results

Porcine AV tissues were cyclically stretched for 48 hours in regular medium and for 1 week in osteogenic medium to approximate the early remodeling and late calcification stages of AV disease, respectively. The expression of miR-214 was then evaluated in the resulting tissue samples using RT-qPCR. Figure 4.5 summarizes the RT-qPCR results for

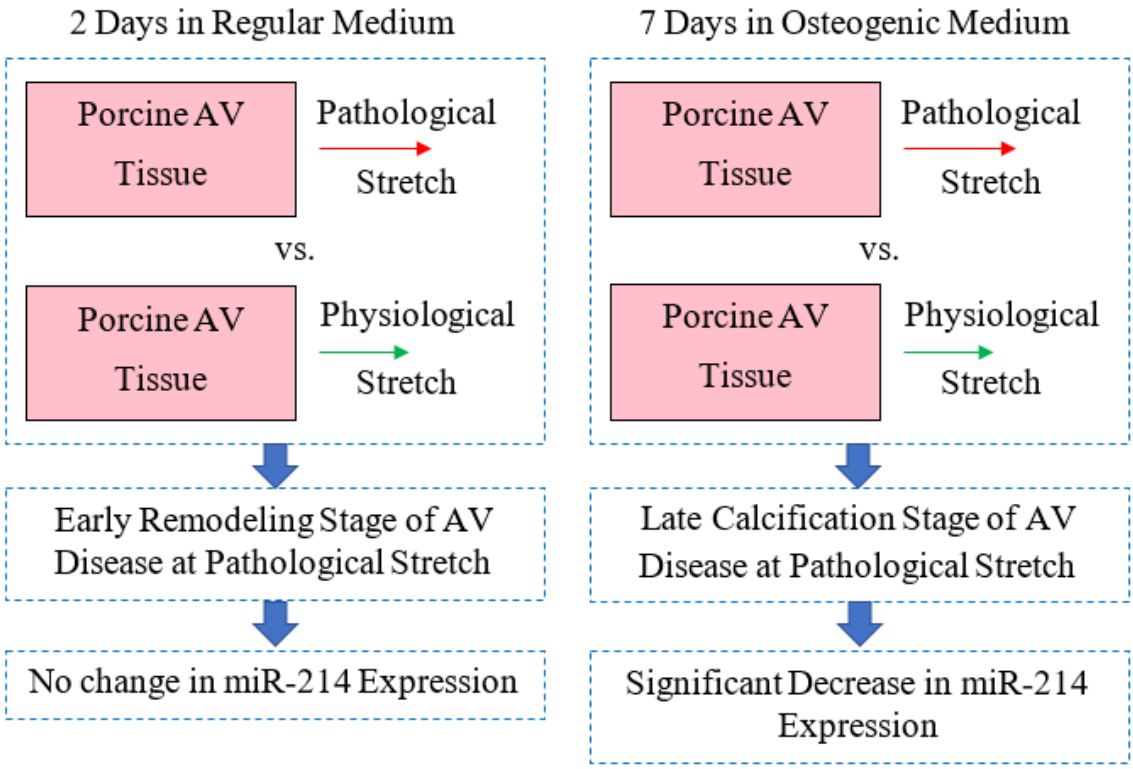

Figure 4.5 – Summary of results for specific aim 1

miR-214 expression. Stretch-induced early AV remodeling did not cause significantly different expression of miR-214. However, it is quite interesting to observe significantly

downregulated expression of miR-214 under conditions of stretch-induced AV calcification. Similar downregulation of miR-214 expression was also found in calcified human aortic valves compared to healthy control (Song et al., 2017; Wang et al., 2017). These observations, in turn, imply a protective role of miR-214 in AV disease and loss of miR-214 is potentially associated with stretch-induced AV calcification.

CHAPTER 5. SPECIFIC AIM 2

5.1 Introduction

Activating Transcription Factor 4 (ATF4) is a major component of the PRKR-Like Endoplasmic Reticulum Kinase (PERK)-Eukaryotic Translation Initiation Factor 2α (eIF2α) signaling pathway, which is one of the three endoplasmic reticulum (ER) stress pathways (Hetz, 2012; Ron et al., 2007). These pathways significantly regulate cellular processes like apoptosis (Puthalakath et al., 2007), autophagy (Kouroku et al., 2006), inflammation (Garg et al., 2012), etc. Interestingly, ER stress has been shown to promote calcification in AV, in which the PERK-eIF2α-ATF4 signaling pathway plays a major role (Cai et al., 2013; Wang et al., 2017).

Mechanical stretch has been found to promote inflammation and apoptosis in smooth muscle cells via induction of ER stress (Jia et al., 2015). Under ER stress, both transcription and translation of ATF4 are increased, resulting in cell death situations via upregulation of C/EBP-Homologous Protein (CHOP) expression (Dey et al., 2010; Han et al., 2013).

Interestingly, ATF4 has been shown to promote mineralization in vascular smooth muscle cells (Masuda et al., 2013; Masuda et al., 2016), osteoblasts (Saito et al, 2011; Xiao et al., 2005), mesenchymal stem cells (Zhou et al., 2016; Yu et al., 2013), etc. It was also found that ATF4 can evoke the expression of osteoblast-specific genes in non-osteoblastic cells (Yang et al., 2004). On the other hand, CHOP has been shown to have a potentially repressive effect on the expression of pro-survival gene BCL2L1 under apoptotic conditions (Noh et al., 2015; Gaudette et al., 2014).

The following diagram shows a linear path of interactions among ATF4, CHOP and BCL2L1 genes under stress conditions, which is adapted from the Apoptosis pathway of the Kyoto Encyclopedia of Genes and Genomes (KEGG) database:

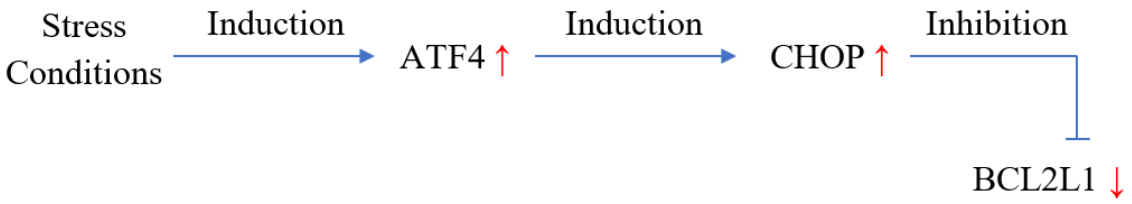

Figure 5.1 – ATF4/CHOP/BCL2L1 pathway.

Since ATF4 has been experimentally validated to be a target of miR-214 in several recent studies (Wang et al., 2013; Li et al., 2015), it will be interesting to see how cyclic stretch modulates the expression of ATF4/CHOP/BCL2L1 genes in AV at the physiological and pathological levels.

5.2 Hypothesis

The hypothesis of this specific aim is that pathologically high cyclic stretch can dysregulate the expression of ATF4, CHOP and BCL2L1 genes in AV tissues.

The anticipated effects of pathological cyclic stretch on these genes are depicted in the following figure:

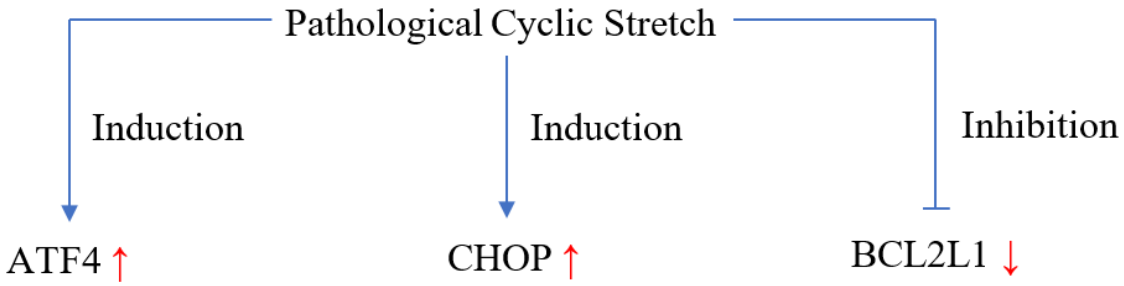

Figure 5.2 – Predicted effects of pathological cyclic stretch on ATF4, CHOP and BCL2L1 genes.

5.3 Experimental Design

The experimental design used to accomplish the goals of the second specific aim is described in the following sections:

5.3.1 Experimental Conditions

The objective of specific aim 2 was to investigate the effects of physiological and pathological cyclic stretch on the mRNA expression of ATF4, CHOP and BCL2L1 genes in porcine AV tissues ex vivo. Therefore, as described in specific aim 1, 10% and 15% were used as the physiological and pathological level of cyclic stretch, respectively and AV leaflet tissues were stretched at 60 cycles/minute under either stretch level.

5.3.2 Experimental Duration and Choice of Culture Medium

As described in specific aim 1, the following combinations of stretch duration and culture medium were used to study the effect of pathological cyclic stretch (15%) on ATF4, CHOP and BCL2L1 genes at the early and late stages of stretch-induced AV disease:

i. Early stage of abnormal AV remodeling → cyclic stretching at 15% in regular medium for 48 hours (in comparison to 10% stretch)
ii. Late stage of AV calcification → cyclic stretching at 15% in osteogenic medium for 1 week (in comparison to 10% stretch)

5.3.3 Pairing of Stretch Experiments

Similar to specific aim 1, two identical stretch bioreactor systems were used to run 10% and 15% stretch experiments in a pairwise fashion using porcine AV tissues harvested

on the same day. This ruled out the effect of day-to-day variability in freshly collected tissues on the tissues' biological responses under 10% and 15% stretch.

5.3.4 Sample Pooling

For assessing the mRNA expression of ATF4, CHOP and BCL2L1 genes using real-time quantitative polymerase chain reaction (RT-qPCR), two stretched tissue samples (either 10% or 15%) were randomly pooled into one qPCR sample to increase the total RNA concentration. So, for example, if 16 tissue samples were obtained from each of the 10% and 15% stretch experiments, the resulting sample size after pooling equaled to 8 for each case.

5.3.5 Primer Sequences for mRNA qPCR

The following table outlines the primer sequences of 18S (housekeeping gene), ATF4, CHOP and BCL2L1 that were used in RT-qPCR. As described in the Methods chapter, the primer pair for each mRNA was designed to be specific for the gene and species (pig) in question.

Table 5.1 – Primer sequences for mRNA qPCR

mRNA	Forward Primer (5'→3')	Reverse Primer (5'→3')
18S	AGGAATTGACGGAAGGGCACCA	GTGCAGCCCCGGACATCTAAG
ATF4	AGTCCTTTTCTGCGAGTGGG	GAGAAGCGCCATGGCCTAAG
CHOP	CCCTGGAAATGAGGAGGAGTC	TGACTGGAATCAGGCGAGTG
BCL2L1	TGACCACCTAGAGCCTTGGA	CGTCAGGAACCATCGGTTGA

5.4 Evaluation of ATF4, CHOP and BCL2L1 mRNA Expression

The mRNA expression of ATF4, CHOP and BCL2L1 genes in stretched AV tissue samples was evaluated using RT-qPCR. As mentioned previously, 18S ribosomal RNA (rRNA) was used as the housekeeping gene. The following sections outline the results from RT-qPCR evaluation of these mRNAs in porcine AV tissue samples from 2-day stretch experiments in regular medium (early stage) and 7-day stretch experiments in osteogenic medium (late stage).

5.4.1 mRNA Expression in 2-Day Stretch Experiment with Regular Medium

For the first part of specific aim 2, freshly obtained porcine AV leaflet tissues were cyclically stretched at 10% and 15% in regular medium for 48 hours, as described earlier. Higher cyclic stretch (15%) in normal culture environment represented the abnormal remodeling (early) stage of AV disease, whereas 10% stretch served as the physiological

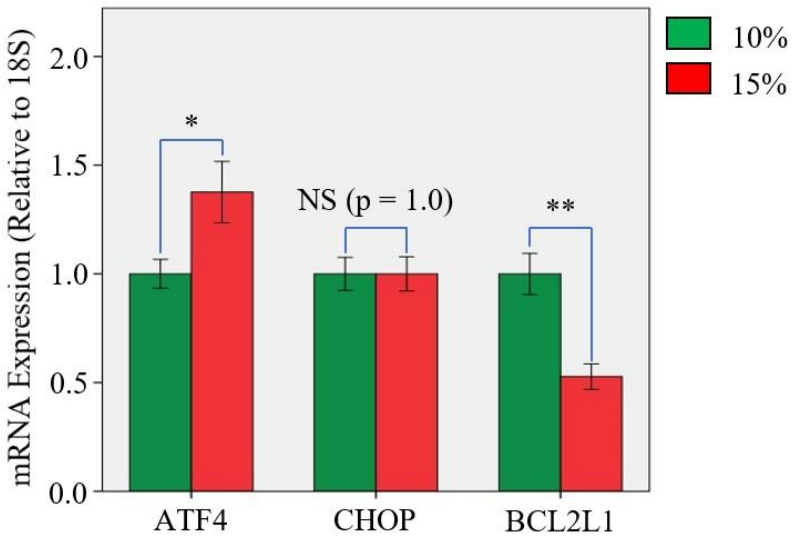

Figure 5.3 – ATF4, CHOP and BCL2L1 mRNA expression in porcine AV tissues after cyclic stretching for 48 hours in regular medium (n = 7 – 8; * p < 0.05; ** p < 0.01; NS = non-significant). Data are presented as mean ± standard error of mean.

counterpart. After completion of the stretch experiments, the expression of ATF4, CHOP and BCL2L1 mRNA (relative to 18S) was evaluated in the stretched tissue samples using RT-qPCR.

As seen in Figure 5.3, ATF4 expression is significantly increased (by 38%) and BCL2L1 expression is significantly decreased (by 47%) at 15% stretch compared to the ones at 10%. However, there is no statistically significant difference (0%) in CHOP expression between 10% and 15% stretch. These may indicate that the early stage of adverse AV remodeling induced by elevated cyclic stretch evokes a significant change in ATF4 and BCL2L1 expression toward the expected trend (increasing and decreasing, respectively). Nonetheless, this increased expression of ATF4 does not cause any significant increase in CHOP expression at 15% stretch compared to 10%.

5.4.2 mRNA Expression in 7-Day Stretch Experiment with Osteogenic Medium

For the second part of specific aim 2, freshly obtained porcine AV leaflet tissues were cyclically stretched at 10% and 15% in osteogenic medium for one week, as described earlier. Higher cyclic stretch (15%) in osteogenic culture environment represented the calcification (late) stage of AV disease, whereas 10% stretch served as the physiological counterpart. After completion of the stretch experiments, the expression of ATF4, CHOP and BCL2L1 mRNA (relative to 18S) was evaluated in the stretched tissue samples using qPCR.

As seen in Figure 5.4, there is 115% increase in ATF4 expression and 53% decrease in BCL2L1 expression at 15% stretch compared to 10%, which are of similar trends to those from 2-day stretch experiments in regular medium. However, these changes in ATF4

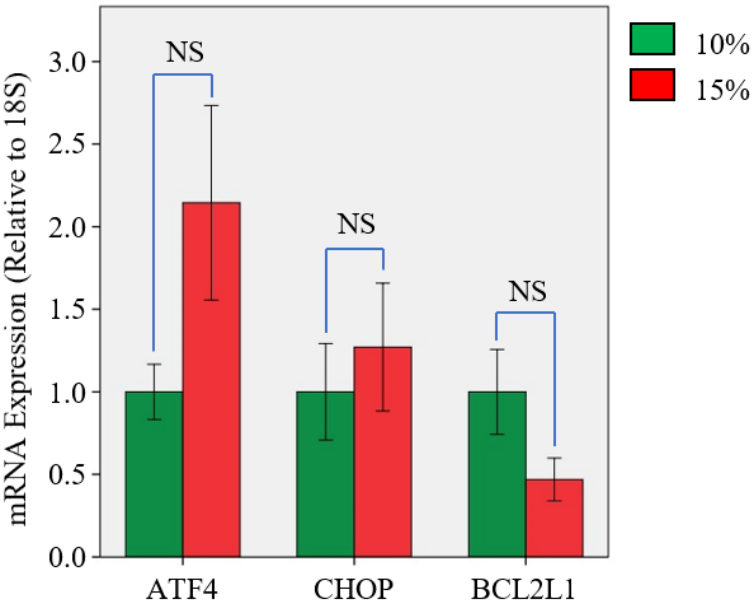

Figure 5.4 – ATF4, CHOP and BCL2L1 mRNA expression in porcine AV tissues after cyclic stretching for 1 week in osteogenic medium (n = 7 – 8; NS = non-significant). Data are presented as mean ± standard error of mean.

and BCL2L1 expression were not statistically significant (corresponding p-values are 0.098 and 0.094, respectively). Additionally, the 27% increase in CHOP expression at 15% stretch compared to 10% was statistically non-significant (p = 0.595). These may indicate that AV calcification induced by elevated cyclic stretch in these experiments (approximating the late stage of AV disease) evokes similar trends in ATF4, CHOP and BCL2L1 expression compared to those in 2-day stretch experiments in regular medium.

5.5 Summary of mRNA RT-qPCR Results

Porcine AV tissues were cyclically stretched for 48 hours in regular medium and for 1 week in osteogenic medium to approximate the early remodeling and late calcification stages of stretch-induced AV disease, respectively. The mRNA expression of ATF4, CHOP and BCL2L1 genes was then evaluated in the resulting tissue samples using RT-

qPCR. It was anticipated that elevated cyclic stretch would significantly upregulate ATF4 and CHOP expression and downregulate BCL2L1 expression in AV tissues.

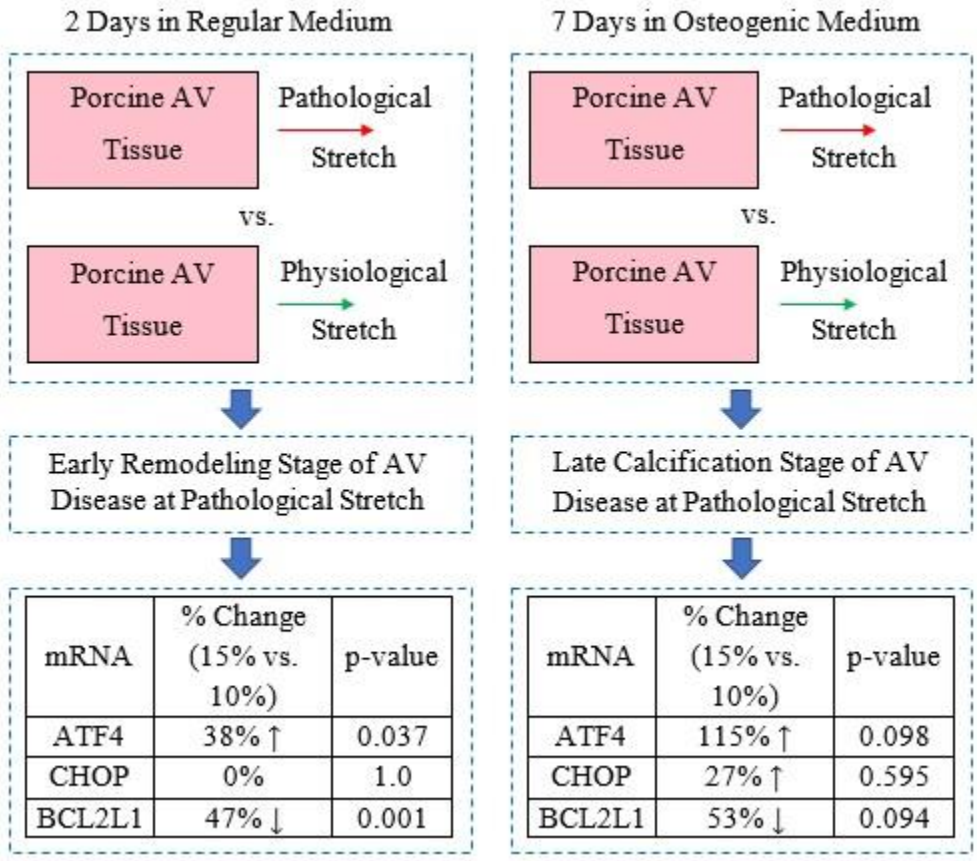

mRNA	% Change (15% vs. 10%)	p-value
ATF4	38% ↑	0.037
CHOP	0%	1.0
BCL2L1	47% ↓	0.001

mRNA	% Change (15% vs. 10%)	p-value
ATF4	115% ↑	0.098
CHOP	27% ↑	0.595
BCL2L1	53% ↓	0.094

Figure 5.5 – Summary of results for specific aim 2.

RT-qPCR results, as summarized in Figure 5.5, showed that stretch-induced early AV remodeling was associated with significant upregulation of ATF4 expression and significant downregulation of BCL2L1 expression. However, there was zero change in CHOP expression between 10% and 15% stretch. Under the condition of stretch-induced AV calcification, mRNA expression of ATF4, CHOP and BCL2L1 genes showed identical trends, although statistically non-significant. Similar upregulation of ATF4 expression was also found in calcified human aortic valves compared to healthy control (Wang et al., 2017), whereas downregulation of BCL2L1 expression was observed in fibrosa-specific human aortic valve endothelial cells (HAVECs) under oscillatory shear flow compared to

pulsatile shear flow (Holliday et al., 2011). These results may underlie the possible association of dysregulated ATF4 and BCL2L1 mRNA expression with the stretch-induced pathogenesis of AV disease.

CHAPTER 6. SPECIFIC AIM 3

6.1 Introduction

As described in the Specific Aim 2 chapter, ATF4 is a major component of the PERK-eIF2α signaling pathway, which is one of the three ER stress pathways (Hetz, 2012; Ron et al., 2007). ATF4 was found to promote osteogenesis in different types of cells, such as vascular smooth muscle cells (Masuda et al., 2016), osteoblasts (Saito et al, 2011), etc. Interestingly, several experimental studies have previously validated ATF4 as a target of miR-214 (Wang et al., 2013; Li et al., 2015). Especially, the study by Wang et al. (2013) showed that miR-214 inhibits bone formation by targeting ATF4. Studies by Zhao et al. (2015) and Li et al. (2016) pointed out the disrupting effect of miR-214 on bone homeostasis by promotion of osteoclastogenesis and consequent increase in bone resorption. Considering the facts that ER stress promotes AV calcification (Cai et al., 2013) and AV calcification is highly similar to the bone formation process (Rajamannan et al., 2003), it won't be surprising if miR-214 is found to have an inhibiting effect on AV calcification via downregulation of ATF4 expression.

On the other hand, CHOP, which is one of the downstream targets of ATF4, has been shown to promote cell apoptosis (Oyadomari et al., 2004). It is well known that increased apoptosis is associated with AV calcification (Jian et al., 2003; Rajamannan et al., 2011). CHOP can promote apoptosis by indirectly repressing the expression of pro-survival gene BCL2L1 (Noh et al., 2015). Therefore, miR-214 overexpression has the potential to suppress cellular apoptosis in AV disease by indirectly repressing CHOP expression via inhibition of ATF4 expression.

ATF4 is also known to transcriptionally regulate the expression of osteocalcin (BGLAP) (Lian et al., 2009; Yang et al., 2004), which is associated with an osteoblast phenotype. Since osteocalcin (BGLAP) is highly expressed in human calcified aortic valve (Rajamannan et al., 2003), miR-214 overexpression has the potential to suppress AV calcification by indirectly repressing BGLAP expression via inhibition of ATF4 expression. The following diagram outlines the altered expression of ATF4, CHOP, BCL2L1 and BGLAP genes in AV calcification:

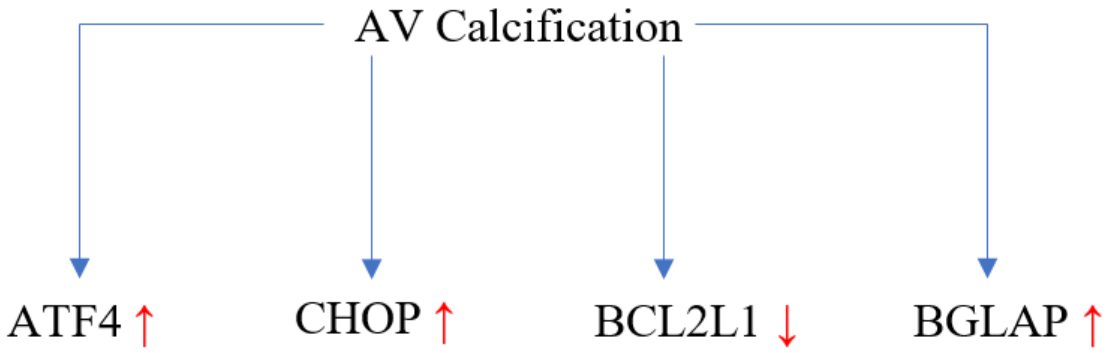

Figure 6.1 – ATF4, CHOP, BCL2L1 and BGLAP expression in AV calcification.

Hence, this specific aim focuses on evaluating the effect of miR-214 overexpression on the mRNA expressions of ATF4, CHOP, BCL2L1 and BGLAP genes, thereby elucidating this miRNA's role in apoptosis and calcification of AV tissues.

6.2 Hypothesis

The hypothesis of this specific aim is that miR-214 overexpression can downregulate the expression of ATF4, CHOP and BGLAP genes and upregulate the expression of BCL2L1 gene in AV tissues.

The anticipated effects of miR-214 overexpression on these genes are depicted in the following figure:

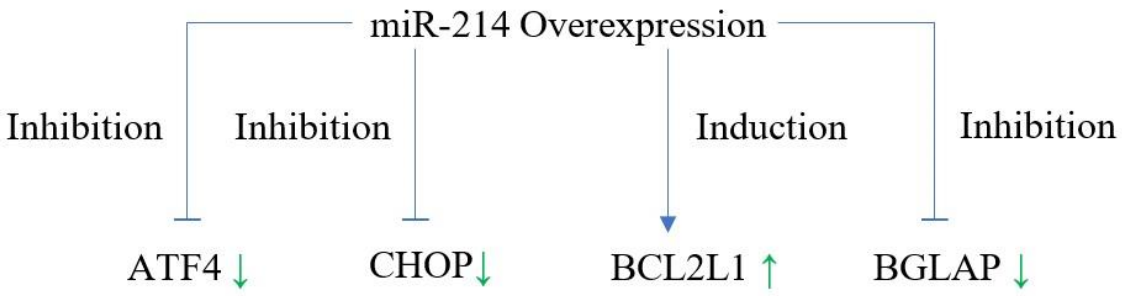

Figure 6.2 – Predicted effects of miR-214 overexpression on ATF4, CHOP, BCL2L1 and BGLAP genes

6.3 Experimental Design

The experimental design used to accomplish the goals of the third specific aim is described in the following sections:

6.3.1 Experimental Conditions

The objective of specific aim 3 was to investigate the effect of miR-214 overexpression on the mRNA expression of ATF4, CHOP, BCL2L1 and BGLAP genes. For this purpose, porcine AV tissues were transfected with negative control mimic and miR-214 mimic in static cultures. Static cultures were used to facilitate the most efficient transfection of AV tissues and consequent effect on mRNA expression with the mimics. As described in the Methods chapter, the final concentrations of both negative control mimic and miR-214 mimic in the static culture medium were 50 nM.

6.3.2 Experimental Duration and Choice of Culture Medium

The above mentioned static transfection experiments were carried out for 48 hours in osteogenic culture medium. A culture duration of 48 hours was deemed to be sufficient for the mimics to have significant effects (if any) on the mRNA expression of the genes of

interest. On the other hand, osteogenic culture medium was used in these experiments to promote a calcific environment for the cultured AV tissues.

6.3.3 Pairing of Transfection Experiments

Static transfection experiments with negative control mimic and miR-214 mimic were run in a pairwise fashion using porcine AV tissues harvested on the same day. This ruled out the effect of day-to-day variability in freshly collected tissues on the tissues' biological responses under static transfection with negative control and miR-214 mimics.

6.3.4 Sample Pooling

The total RNA yield from each tissue sample was quite high (total RNA concentration $\geq$ 100 ng/μL) for these static transfection experiments. Therefore, no sample pooling was deemed necessary.

6.3.5 Primer Sequences for mRNA RT-qPCR

The following table outlines the primer sequences of 18S (housekeeping gene), ATF4, CHOP, BCL2L1 and BGLAP that were used in real-time quantitative polymerase chain reaction (RT-qPCR). As described in the Methods chapter, the primer pair for each mRNA was designed to be specific for the gene and species (pig) in question.

Table 6.1 – Primer sequences for mRNA qPCR

mRNA	Forward Primer (5'→3')	Reverse Primer (5'→3')
18S	AGGAATTGACGGAAGGGCACCA	GTGCAGCCCCGGACATCTAAG
ATF4	AGTCCTTTTCTGCGAGTGGG	GAGAAGCGCCATGGCCTAAG
CHOP	CCCTGGAAATGAGGAGGAGTC	TGACTGGAATCAGGCGAGTG
BCL2L1	TGACCACCTAGAGCCTTGGA	CGTCAGGAACCATCGGTTGA
BGLAP	AAAGGTGCAGCCTTCGTGT	AAGCCGATGTGATCAGCCAG

6.4 Evaluation of miR-214 and mRNA Expression

The expression of miR-214 and mRNAs (ATF4, CHOP, BCL2L1 and BGLAP) in statically transfected AV tissue samples was evaluated using RT-qPCR. Here, U6 small nuclear RNA (snRNA) and 18S ribosomal RNA (rRNA) were used as the housekeeping genes for miRNA and mRNA RT-qPCR, respectively. The following sections outline the results from RT-qPCR evaluation of miR-214 and mRNA expression in porcine AV tissue samples from static transfection experiments in osteogenic medium.

6.4.1 Evaluation of miR-214 Expression

Freshly obtained porcine AV leaflet tissues were statically cultured in osteogenic medium for 48 hours in the presence of negative control mimic and miR-214 mimic separately, as described earlier. Static transfection with miR-214 mimic at a final concentration of 50 nM represented the miR-214 overexpression case, whereas the one with negative control mimic at the same final concentration served as the control case.

After completion of the transfection experiments, the expression of miR-214 (relative to U6) was evaluated in the statically cultured tissue samples using RT-qPCR.

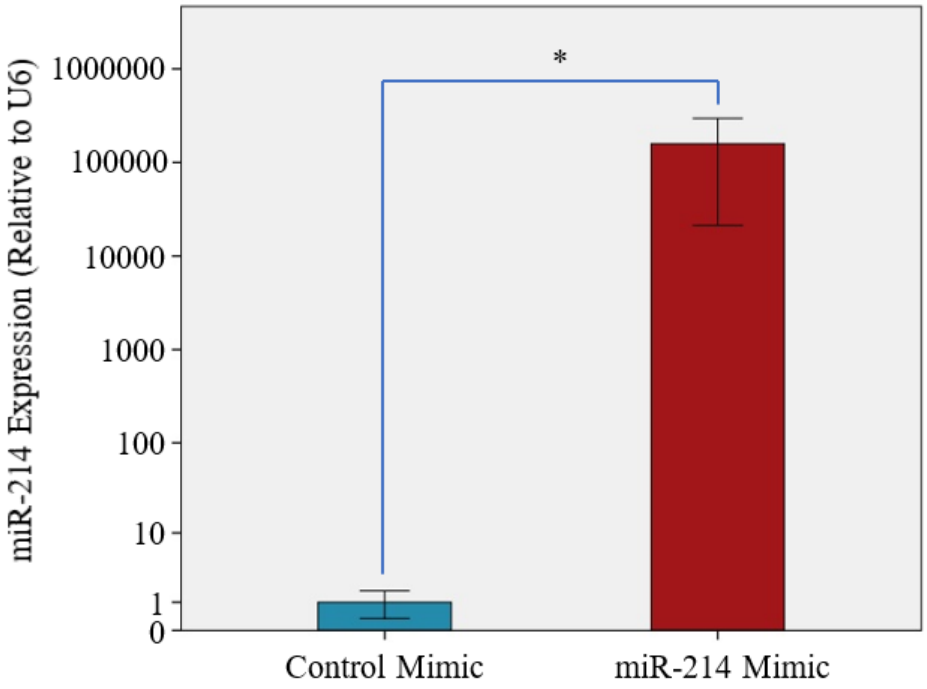

Figure 6.3 – miR-214 expression in porcine AV tissues after static transfection for 48 hours in osteogenic medium (n = 4; * p < 0.05). Data are presented as mean ± standard error of mean.

As seen in Figure 6.3, static transfection with miR-214 mimic resulted in significantly higher expression of miR-214 (more than 100,000-fold increase) in AV leaflet tissues compared to the control mimic case. This, in turn, indicates that the static transfection protocol (as described in the Methods chapter) was proved to be effective in overexpressing miR-214 in porcine AV tissues.

6.4.2 Evaluation of mRNA Expression

Freshly obtained porcine AV leaflet tissues were statically cultured in osteogenic medium for 48 hours in the presence of negative control mimic and miR-214 mimic separately, as described earlier. Static transfection with miR-214 mimic at a final

concentration of 50 nM represented the miR-214 overexpression case, whereas the one with negative control mimic at the same final concentration served as the control case. After completion of the transfection experiments, the mRNA expression of ATF4, CHOP, BCL2L1 and BGLAP genes (relative to 18S) was evaluated in the statically cultured tissue samples using RT-qPCR.

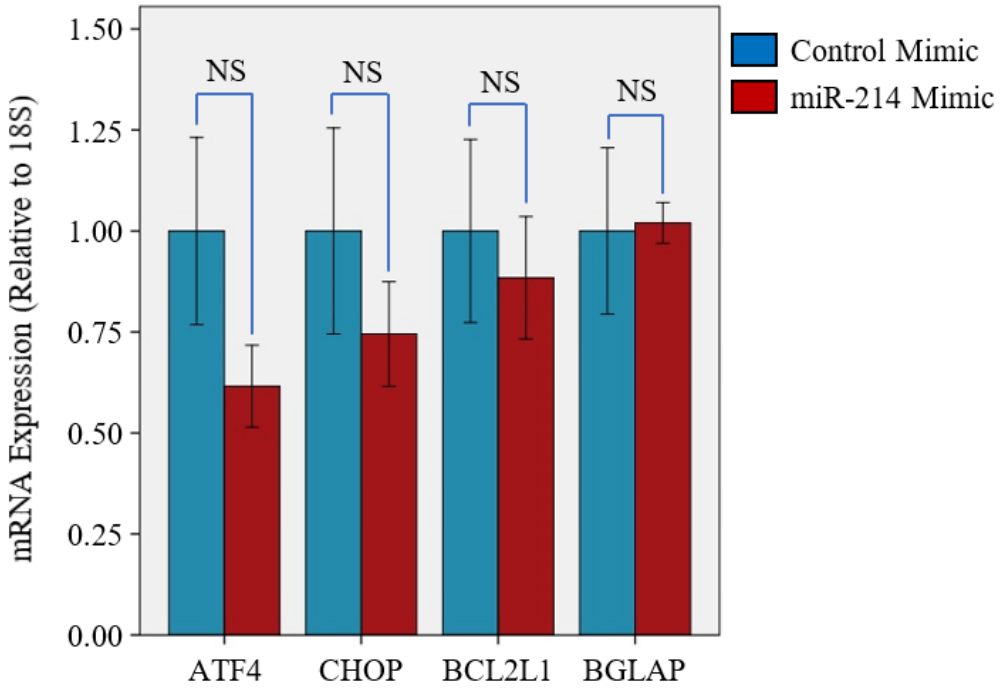

Figure 6.4 – ATF4, CHOP, BCL2L1 and BGLAP mRNA expression in porcine AV tissues after static transfection for 48 hours in osteogenic medium (n = 7 – 8; NS = non-significant). Data are presented as mean ± standard error of mean.

As seen in Figure 6.4, static transfection with miR-214 mimic resulted in 38%, 25% and 12% decrease in mRNA expression of ATF4, CHOP and BCL2L1 genes, respectively, compared to the control mimic cases. However, none of these differences were statistically significant (p-values for ATF4, CHOP and BCL2L1 genes were 0.161, 0.396 and 0.678, respectively). On the other hand, the mRNA expressions of BGLAP remained practically the same between the control mimic and miR-214 mimic cases. These decreases in ATF4 and CHOP expression strengthen the notion that miR-214 overexpression may have an

inhibiting effect on these mRNAs in AV tissues. Nonetheless, these did not result into a downregulation of BGLAP expression with miR-214 mimic. Interestingly, the 12% decrease in average BCL2L1 expression upon miR-214 overexpression is contrary to the prediction that CHOP may negatively regulate the expression of BCL2L1.

6.5 Summary of RT-qPCR Results from Transfection Experiments

Porcine AV tissues were statically cultured for 48 hours in osteogenic medium with negative control mimic and miR-214 mimic separately. The expression of miR-214 as well as those of ATF4, CHOP, BCL2L1 and BGLAP mRNAs were then evaluated using RT-qPCR. It was anticipated that miR-214 overexpression would significantly downregulate ATF4, CHOP and BGLAP expression and upregulate BCL2L1 expression in AV tissues.

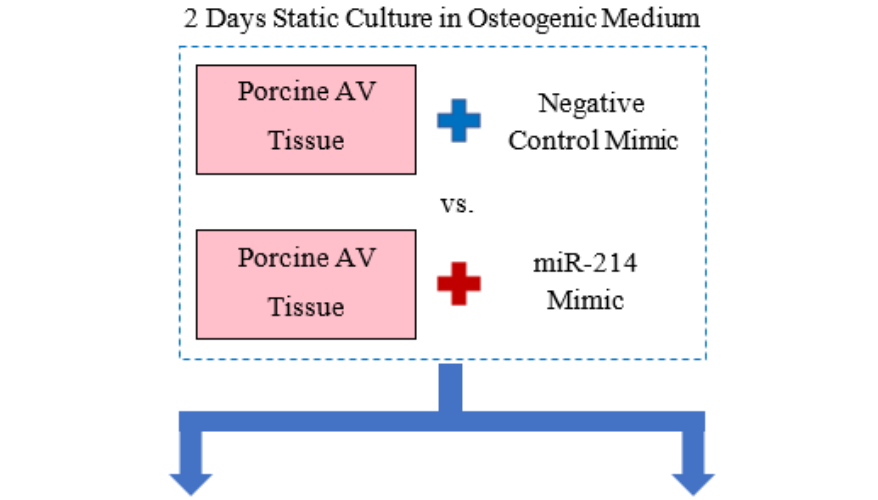

mRNA	% Change (miR-214 mimic vs. control mimic)	p-value
ATF4	38%↓	0.161
CHOP	25%↓	0.396
BCL2L1	12%↓	0.678
BGLAP	2%↑	0.928

Figure 6.5 – Summary of results for specific aim 3.

RT-qPCR results (Figure 6.5) showed that static transfection with miR-214 mimic caused significant upregulation of miR-214 expression in porcine AV tissues compared to the control mimic case. miR-214 overexpression resulted in 38%, 25% and 12% decrease in mRNA expression of ATF4, CHOP and BCL2L1 genes with no statistical significance. On the other hand, BGLAP expressions were found to be effectively the same between the control mimic and miR-214 mimic cases. These observations may underlie the possible inhibiting effect of miR-214 on the ATF4/CHOP pathway in AV tissues, thereby indicating this miRNA's potentially protective role in AV disease.

CHAPTER 7. DISCUSSIONS

7.1 Discussion of Specific Aim 1 Results

As described in Specific Aim 1 chapter, 2-day 15% stretch in regular medium, which represents stretch-induced early remodeling stage of AV disease, did not exhibit statistically significant difference in miR-214 expression compared to the physiological counterpart (2-day 10% stretch in regular medium). However, 7-day 15% stretch in osteogenic medium, which represents stretch-induced late calcification stage of AV disease, showed statistically significant decrease in miR-214 expression compared to the physiological counterpart (7-day 10% stretch in osteogenic medium). The possible reasons behind these results are discussed in the following sections:

7.1.1 Why didn't miR-214 expression significantly change at the stretch-induced early remodeling stage of AV disease?

It is intriguing to observe no significant change in miR-214 expression at the stretch-induced early remodeling stage of AV disease (2-day 15% stretch in regular medium) compared to the physiological counterpart (2-day 10% stretch in regular medium). miR-214 transcription is positively regulated by TWIST1, a basic helix-loop-helix (bHLH) transcription factor (Lee et al., 2009). TWIST1 expression was previously shown to be induced by TIMP1 (Tissue Inhibitor of Metalloproteinases 1) (D'Angelo et al., 2014). TIMP1, along with MMP2 (Matrix Metalloproteinase 2), are major indicators of adverse extracellular matrix (ECM) remodeling in AV disease (Kaden et al., 2004; Kaden et al., 2005; Balachandran et al. 2009).

Interestingly, Balachandran et al. (2009) showed using porcine AV tissues that there was no statistically significant difference in TIMP1 expression between 10% and 15% stretch after 2 days of cyclic stretching in regular medium, although the expression of MMP2 showed significant increase at 15% stretch compared to 10%. Consequently, similar TIMP1 expression under both stretch levels implies that there may be no significant change in TWIST1 expression, justifying the observed non-significant difference in miR-214 expression at the stretch-induced early remodeling stage of AV disease.

Therefore, considering all these evidences, it can be concluded that miR-214 is not associated with stretch-induced adverse AV remodeling. Furthermore, it can be hypothesized that non-significant change in TWIST1 expression may be responsible for the non-significant difference in miR-214 expression observed during stretch-induced adverse AV remodeling.

7.1.2 Why was miR-214 expression significantly downregulated at the stretch-induced late calcification stage of AV disease?

It is highly interesting to observe significant downregulation of miR-214 expression at the stretch-induced late calcification stage of AV disease (7-day 15% stretch in osteogenic medium) compared to the physiological counterpart (7-day 10% stretch in osteogenic medium). Similar downregulation of miR-214 expression was also found in calcified human aortic valves compared to healthy control (Song et al., 2017; Wang et al., 2017). Together, these results imply a negative correlation between miR-214 expression and AV calcification. This implication can be further corroborated by the inhibiting effect of miR-214 on osteogenic differentiation of osteoblasts (Wang et al., 2013; Zhao et al.,

2015; Li et al., 2016), myoblasts (Shi et al., 2013), mesenchymal stem cells (Yang et al., 2016), etc.

As mentioned previously, TWIST1, a basic helix-loop-helix (bHLH) transcription factor, is a positive regulator of miR-214 transcription (Lee et al., 2009). Interestingly, TWIST1 expression was found to be significantly downregulated in calcified human aortic valves compared to healthy control (Zhang et al., 2014; Zhu et al., 2016). In addition to that, TWIST1 has an inhibiting effect on the osteogenic differentiation of aortic valve interstitial cells (Zhang et al., 2014; Zhu et al., 2016), osteoblasts (Bialek et al., 2004), mesenchymal stem cells (Miraoui et al., 2010), etc.

From a biomechanics point of view, elevated cyclic stretch (15%) over a long culture duration (much greater than 48 hours) can downregulate TWIST1 expression via downregulation of its positive regulator, Scleraxis (SCX), another basic helix-loop-helix (bHLH) transcription factor, compared to 10% stretch (Morita et al., 2013; Roche et al., 2016; Bagchi et al., 2016).

Therefore, considering all these evidences, it can be concluded that miR-214 has a protective role in stretch-induced AV calcification. Furthermore, it can be hypothesized that downregulation of TWIST1 expression may be responsible for the downregulation of miR-214 expression in stretch-induced AV calcification, as outlined in Figure 7.1:

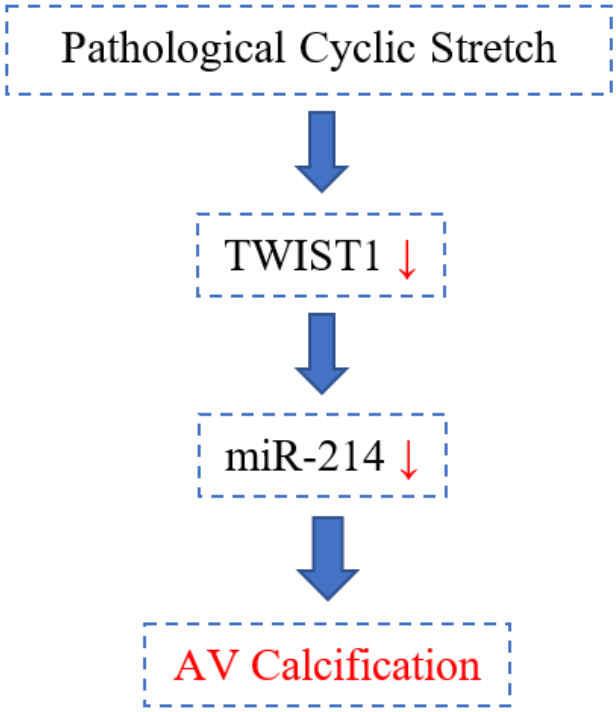

Figure 7.1 – miR-214 in stretch-induced AV calcification.

7.1.3 Do stretch and shear regulate miR-214 expression in AV similarly? If not, why?

Previous studies have established that both low magnitude (± 5 dyne/cm^2 peak value and 1 Hz frequency) and high magnitude (± 25 dyne/cm^2 peak value and 1 Hz frequency) oscillatory shear stress, when applied to the fibrosa side of porcine AV in an osteogenic environment, induce higher AV calcification compared to the physiological oscillatory shear stress (± 10 dyne/cm^2 peak value and 1 Hz frequency) (Rathan et al., 2011). In addition to that, Rathan et al. (2016) assessed miR-214 expression in porcine AV tissues under the following conditions:

i. FPS: Fibrosa exposed to unidirectional pulsatile shear stress (79 dyne/cm^2 peak value and 1 Hz frequency)

ii. FOS: Fibrosa exposed to low magnitude oscillatory shear stress (± 5 dyne/cm^2 peak value and 1 Hz frequency)

iii. VPS: Ventricularis exposed to unidirectional pulsatile shear stress (79 dyne/cm^2 peak value and 1 Hz frequency)

iv. VOS: Ventricularis exposed to low magnitude oscillatory shear stress (± 5 dyne/cm^2 peak value and 1 Hz frequency)

It was found that FOS condition significantly upregulates miR-214 expression in AV compared to each of the other three conditions, as outlined in the following diagram:

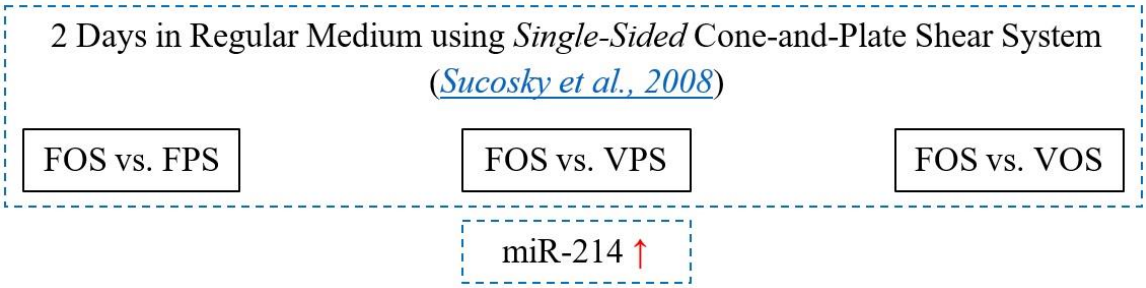

Figure 7.2 – Shear stress and miR-214 expression in AV (Rathan et al., 2016).

At this point, it should be noted that the low magnitude oscillatory shear stress (± 5 dyne/cm^2 peak value and 1 Hz frequency) is representative of the bidirectional oscillatory shear stress experienced by the fibrosa side of a diseased AV, whereas the unidirectional pulsatile shear stress (79 dyne/cm^2 peak value and 1 Hz frequency) is representative of the pulsatile shear stress experienced by the ventricularis side of a normal AV (Rathan et al., 2016; Yap et al., 2012; Yap et al., 2012; Rathan et al., 2011; Ge et al., 2009; Cao et al., 2016).

Since the fibrosa and ventricularis side of AV (whether healthy or diseased) experiences bidirectional oscillatory shear stress and unidirectional pulsatile shear stress, respectively (Ge et al., 2009), the abovementioned comparisons of miR-214 expression are

debatable from a physiological perspective. Considering that exposure of fibrosa to either sub-physiological (± 5 dyne/cm^2 peak value and 1 Hz frequency) or supra-physiological (± 25 dyne/cm^2 peak value and 1 Hz frequency) oscillatory shear stress causes higher AV calcification compared to the physiological oscillatory shear stress (± 10 dyne/cm^2 peak value and 1 Hz frequency) (Rathan et al., 2011), the more realistic conditions, using a single-sided cone-and-plate shear system (Sucosky et al., 2008), are listed below:

i. Fibrosa exposed to physiological oscillatory shear stress (± 10 dyne/cm^2 peak value and 1 Hz frequency)
ii. Fibrosa exposed to sub-physiological oscillatory shear stress (± 5 dyne/cm^2 peak value and 1 Hz frequency)
iii. Fibrosa exposed to supra-physiological oscillatory shear stress (± 25 dyne/cm^2 peak value and 1 Hz frequency)

In case of a double-sided cone-and-plate shear system (Sun et al., 2011), the more realistic conditions, following the approach of Sun et al. (2013), are listed below:

i. Fibrosa exposed to physiological oscillatory shear stress (~ ± 10 dyne/cm^2 peak value and 1 Hz frequency) and ventricularis exposed to physiological pulsatile shear stress (~ 80 dyne/cm^2 peak value and 1 Hz frequency) simultaneously
ii. Fibrosa exposed to sub-physiological oscillatory shear stress (~ ± 5 dyne/cm^2 peak value and 1 Hz frequency) and ventricularis exposed to sub-physiological pulsatile shear stress (~ 40 dyne/cm^2 peak value and 1 Hz frequency) simultaneously
iii. Fibrosa exposed to supra-physiological oscillatory shear stress (~ ± 20 dyne/cm^2 peak value and 1 Hz frequency) and ventricularis exposed to supra-physiological

pulsatile shear stress (~ 160 dyne/cm^2 peak value and 1 Hz frequency) simultaneously

Especially, Sun et al. (2013) showed that the supra-physiological case [condition (iii) above] with porcine AV resulted in significantly higher expression of Bone Morphogenetic Protein-4 (BMP-4), Transforming Growth Factor-β1 (TGF-β1), Matrix Metalloproteinase-2 and -9 (MMP-2 and -9), and Cathepsin-L and -S compared to the physiological case [condition (i) above]. However, there was no significant difference in these genes' expression between the sub-physiological [condition (ii) above] and the physiological case [condition (i) above].

Mahler et al. (2014) reported that when porcine aortic valve endothelial cells (PAVECs) were exposed to low (± 2 dyne/cm^2 peak value and 1 Hz frequency), moderate (± 10 dyne/cm^2 peak value and 1 Hz frequency) and high (± 20 dyne/cm^2 peak value and 1 Hz frequency) oscillatory shear stress, there was no significant difference in the expression of endothelial-to-mesenchymal transformation (EndMT) related genes (PECAM, ACTA2, Snail and TGF-β1). Since TWIST1 is an EndMT gene and a positive regulator of miR-214 transcription (Lee et al., 2009), similar non-significant difference in miR-214 expression can be expected when AV fibrosa is exposed to sub-physiological (~ ± 5 dyne/cm^2 peak value and 1 Hz frequency), physiological (~ ± 10 dyne/cm^2 peak value and 1 Hz frequency) and supra-physiological (~ ± 20 dyne/cm^2 peak value and 1 Hz frequency) oscillatory shear stress for 48 hours. This expectation is also strengthened by the regulatory relation between miR-214 and Snail expression (Lv et al., 2017), in addition to the fact that Snail has an inhibiting effect on osteogenic differentiation (Park et al., 2010) like TWIST1.

7.2 Discussion of Specific Aim 2 Results

As described in Specific Aim 2 chapter, 2-day 15% stretch in regular medium, which represents stretch-induced early remodeling stage of AV disease, exhibited statistically significant increase in ATF4 expression and decrease in BCL2L1 expression compared to the physiological counterpart (2-day 10% stretch in regular medium). In addition to that, 7-day 15% stretch in osteogenic medium, which represents stretch-induced late calcification stage of AV disease, showed identical trends (although non-significant) in ATF4 and BCL2L1 expression compared to the physiological counterpart (7-day 10% stretch in osteogenic medium). For both stages, CHOP expression was effectively the same between 10% and 15% stretch. The possible reasons behind these results are discussed in the following sections:

7.2.1 Why was ATF4 expression upregulated and BCL2L1 expression downregulated at the stretch-induced early remodeling and late calcification stages of AV disease?

It is highly interesting to observe upregulation of ATF4 expression and downregulation of BCL2L1 expression at the stretch-induced early remodeling (2-day 15% stretch in regular medium) and late calcification (7-day 15% stretch in osteogenic medium) stages of AV disease compared to the respective physiological counterparts (2-day 10% stretch in regular medium and 7-day 10% stretch in osteogenic medium). Similar upregulation of ATF4 expression was also found in calcified human aortic valves compared to normal ones (Wang et al., 2017). On the other hand, Balachandran et al. (2009) showed that pathological cyclic stretch (15%) induces significant increase in cell apoptosis (as determined by TUNEL staining) of porcine AV tissues compared to the physiological

level (10%), which is consistent with the observed downregulation of pro-survival BCL2L1 gene at 15% stretch (Finucane et al., 1999).

It has been well established that ATF4 is a pro-osteogenic transcription factor (Masuda et al., 2016; Cai et al., 2013; Masuda et al., 2013; Yang et al., 2004). Valentine et al. (2017) showed that exposure of mouse (20 months-old) type II alveolar epithelial cells (ATII) to 15% cyclic stretch (at 0.86 Hz) resulted in significant increase of ATF4 expression compared to static control. Yang et al. (2016) reported that 10% cyclic stretch (at 0.5 Hz) significantly upregulated ATF4 expression in human periodontal ligament cells (hPDLCs) compared to static control. Since elevated cyclic stretch (15%) induces higher AV calcification compared to the physiological level (10%) (Specific Aim 1 chapter and Balachandran et al., 2010), the observed upregulation of ATF4 expression (15% vs. 10% stretch) in porcine AV tissues makes sense from both biomechanical and functional point of view.

ATF4 can upregulate the expression of MMP2 and MMP9 in cancer cells (Zhu et al., 2014; Dey et al., 2015; Liu et al., 2010). Similar upregulation of MMP2 and MMP9 expression was observed in porcine AV tissues under pathological cyclic stretch (15%) compared to the physiological level (10%) (Balachandran et al., 2009). Additionally, ATF4 has been shown to be a positive regulator of autophagy (B'chir et al., 2013; Matsumoto et al., 2013). This is interesting because autophagic cell death has been proposed to be the main cell death mechanism in AV calcification (Somers et al., 2006; Mistiaen et al., 2006; Mistiaen, 2012). On the other hand, ATF4 has been found to be essential for the proliferation of different types of cells, such as chondrocytes (Wang et al., 2009), osteoblasts (Zhang et al., 2008), tumor cells (Ye et al., 2010), etc. This is especially

important since pathological cyclic stretch (15%) causes significant increase in cell proliferation (as determined by BrdU staining) of porcine AV tissues compared to the physiological level (10%) (Balachandran et al., 2009).

ATF4 is a major component of the PERK-eIF2α ER stress pathway (Xu et al., 2005; Wang et al., 2014). Upregulation of ATF4 expression is mediated by the sequential phosphorylation of PERK and eIF2α under ER stress conditions (Ron et al., 2007; Walter et al., 2011). Interestingly, higher degree of PERK and eIF2α phosphorylation and ATF4 expression have been observed in calcified human aortic valves compared to normal control (Cai et al., 2013; Wang et al., 2017). Therefore, it can be hypothesized that increase in ATF4 expression during the stretch-induced early remodeling and late calcification stages of AV disease may be potentiated by the sequential phosphorylation of PERK and eIF2α (as shown in Figure 7.3).

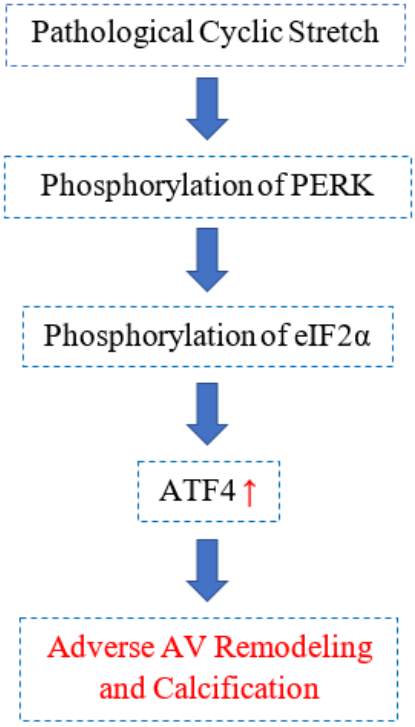

Figure 7.3 – ATF4 in stretch-induced AV remodeling and calcification.

As mentioned earlier, BCL2L1 is mainly a pro-survival gene (Shimizu et al., 1994; Kovalovich et al., 2001) due to its predominant anti-apoptotic isoform, BCL-XL (Gonzalez-Garcia et al., 1994; Xerri et al., 1996; Taylor et al., 1999; Bai et al., 2005). Downregulation of BCL2L1 expression has been shown to be associated with increased cell apoptosis (Hagenbuchner et al., 2010). In addition to that, decreased BCL2L1 expression may initiate and/or stimulate autophagy (Lindqvist et al., 2014; Kim et al., 2014; Maejima et al., 2013; Han et al., 2011), which is consistent with the pro-autophagic effect of increased ATF4 expression (B'chir et al., 2013; Matsumoto et al., 2013). This is especially interesting since downregulation of BCL2L1 expression may result in autophagic cell death (Yanagisawa et al., 2003).

B-Cell Lymphoma/Leukemia 11B (BCL11B) is a pro-survival gene (Wakabayashi et al., 2003) that has been shown to be a positive regulator of BCL2L1 expression (Grabarczyk et al., 2007; Kamimura et al., 2007). Furthermore, BCL11B expression has been found to be downregulated with increased arterial stiffness (Valisno et al., 2017; Al Maskari et al., 2016; Wu et al., 2014; Mitchell et al., 2012). Therefore, it can be hypothesized that decrease in BCL2L1 expression during the stretch-induced early remodeling and late calcification stages of AV disease may be mediated by downregulation of BCL11B expression (as shown in Figure 7.4).

Interestingly, both BCL11B and BCL2L1 expression was found to be upregulated in calcified human aortic valves compared to normal control (Li et al., 2017; Bossé et al., 2009), which is counterintuitive. This may indicate the occurrence of autophagy inhibition and associated increase in calcification during the very late stage of AV disease (Deng et al., 2017; Peng et al., 2017; Dai et al., 2013).

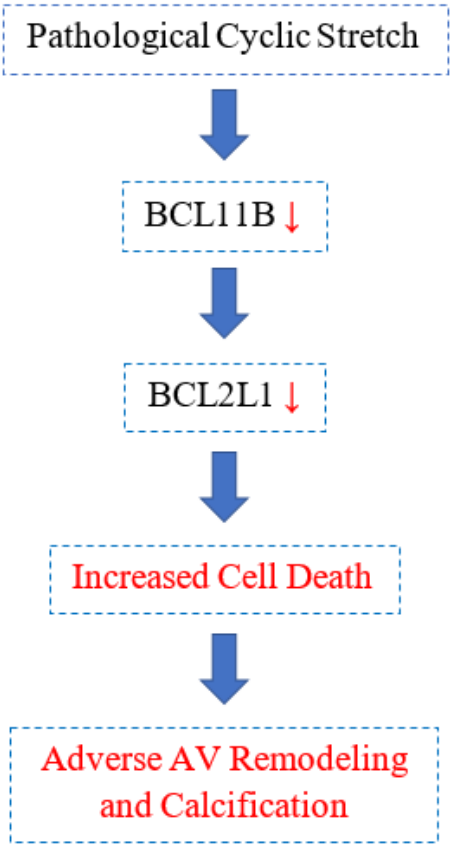

Figure 7.4 – BCL2L1 in stretch-induced AV remodeling and calcification.

7.2.2 Why did CHOP expression remain effectively the same at the stretch-induced early remodeling and late calcification stages of AV disease?

It is surprising to observe that CHOP expression remains effectively the same at the stretch-induced early remodeling (2-day 15% stretch in regular medium) and late calcification (7-day 15% stretch in osteogenic medium) stages of AV disease compared to the respective physiological counterparts (2-day 10% stretch in regular medium and 7-day 10% stretch in osteogenic medium). However, CHOP expression was found to be significantly upregulated in calcified human aortic valves compared to healthy control (Wang et al., 2017; Cai et al., 2013). In addition to that, CHOP has been shown to promote both valvular and vascular calcification (Masuda et al., 2013; Cai et al., 2017).

Jia et al. (2017) and Jia et al. (2015) reported that cyclic stretch of 18% significantly upregulates CHOP expression in mouse aortic smooth muscle cells (SMCs) compared to static control. However, Cheng et al. (2008) showed that 20% stretch induced a brief (during the culture period from 12 to 18 hours) increase in CHOP expression of vascular smooth muscle cells (VSMCs) compared to 10% stretch, which was attenuated afterwards (culture period > 18 hours). Therefore, it is possible that pathological cyclic stretch (15%) induces similar transient increase of CHOP expression in porcine AV tissues compared to the physiological level (10%), which is later attenuated by some adaptive response of the tissue itself.

Tribbles Homolog 3 (TRB3) is one of the transcriptional targets of both ATF4 and CHOP (Ohoka et al., 2005; Han et al., 2013). It should be noted here that CHOP, itself, is another transcriptional target of ATF4. Interestingly, increased TRB3 expression works in a negative feedback loop to inhibit the transcriptional induction of CHOP (Jousse et al., 2007). In addition to that, 20% cyclic stretch has been shown to upregulate TRB3 expression in rat cardiomyocytes compared to 10% stretch, which results in increased cell apoptosis (Cheng et al., 2015). TRB3 was also found to promote osteogenic differentiation (Zhang et al., 2017; Fan et al., 2016; Park et al., 2009) and to be positively regulated by TWIST1 (Lee et al., 2011).

Therefore, it can be hypothesized that the insensitivity of CHOP expression to pathological cyclic stretch (15%) during the stretch-induced early remodeling and late calcification stages of AV disease may be caused by TRB3-mediated inhibition of its transiently increased expression at 15% stretch compared to 10%, whereas increased TRB3 expression promotes adverse AV remodeling and calcification (as shown in Figure 7.5).

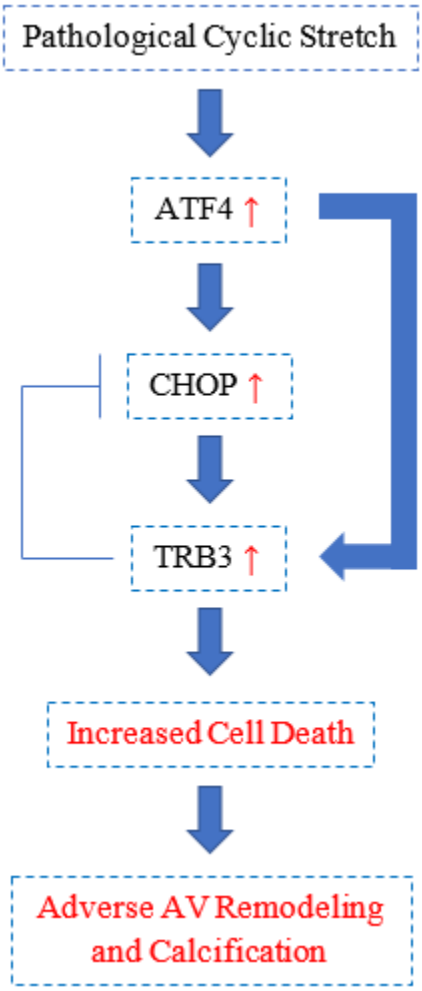

Figure 7.5 – CHOP in stretch-induced AV remodeling and calcification.

7.3 Discussion of Specific Aim 3 Results

As described in Specific Aim 3 chapter, application of miR-214 mimic significantly upregulated miR-214 expression in statically cultured porcine AV tissues. However, this didn't result in significant inhibition of the mRNA expression of ATF4, CHOP and BGLAP genes. Nonetheless, the resulting mRNA expression of ATF4 and CHOP genes exhibited decreasing trends, as expected (38% and 25% decrease, respectively), while the mRNA expression of BGLAP was literally unaffected. Additionally, transfection of porcine AV tissues with miR-214 mimic resulted in a slight decrease (12%) of pro-survival

gene BCL2L1 expression, which was opposite to the anticipated effect. One of the implications of the observed results is that the used concentration of miR-214 mimic (50 nM) may not be sufficient and higher concentration (such as 100 nM) may have to be used to induce significant effects on the mRNA expression of ATF4, CHOP, BCL2L1 and BGLAP genes.

The most prominent effect of miR-214 mimic was on the mRNA expression of ATF4 gene (38% decrease with a p-value of 0.161). Since ATF4 is a validated target of miR-214 (Wang et al., 2013), application of miR-214 mimic should be able to inhibit its expression (whether mRNA or protein). Interestingly, it was found that miR-214 mimic inhibits ATF4 expression in mouse osteoblasts only at the protein level (Wang et al., 2013). Therefore, it is a possibility that miR-214 may inhibit the expression of ATF4 gene more efficiently at the protein level. Subsequently, it may be able to indirectly inhibit the protein expression of CHOP and BGLAP genes.

7.4 Limitations of the Study

The research work presented in this dissertation has some limitations. These limitations are outlined as follows:

i. The *ex vivo* stretch bioreactor applies uniaxial stretch in the circumferential direction. This is in contrary to the in vivo condition since AV leaflets undergo biaxial stretching, with ~ 10% stretch in the circumferential direction and ~ 30% stretch in the radial direction. However, preliminary work in our laboratory showed that application of 30% cyclic stretch in the radial direction does not induce

significant changes in the collagen and sulfated glycosaminoglycan (sGAG) content of AV (Balachandran, 2010).

ii. There may be biological variability among porcine AV tissues collected on the same day. This is due to the inter-animal and intra-animal differences in AV tissue properties. The effect of this variability was nullified by always running 10% and 15% stretch or negative control and miR-214 mimic experiments in a pairwise fashion. Additionally, there may be day-to-day variability among porcine AV tissues. To counteract this, AV tissue samples collected on (at least) two separate days were used for each group in a comparison case.

iii. In specific aim 3, static cultures of porcine AV tissues were used in the transfection experiments, which contrasts with the dynamic AV function in vivo. However, these static transfection experiments were justified as the main objective was to see the effect of miR-214 overexpression of ATF4, CHOP, BCL2L1 and BGLAP genes in AV.

CHAPTER 8. CONCLUSIONS AND FUTURE WORKS

This thesis work demonstrated, for the first time, the effect of physiological and pathological cyclic stretch on miR-214 expression in porcine AVs. It also showed that the expression of ATF4 gene, which is a target of miR-214, is stretch-sensitive. The key findings from this research work can be outlined as follows:

- Pathological cyclic stretch downregulates miR-214 expression in AV, especially in the late stage of stretch-induced AV calcification.
- Pathological cyclic stretch upregulates ATF4 expression and downregulates BCL2L1 expression in both the early remodeling stage and late calcification stage of stretch-induced AV disease.
- Pathological cyclic stretch does not affect CHOP expression in AV.
- miR-214 overexpression has the potential to significantly inhibit ATF4 expression in AV.

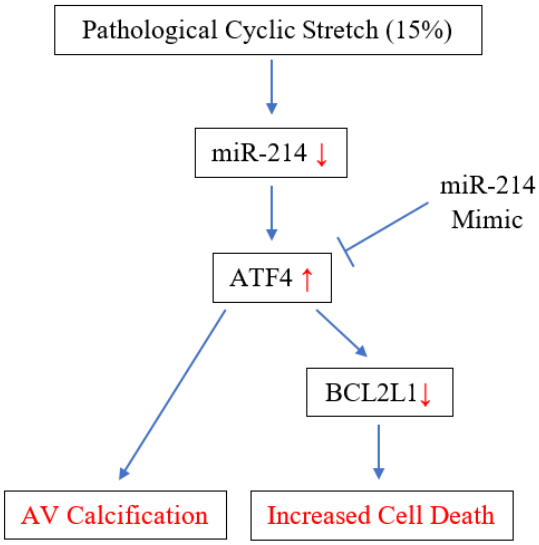

Figure 8.1 – Proposed pathway involving stretch/miR-214/ATF4/BCL2L1.

Figure 8.1 represents the proposed functional pathway via which pathological cyclic stretch may regulate the expression of miR-214 and its target gene ATF4 in AV, potentially leading to increased cell death and AV calcification. To validate this proposed pathway, the following future works are suggested:

- It will be interesting to see whether pathological cyclic stretch exerts similar effects on the mRNA and protein expression of ATF4, CHOP and BCL2L1 genes in porcine AV tissues. Therefore, western blotting and immunostaining of stretched tissue samples can be completed for assessing the protein expression of ATF4, CHOP and BCL2L1 genes.
- Mechanical stretch mainly affects the interstitial cells (ICs) in AV. Hence, from a cellular point of view, it will be worthwhile to evaluate the effect of cyclic stretch on the mRNA and protein expression of ATF4, CHOP and BCL2L1 genes in valvular interstitial cells (VICs). In addition to that, the expression of miR-214 should be assessed in cyclically stretched VICs.
- The current research work evaluated the effect of miR-214 mimic on the mRNA expression of ATF4, CHOP, BCL2L1 and BGLAP genes in statically cultured AV tissues. Similar assessment of the effect of miR-214 overexpression on the mRNA and protein expression of above-mentioned genes needs to be completed with stretched tissue samples.
- The functional effect of miR-214 on the mRNA and protein expression of ATF4, CHOP, BCL2L1 and BGLAP genes can be further validated by evaluating the effect of anti-miR-214 on these genes in static and stretched tissue samples. Identical functional studies can also be carried out with static and cyclically stretched VICs.

- miR-214 mimic and anti-miR-214 can be used to elucidate the effect of miR-214 on cellular processes (such as apoptosis and proliferation) in VICs and AV tissues, under both static and stretch conditions.
- The current research work did not assess the inter-dependency of ATF4, CHOP and BCL2L1 genes in AV tissues. Therefore, adenoviral vector (for overexpression) and siRNA (for inhibition of expression) based approaches can be implemented to assess the inter-dependency of ATF4, CHOP and BCL2L1 genes in VICs and AV tissues, under both static and stretch conditions.
- The adenoviral vector and siRNA based approached can similarly be used to evaluate the effect of ATF4, CHOP and BCL2L1 genes on apoptosis, proliferation and calcification of VICs and AV tissues.
- TWIST1 is a positive regulator of miR-214 (Lee et al., 2009). Therefore, adenoviral vector mediated overexpression and siRNA mediated inhibition of TWIST1 can be used to validate this regulatory role in static and cyclically stretched VICs and AV tissues.

Together, these future works will enhance the current understanding of stretch-mediated regulation of miR-214 expression and its relation to AV pathogenesis.

APPENDIX

A.1 Stretch Programs (Si Programmer™ Software)

(a) 10% stretch program

(b) 15% stretch program

Figure A.1: Stretch programs

A.2 Calcium Arsenazo Assay

A.2.1 Reagents:

- DPBS (THERMO FISHER SCIENTIFIC catalog no. 21600044)
- Acetic Acid 1 M (SIGMA ALDRICH catalog no. AX0073)
- Arsenazo III Reagent (POINTE SCIENTIFIC catalog no. C7529)
- Calcium Standard (0.5 mg/mL) (RICCA CHEMICAL COMPANY catalog no. 1799-16)

A.2.2 Procedure:

1. Measure the empty weight of each microcentrifuge tube.
2. Wash tissue samples three times with DPBS.
3. Use mortar and pestle to grind the tissue samples with liquid nitrogen and transfer each of these to a microcentrifuge tube.
4. Measure the combined weight of each microcentrifuge tube containing a wet tissue sample.
5. Incubate the tissue samples in a dryer at 37°C for 24 hours. Remember to keep the lids of the microcentrifuge tubes open.
6. Measure the combined weight of each microcentrifuge tube containing a dry tissue sample.
7. Add 500 µL of 1 M acetic acid to each microcentrifuge tube.
8. Vortex the tissue samples overnight (12 hours) in refrigerator.
9. Centrifuge the samples at 13,000xg for 10 minutes.
10. Transfer the supernatants to new microcentrifuge tubes.

11. Prepare calcium standards in 1 M acetic acid (0, 20, 40, 60, 80, 100 µg/mL).
12. Pipet 25 µL of each standard and sample in triplicate to a clear 96-well plate.
13. Add 300 µL of Arsenazo III reagent to each well (dilute sample if color change is more than that of maximum calcium standard).
14. Incubate for 30 seconds at room temperature.
15. Read the absorbance of each well in a plate reader at 650 nm (color is stable for 30 minutes).

A.3 Alizarin Red Stain

A.3.1 Reagents:

- For Alizarin Red Solution
- Alizarin Red S 2 g (SIGMA ALDRICH catalog no. A5533)
- DI water 100 mL
- 0.5% Ammonium Hydroxide (SIGMA ALDRICH catalog no. 320145)

Mix the solution, adjust the pH to 4.1 – 4.3 using 0.5% Ammonium Hydroxide. The pH is critical. Make fresh.

A.3.2 Procedure:

1. Rehydrate frozen sections in 70% ethanol.
2. Rinse with DI water at room temperature.
3. Incubate with Alizarin Red S solution for 30 seconds.
4. Shake off excess dye and blot sections using Kimwipes.

5. Dehydrate the slides in the autostainer.
6. Coverslip the slides and store at room temperature.

A.4 Von Kossa Stain

A.4.1 Reagents:

For 5% Silver Nitrate Solution (Stable for 1 year):

- Silver Nitrate 25 g (SIGMA ALDRICH catalog no. S8157)
- DI water 500 mL

Mix well, pour into a clean brown bottle and store in refrigerator at 4°C.

For 5% Sodium Thiosulfate (Make fresh):

- Sodium Thiosulfate 5 g (SIGMA ALDRICH catalog no. S7026)
- DI water 100 mL

For Nuclear Fast Red (Kernechtrot) Solution:

- Nuclear Fast Red 0.1 g (SIGMA ALDRICH catalog no. 229113)
- Aluminum Sulfate 5 g (SIGMA ALDRICH catalog no. 368458)
- DI water 100 mL
- Thymol 1 grain (SIGMA ALDRICH catalog no. T0501)

Dissolve aluminum sulfate in DI water. Add Nuclear Fast Red and slowly heat to boil and cool. Filter and add a grain of thymol as a preservative.

A.4.2 Procedure:

1. Rehydrate frozen sections in DI water at room temperature.
2. Incubate slides with 5% silver nitrate solution placed under a UV lamp. Place foil or mirror beneath the jar/tray to reflect the light. Leave for 1 hour or until calcium turns black.
3. Wash three times with DI water for 5 minutes at room temperature.
4. Wash one time with 5% sodium thiosulfate for 5 minutes at room temperature.
5. Wash one time with tap water, one time with DI water.
6. Incubate slides with Nuclear Fast Red for 5 minutes at room temperature.
7. Wash briefly with DI water.
8. Dehydrate the slides in the autostainer.
9. Coverslip the slides and store at room temperature.

A.5 Raw Data

A.5.1 Specific Aim 1

Table A.1 – Calcification of Porcine AV Tissues under Cyclic Stretch

Quantification of AV Calcification (Determined by Arsenazo Assay)			
Wet Basis (μg Ca/mg wet tissue)		Dry Basis (μg Ca/mg dry tissue)	
10% (n = 6)	15% (n = 6)	10% (n = 6)	15% (n = 6)
1.2325	1.6414	12.9534	14.9262
0.2177	1.2528	3.5781	11.9958
0.5118	1.7425	6.0766	21.7276
0.9913	1.0992	14.1118	12.7887
0.2442	1.3216	3.4662	15.2247
0.1309	1.3602	2.0088	15.7760

Table A.2 – miR-214 Expression in Stretched Porcine AV Tissues

miR-214 Expression Relative to U6 (Determined by qPCR)			
2-Day Stretch in Regular Medium		7-Day Stretch in Osteogenic Medium	
10% (n = 8)	15% (n = 8)	10% (n = 9)	15% (n = 10)
1.2713	2.0131	2.0682	0.6409
1.3465	1.8832	1.4208	0.1765

1.4352	1.4960	0.9370	0.4888
2.05	1.5816	0.5601	0.0789
0.5233	0.2272	0.5579	0.3547
0.5045	0.1958	1.9454	0.3685
0.5279	0.1343	0.2685	0.1212
0.3411	1.2596	0.7248	0.2153
_	_	0.5174	0.3181
_	_	_	0.0789

A.5.2 Specific Aim 2

Table A.3 – ATF4 mRNA Expression in Stretched Porcine AV Tissues

ATF4 mRNA Expression Relative to 18S (Determined by RT-qPCR)			
2-Day Stretch in Regular Medium		7-Day Stretch in Osteogenic Medium	
10% (n = 7)	15% (n = 8)	10% (n = 7)	15% (n = 8)
1.0351	1.6767	0.7260	4.0669
1.2407	1.7596	1.1605	5.0411
1.0941	1.5361	1.7357	2.6404
0.7869	1.0457	1.3927	1.9428
1.1528	1.0583	0.5576	1.2145
0.8189	1.4803	0.8129	1.2426
0.8715	1.7676	0.6147	0.5256
_	0.6848	_	0.4871

Table A.4 – CHOP mRNA Expression in Stretched Porcine AV Tissues

CHOP mRNA Expression Relative to 18S (Determined by RT-qPCR)			
2-Day Stretch in Regular Medium		7-Day Stretch in Osteogenic Medium	
10% (n = 8)	15% (n = 8)	10% (n = 7)	15% (n = 8)
0.9018	1.2171	0.5876	0.5369
1.2159	1.2843	0.4951	0.7403

0.9731	0.8667	0.2311	0.0491
1.1270	0.8915	0.2941	0.4921
0.8137	0.6827	2.0633	2.9788
1.2630	0.9504	1.5007	2.8499
0.6284	1.2555	1.8282	1.4266
1.0771	0.8513	_	1.0928

Table A.5 – BCL2L1 mRNA Expression in Stretched Porcine AV Tissues

BCL2L1 mRNA Expression Relative to 18S (Determined by RT-qPCR)			
2-Day Stretch in Regular Medium		7-Day Stretch in Osteogenic Medium	
10% (n = 7)	15% (n = 8)	10% (n = 8)	15% (n = 7)
0.6282	0.5382	1.8791	1.0314
1.0388	0.5012	1.2925	0.8472
0.7282	0.6404	0.9256	0.4764
1.2812	0.8454	2.2099	0.3040
1.1111	0.3514	0.5893	0.2968
0.9466	0.3474	0.3379	0.2108
1.2658	0.5857	0.3287	0.1172
_	0.4095	0.4370	_

A.5.3 Specific Aim 3

Table A.6 – miR-214 Expression in Transfected Porcine AV Tissues

miR-214 Expression Relative to U6 (Determined by RT-qPCR)	
Negative Control Mimic (n = 4)	miR-214 mimic (n = 4)
2.9205	12603.1162
0.0598	29685.8705
0.2699	21714.0121
0.7498	570725.8718

Table A.7 – ATF4 and BGLAP mRNA Expression in Transfected Porcine AV Tissues

ATF4 and BGLAP mRNA Expression Relative to 18S (Determined by RT-qPCR)			
ATF4		BGLAP	
Negative Control Mimic (n = 8)	miR-214 Mimic (n = 7)	Negative Control Mimic (n = 8)	miR-214 Mimic (n = 7)
1.5730	0.2230	1.3563	1.1127
0.6780	0.7801	1.5383	0.9893
0.9003	0.4315	0.5437	0.8045
0.3016	1.0301	0.5676	1.0578
0.4128	0.5919	0.5638	0.9878

1.7468	0.4771	1.3187	0.9550
0.4533	0.7766	0.2621	1.2311
1.9342	_	1.8495	_

REFERENCES

[1] Al Maskari, R., Cleary, S., Li, Y., Khir, A., Mitchell, G., Wilkinson, I., & O'Shaughnessy, K. (2016). Genetic Variations on Chromosome 14 Influence BCL11B Gene Expression Levels and Aortic Stiffness. The FASEB Journal, 30(1 Supplement), 1260-8.

[2] Arjunon, S., Rathan, S., Jo, H., & Yoganathan, A. P. (2013). Aortic valve: mechanical environment and mechanobiology. Annals of biomedical engineering, 41(7), 1331-1346.

[3] Aurora, A. B., Mahmoud, A. I., Luo, X., Johnson, B. A., van Rooij, E., Matsuzaki, S., ... & Olson, E. N. (2012). MicroRNA-214 protects the mouse heart from ischemic injury by controlling Ca2+ overload and cell death. The Journal of clinical investigation, 122(4), 1222.

[4] Bai, J., Sui, J., Demirjian, A., Vollmer, C. M., Marasco, W., & Callery, M. P. (2005). Predominant Bcl-XL Knockdown Disables Antiapoptotic Mechanisms: Tumor Necrosis Factor–Related Apoptosis-Inducing Ligand–Based Triple Chemotherapy Overcomes Chemoresistance in Pancreatic Cancer Cells In vitro. Cancer research, 65(6), 2344-2352.

[5] Balachandran, K., Sucosky, P., Jo, H., & Yoganathan, A. P. (2009). Elevated cyclic stretch alters matrix remodeling in aortic valve cusps: implications for degenerative aortic valve disease. American Journal of Physiology-Heart and Circulatory Physiology, 296(3), H756-H764.

[6] Balachandran, K., Sucosky, P., Jo, H., & Yoganathan, A. P. (2010). Elevated cyclic stretch induces aortic valve calcification in a bone morphogenic protein-dependent manner. The American journal of pathology, 177(1), 49-57.

[7] Balachandran, K., Sucosky, P., & Yoganathan, A. P. (2011). Hemodynamics and mechanobiology of aortic valve inflammation and calcification. International journal of inflammation, 2011.

[8] Bagchi, R. A., Roche, P., Aroutiounova, N., Espira, L., Abrenica, B., Schweitzer, R., & Czubryt, M. P. (2016). The transcription factor scleraxis is a critical regulator of cardiac fibroblast phenotype. BMC biology, 14(1), 21.

[9] Baumgarten, A., Bang, C., Tschirner, A., Engelmann, A., Adams, V., von Haehling, S., ... & Meyer, R. (2013). TWIST1 regulates the activity of ubiquitin proteasome system via the miR-199/214 cluster in human end-stage dilated cardiomyopathy. International journal of cardiology, 168(2), 1447-1452.

[10] B'chir, W., Maurin, A. C., Carraro, V., Averous, J., Jousse, C., Muranishi, Y., ... & Bruhat, A. (2013). The eIF2α/ATF4 pathway is essential for stress-induced autophagy gene expression. Nucleic acids research, 41(16), 7683-7699.

[11] Bialek, P., Kern, B., Yang, X., Schrock, M., Sosic, D., Hong, N., ... & Justice, M. J. (2004). A twist code determines the onset of osteoblast differentiation. Developmental cell, 6(3), 423-435.

[12] Billiar, K. L., & Sacks, M. S. (2000). Biaxial mechanical properties of the natural and glutaraldehyde treated aortic valve cusp-Part I: Experimental results. Transactions-American Society of Mechanical Engineers Journal of Biomechanical Engineering, 122(1), 23-30.

[13] Billiar, K. L., & Sacks, M. S. (2000). Biaxial mechanical properties of the native and glutaraldehyde-treated aortic valve cusp: part II—a structural constitutive model. Journal of biomechanical engineering, 122(4), 327-335.

[14] Bossé, Y., Miqdad, A., Fournier, D., Pépin, A., Pibarot, P., & Mathieu, P. (2009). Refining molecular pathways leading to calcific aortic valve stenosis by studying gene expression profile of normal and calcified stenotic human aortic valves. Circulation: Cardiovascular Genetics, CIRCGENETICS-108.

[15] Butcher, J. T., & Nerem, R. M. (2006). Valvular endothelial cells regulate the phenotype of interstitial cells in co-culture: effects of steady shear stress. Tissue engineering, 12(4), 905-915.

[16] Butcher, J. T., Penrod, A. M., García, A. J., & Nerem, R. M. (2004). Unique morphology and focal adhesion development of valvular endothelial cells in static and fluid flow environments. Arteriosclerosis, thrombosis, and vascular biology, 24(8), 1429-1434.

[17] Butcher, J. T., Tressel, S., Johnson, T., Turner, D., Sorescu, G., Jo, H., & Nerem, R. M. (2005). Transcriptional profiles of valvular and vascular endothelial cells reveal phenotypic differences. Arteriosclerosis, thrombosis, and vascular biology, 26(1), 69-77.

[18] Cai, Z., Li, F., Gong, W., Liu, W., Duan, Q., Chen, C., ... & Wang, D. W. (2013). Endoplasmic Reticulum Stress Participates in Aortic Valve Calcification in Hypercholesterolemic Animals. Arteriosclerosis, thrombosis, and vascular biology, 33(10), 2345-2354.

[19] Cai, Z., Liu, B., Wei, J., Fu, Z., Wang, Y., Wang, Y., ... & Lin, X. (2017). Deficiency of CCAAT/enhancer-binding protein homologous protein (CHOP) prevents diet-induced aortic valve calcification in vivo. Aging Cell.

[20] Cao, K., Bukač, M., & Sucosky, P. (2016). Three-dimensional macro-scale assessment of regional and temporal wall shear stress characteristics on aortic valve leaflets. Computer methods in biomechanics and biomedical engineering, 19(6), 603-613.

[21] Chakraborty, S., Wirrig, E. E., Hinton, R. B., Merrill, W. H., Spicer, D. B., & Yutzey, K. E. (2010). Twist1 promotes heart valve cell proliferation and extracellular matrix gene expression during development in vivo and is expressed in human diseased aortic valves. Developmental biology, 347(1), 167-179.

[22] Charitos, E. I., & Sievers, H. H. (2012). Anatomy of the aortic root: implications for valve-sparing surgery. Annals of cardiothoracic surgery, 2(1), 53.

[23] Chen, J. H., & Simmons, C. A. (2011). Cell–matrix interactions in the pathobiology of calcific aortic valve disease. Circulation research, 108(12), 1510-1524.

[24] Cheng, W. P., Hung, H. F., Wang, B. W., & Shyu, K. G. (2007). The molecular regulation of GADD153 in apoptosis of cultured vascular smooth muscle cells by cyclic mechanical stretch. Cardiovascular research, 77(3), 551-559.

[25] Cheng, W. P., Wang, B. W., Lo, H. M., & Shyu, K. G. (2015). Mechanical stretch induces apoptosis regulator TRB3 in cultured cardiomyocytes and volume-overloaded heart. PloS one, 10(4), e0123235.

[26] Choi, B., Lee, S., Kim, S. M., Lee, E. J., Lee, S. R., Kim, D. H., ... & Song, J. K. (2017). Dipeptidyl Peptidase-4 Induces Aortic Valve Calcification by Inhibiting

Insulin-like Growth Factor-1 Signaling in Valvular Interstitial Cells. Circulation, CIRCULATIONAHA-116.

[27] Cleveland Clinic: http://www.clevelandclinicmeded.com/medicalpubs/diseasemanagement/cardiology/aortic-valve-disease/

[28] Dahal, S., Huang, P., Murray, B. T., & Mahler, G. J. (2017). Endothelial to Mesenchymal Transformation is Induced by Altered Extracellular Matrix in Aortic Valve Endothelial Cells. Journal of Biomedical Materials Research Part A.

[29] Dai, X. Y., Zhao, M. M., Cai, Y., Guan, Q. C., Zhao, Y., Guan, Y., ... & Wang, X. (2013). Phosphate-induced autophagy counteracts vascular calcification by reducing matrix vesicle release. Kidney international, 83(6), 1042-1051.

[30] D'Angelo, R. C., Liu, X. W., Najy, A. J., Jung, Y. S., Won, J., Chai, K. X., ... & Kim, H. R. C. (2014). TIMP-1 via TWIST1 induces EMT phenotypes in human breast epithelial cells. Molecular Cancer Research, 12(9), 1324-1333.

[31] Deck, J. D. (1986). Endothelial cell orientation on aortic valve leaflets. Cardiovascular research, 20(10), 760-767.

[32] Deng, X. S., Meng, X., Venardos, N., Song, R., Yamanaka, K., Fullerton, D., & Jaggers, J. (2017). Autophagy negatively regulates pro-osteogenic activity in human aortic valve interstitial cells. journal of surgical research, 218, 285-291.

[33] Dey, S., Baird, T. D., Zhou, D., Palam, L. R., Spandau, D. F., & Wek, R. C. (2010). Both transcriptional regulation and translational control of ATF4 are central to the integrated stress response. Journal of Biological Chemistry, 285(43), 33165-33174.

[34] Dey, S., Sayers, C. M., Verginadis, I. I., Lehman, S. L., Cheng, Y., Cerniglia, G. J., ... & Diehl, J. A. (2015). ATF4-dependent induction of heme oxygenase 1 prevents anoikis and promotes metastasis. The Journal of clinical investigation, 125(7), 2592.

[35] Dong, H., Dong, S., Zhang, L., Gao, X., Lv, G., Chen, W., & Shao, S. (2016). MicroRNA-214 exerts a Cardio-protective effect by inhibition of fibrosis. The Anatomical Record, 299(10), 1348-1357.

[36] Duan, Q., Yang, L., Gong, W., Wang, F., Chen, C., Wang, P., ... & Wang, D. W. (2015). MicroRNA-214 is upregulated in heart failure patients and suppresses XBP1-

mediated endothelial cells angiogenesis. Journal of cellular physiology, 230(8), 1964-1973.

[37] El Accaoui, R. N., Gould, S. T., Hajj, G. P., Chu, Y., Davis, M. K., Kraft, D. C., ... & Kutschke, W. (2014). Aortic valve sclerosis in mice deficient in endothelial nitric oxide synthase. American Journal of Physiology-Heart and Circulatory Physiology, 306(9), H1302-H1313.

[38] Fan, J., Im, C. S., Guo, M., Cui, Z. K., Fartash, A., Kim, S., ... & Aghaloo, T. L. (2016). Enhanced Osteogenesis of Adipose-Derived Stem Cells by Regulating Bone Morphogenetic Protein Signaling Antagonists and Agonists. Stem cells translational medicine, 5(4), 539-551.

[39] Fernández Esmerats, J., Heath, J., & Jo, H. (2016). Shear-sensitive genes in aortic valve endothelium. Antioxidants & redox signaling, 25(7), 401-414.

[40] Finucane, D. M., Bossy-Wetzel, E., Waterhouse, N. J., Cotter, T. G., & Green, D. R. (1999). Bax-induced caspase activation and apoptosis via cytochromec release from mitochondria is inhibitable by Bcl-xL. Journal of Biological Chemistry, 274(4), 2225-2233.

[41] Freeman, R. V., & Otto, C. M. (2005). Spectrum of calcific aortic valve disease. Circulation, 111(24), 3316-3326.

[42] Fu, H. Y., Okada, K. I., Liao, Y., Tsukamoto, O., Isomura, T., Asai, M., ... & Asanuma, H. (2010). Ablation of C/EBP homologous protein attenuates endoplasmic reticulum–mediated apoptosis and cardiac dysfunction induced by pressure overload. Circulation, 122(4), 361-369.

[43] Ge, L., & Sotiropoulos, F. (2010). Direction and magnitude of blood flow shear stresses on the leaflets of aortic valves: is there a link with valve calcification? Journal of biomechanical engineering, 132(1), 014505.

[44] Garg, A. D., Kaczmarek, A., Krysko, O., Vandenabeele, P., Krysko, D. V., & Agostinis, P. (2012). ER stress-induced inflammation: does it aid or impede disease progression? Trends in molecular medicine, 18(10), 589-598.

[45] Gaudette, B. T., Iwakoshi, N. N., & Boise, L. H. (2014). Bcl-xL protein protects from C/EBP homologous protein (CHOP)-dependent apoptosis during plasma cell differentiation. Journal of Biological Chemistry, 289(34), 23629-23640.

[46] González-García, M., Pérez-Ballestero, R., Ding, L., Duan, L., Boise, L. H., Thompson, C. B., & Nunez, G. (1994). bcl-XL is the major bcl-x mRNA form expressed during murine development and its product localizes to mitochondria. Development, 120(10), 3033-3042.

[47] Grabarczyk, P., Przybylski, G. K., Depke, M., Völker, U., Bahr, J., Assmus, K., ... & Schmidt, C. A. (2007). Inhibition of BCL11B expression leads to apoptosis of malignant but not normal mature T cells. Oncogene, 26(26), 3797.

[48] Ha, M., & Kim, V. N. (2014). Regulation of microRNA biogenesis. Nature reviews Molecular cell biology, 15(8), 509-524.

[49] Han, Y. K., Ha, T. K., Kim, Y. G., & Lee, G. M. (2011). Bcl-x L overexpression delays the onset of autophagy and apoptosis in hyperosmotic recombinant Chinese hamster ovary cell cultures. Journal of biotechnology, 156(1), 52-55.

[50] Han, J., Back, S. H., Hur, J., Lin, Y. H., Gildersleeve, R., Shan, J., ... & Kilberg, M. S. (2013). ER-stress-induced transcriptional regulation increases protein synthesis leading to cell death. Nature cell biology, 15(5), 481.

[51] Hagenbuchner, J., Ausserlechner, M. J., Porto, V., David, R., Meister, B., Bodner, M., ... & Obexer, P. (2010). The anti-apoptotic protein BCL2L1/Bcl-xL is neutralized by pro-apoptotic PMAIP1/Noxa in neuroblastoma, thereby determining bortezomib sensitivity independent of prosurvival MCL1 expression. Journal of Biological Chemistry, 285(10), 6904-6912.

[52] Han, J., Back, S. H., Hur, J., Lin, Y. H., Gildersleeve, R., Shan, J., ... & Kilberg, M. S. (2013). ER-stress-induced transcriptional regulation increases protein synthesis leading to cell death. Nature cell biology, 15(5), 481.

[53] Hetz, C. (2012). The unfolded protein response: controlling cell fate decisions under ER stress and beyond. Nature reviews. Molecular cell biology, 13(2), 89.

[54] Holliday, C. J., Ankeny, R. F., Jo, H., & Nerem, R. M. (2011). Discovery of shear- and side-specific mRNAs and miRNAs in human aortic valvular endothelial cells. American Journal of Physiology-Heart and Circulatory Physiology, 301(3), H856-H867.

[55] Hjortnaes, J., Shapero, K., Goettsch, C., Hutcheson, J. D., Keegan, J., Kluin, J., ... & Aikawa, E. (2015). Valvular interstitial cells suppress calcification of valvular endothelial cells. Atherosclerosis, 242(1), 251-260.

[56] Jia, L. X., Zhang, W. M., Li, T. T., Liu, Y., Piao, C. M., Ma, Y. C., ... & Du, J. (2017). ER stress dependent microparticles derived from smooth muscle cells promote endothelial dysfunction during thoracic aortic aneurysm and dissection. Clinical Science, 131(12), 1287-1299.

[57] Jia, L. X., Zhang, W. M., Zhang, H. J., Li, T. T., Wang, Y. L., Qin, Y. W., ... & Du, J. (2015). Mechanical stretch-induced endoplasmic reticulum stress, apoptosis and inflammation contribute to thoracic aortic aneurysm and dissection. The Journal of pathology, 236(3), 373-383.

[58] Jian, B., Narula, N., Li, Q. Y., Mohler, E. R., & Levy, R. J. (2003). Progression of aortic valve stenosis: TGF-β1 is present in calcified aortic valve cusps and promotes aortic valve interstitial cell calcification via apoptosis. The Annals of thoracic surgery, 75(2), 457-465.

[59] Jin, Y., Yang, C. J., Xu, X., Cao, J. N., Feng, Q. T., & Yang, J. (2015). MiR-214 regulates the pathogenesis of patients with coronary artery disease by targeting VEGF. Molecular and cellular biochemistry, 402(1-2), 111-122.

[60] Jousse, C., Deval, C., Maurin, A. C., Parry, L., Chérasse, Y., Chaveroux, C., ... & Fafournoux, P. (2007). TRB3 inhibits the transcriptional activation of stress-regulated genes by a negative feedback on the ATF4 pathway. Journal of Biological Chemistry, 282(21), 15851-15861.

[61] Kaden, J. J., Dempfle, C. E., Grobholz, R., Fischer, C. S., Vocke, D. C., Kılıç, R., ... & Brueckmann, M. (2005). Inflammatory regulation of extracellular matrix remodeling in calcific aortic valve stenosis. Cardiovascular Pathology, 14(2), 80-87.

[62] Kaden, J. J., Vocke, D. C., Fischer, C. S., Grobholz, R., Brueckmann, M., Vahl, C. F., ... & Borggrefe, M. (2004). Expression and activity of matrix metalloproteinase-2 in calcific aortic stenosis. Zeitschrift für Kardiologie, 93(2), 124-130.

[63] Kamimura, K., Mishima, Y., Obata, M., Endo, T., Aoyagi, Y., & Kominami, R. (2007). Lack of Bcl11b tumor suppressor results in vulnerability to DNA replication stress and damages. Oncogene, 26(40), 5840.

[64] KEGG apoptosis pathway: http://www.genome.jp/kegg/pathway/hsa/hsa04210.html

[65] Kim, S. Y., Song, X., Zhang, L., Bartlett, D. L., & Lee, Y. J. (2014). Role of Bcl-xL/Beclin-1 in interplay between apoptosis and autophagy in oxaliplatin and bortezomib-induced cell death. Biochemical pharmacology, 88(2), 178-188.

[66] Kodali, S. K., Williams, M. R., Smith, C. R., Svensson, L. G., Webb, J. G., Makkar, R. R., ... & Fischbein, M. (2012). Two-year outcomes after transcatheter or surgical aortic-valve replacement. New England Journal of Medicine, 366(18), 1686-1695.

[67] Kovalovich, K., Li, W., DeAngelis, R., Greenbaum, L. E., Ciliberto, G., & Taub, R. (2001). Interleukin-6 protects against Fas-mediated death by establishing a critical level of anti-apoptotic hepatic proteins FLIP, Bcl-2, and Bcl-xL. Journal of Biological Chemistry, 276(28), 26605-26613.

[68] Ku, C. H., Johnson, P. H., Batten, P., Sarathchandra, P., Chambers, R. C., Taylor, P. M., ... & Chester, A. H. (2006). Collagen synthesis by mesenchymal stem cells and aortic valve interstitial cells in response to mechanical stretch. Cardiovascular research, 71(3), 548-556.

[69] Kvitting, J. P. E., Ebbers, T., Wigström, L., Engvall, J., Olin, C. L., & Bolger, A. F. (2004). Flow patterns in the aortic root and the aorta studied with time-resolved, 3-dimensional, phase-contrast magnetic resonance imaging: implications for aortic valve–sparing surgery. The Journal of thoracic and cardiovascular surgery, 127(6), 1602-1607.

[70] Kouroku, Y., Fujita, E., Tanida, I., Ueno, T., Isoai, A., Kumagai, H., ... & Momoi, T. (2007). ER stress (PERK/eIF2 [alpha] phosphorylation) mediates the polyglutamine-induced LC3 conversion, an essential step for autophagy formation. Cell death and differentiation, 14(2), 230.

[71] Langille, B. L., & Adamson, S. L. (1981). Relationship between blood flow direction and endothelial cell orientation at arterial branch sites in rabbits and mice. Circulation Research, 48(4), 481-488.

[72] Lee, Y. B., Bantounas, I., Lee, D. Y., Phylactou, L., Caldwell, M. A., & Uney, J. B. (2008). Twist-1 regulates the miR-199a/214 cluster during development. Nucleic acids research, 37(1), 123-128.

[73] Lee, R. C., Feinbaum, R. L., & Ambros, V. (1993). The C. elegans heterochronic gene lin-4 encodes small RNAs with antisense complementarity to lin-14. Cell, 75(5), 843-854.

[74] Lee, M. P., & Yutzey, K. E. (2011). Twist1 directly regulates genes that promote cell proliferation and migration in developing heart valves. PLoS One, 6(12), e29758.

[75] Lei, Y., Masjedi, S., & Ferdous, Z. (2017). A study of extracellular matrix remodeling in aortic heart valves using a novel biaxial stretch bioreactor. Journal of the Mechanical Behavior of Biomedical Materials, 75, 351-358.

[76] Leon, M. B., Smith, C. R., Mack, M. J., Makkar, R. R., Svensson, L. G., Kodali, S. K., ... & Doshi, D. (2016). Transcatheter or surgical aortic-valve replacement in intermediate-risk patients. N Engl J Med, 2016(374), 1609-1620.

[77] Li, D., Liu, J., Guo, B., Liang, C., Dang, L., Lu, C., ... & He, B. (2016). Osteoclast-derived exosomal miR-214-3p inhibits osteoblastic bone formation. Nature communications, 7.

[78] Li, F., Song, R., Ao, L., Reece, T. B., Cleveland, J. C., Dong, N., ... & Meng, X. (2017). ADAMTS5 Deficiency in Calcified Aortic Valves Is Associated with Elevated Pro-Osteogenic Activity in Valvular Interstitial Cells. Arteriosclerosis, Thrombosis, and Vascular Biology, ATVBAHA-117.

[79] Li, X. F., Wang, Y., Zheng, D. D., Xu, H. X., Wang, T., Pan, M., ... & Zhu, J. H. (2016). M1 macrophages promote aortic valve calcification mediated by microRNA-214/TWIST1 pathway in valvular interstitial cells. American journal of translational research, 8(12), 5773.

[80] Li, F., Yao, Q., Ao, L., Cleveland, J. C., Dong, N., Fullerton, D. A., & Meng, X. (2017). Klotho suppresses high phosphate-induced osteogenic responses in human aortic valve interstitial cells through inhibition of Sox9. Journal of Molecular Medicine, 95(7), 739-751.

[81] Li, K., Zhang, J., Yu, J., Liu, B., Guo, Y., Deng, J., ... & Guo, F. (2015). MicroRNA-214 suppresses gluconeogenesis by targeting activating transcriptional factor 4. Journal of Biological Chemistry, jbc-M114.

[82] Lindqvist, L. M., Heinlein, M., Huang, D. C., & Vaux, D. L. (2014). Prosurvival Bcl-2 family members affect autophagy only indirectly, by inhibiting Bax and Bak. Proceedings of the National Academy of Sciences, 111(23), 8512-8517.

[83] Liu, A. C., Joag, V. R., & Gotlieb, A. I. (2007). The emerging role of valve interstitial cell phenotypes in regulating heart valve pathobiology. The American journal of pathology, 171(5), 1407-1418.

[84] Liu, H., Tao, Y., Chen, M., Yu, J., Li, W. J., Tao, L., ... & Li, F. (2016). Upregulation of microRNA-214 contributes to the development of vascular remodeling in hypoxia-induced pulmonary hypertension via targeting CCNL2. Scientific reports, 6.

[85] Liu, P. L., Tsai, J. R., Charles, A. L., Hwang, J. J., Chou, S. H., Ping, Y. H., ... & Chen, Y. H. (2010). Resveratrol inhibits human lung adenocarcinoma cell metastasis by suppressing heme oxygenase 1-mediated nuclear factor-κB pathway and subsequently downregulating expression of matrix metalloproteinases. Molecular nutrition & food research, 54(S2).

[86] Lu, H. Q., Liang, C., He, Z. Q., Fan, M., & Wu, Z. G. (2013). Circulating miR-214 is associated with the severity of coronary artery disease. Journal of geriatric cardiology: JGC, 10(1), 34.

[87] Lv, J. W., Wen, W., Jiang, C., Fu, Q. B., Gu, Y. J., Lv, T. T., ... & Xue, W. (2017). Inhibition of microRNA-214 promotes epithelial–mesenchymal transition process and induces interstitial cystitis in postmenopausal women by upregulating Mfn2. Experimental & molecular medicine, 49(7), e357.

[88] Ma, H., Killaars, A. R., DelRio, F. W., Yang, C., & Anseth, K. S. (2017). Myofibroblastic activation of valvular interstitial cells is modulated by spatial variations in matrix elasticity and its organization. Biomaterials, 131, 131-144.

[89] Maejima, Y., Kyoi, S., Zhai, P., Liu, T., Li, H., Ivessa, A., ... & Lim, D. S. (2013). Mst1 inhibits autophagy by promoting the interaction between Beclin1 and Bcl-2. Nature medicine, 19(11), 1478-1488.

[90] Mahler, G. J., Frendl, C. M., Cao, Q., & Butcher, J. T. (2014). Effects of shear stress pattern and magnitude on mesenchymal transformation and invasion of aortic valve endothelial cells. Biotechnology and bioengineering, 111(11), 2326-2337.

[91] Markl, M., Draney, M. T., Miller, D. C., Levin, J. M., Williamson, E. E., Pelc, N. J., ... & Herfkens, R. J. (2005). Time-resolved three-dimensional magnetic resonance velocity mapping of aortic flow in healthy volunteers and patients after valve-sparing aortic root replacement. The Journal of thoracic and cardiovascular surgery, 130(2), 456-463.

[92] Masuda, M., Miyazaki-Anzai, S., Keenan, A. L., Shiozaki, Y., Okamura, K., Chick, W. S., ... & Adams, C. M. (2016). Activating transcription factor-4 promotes mineralization in vascular smooth muscle cells. JCI insight, 1(18).

[93] Masuda, M., Miyazaki-Anzai, S., Levi, M., Ting, T. C., & Miyazaki, M. (2013). PERK-eIF2α-ATF4-CHOP signaling contributes to TNFα-induced vascular calcification. Journal of the American Heart Association, 2(5), e000238.

[94] Matsumoto, H., Miyazaki, S., Matsuyama, S., Takeda, M., Kawano, M., Nakagawa, H., ... & Matsuo, S. (2013). Selection of autophagy or apoptosis in cells exposed to ER-stress depends on ATF4 expression pattern with or without CHOP expression. Biology open, 2(10), 1084-1090.

[95] Mayo Clinic: http://www.mayoclinic.org/diseases-conditions/aortic-stenosis/symptoms-causes/dxc-20344145

[96] McGinnigle, E., Nosalski, R., Skiba, D., Denby, L., Graham, D., Baker, A. H., & Guzik, T. J. (2017). 191 Role of mir-214 in angiotensin ii induced hypertensive heart disease. Heart, 103(Suppl 5), A130-A131.

[97] McManus, D. D., & Freedman, J. E. (2015). MicroRNAs in platelet function and cardiovascular disease. Nature Reviews Cardiology, 12(12), 711-717.

[98] Miller, J. D., Weiss, R. M., & Heistad, D. D. (2011). Calcific aortic valve stenosis: methods, models, and mechanisms. Circulation research, 108(11), 1392-1412.

[99] Minamino, T., Komuro, I., & Kitakaze, M. (2010). Endoplasmic reticulum stress as a therapeutic target in cardiovascular disease. Circulation research, 107(9), 1071-1082.

[100] Miraoui, H., Severe, N., Vaudin, P., & Marie, P. J. (2010). Molecular silencing of Twist1 enhances osteogenic differentiation of murine mesenchymal stem cells: implication of FGFR2 signaling. Journal of cellular biochemistry, 110(5), 1147-1154.

[101] Mistiaen, W. (2013). Degenerative aortic valve disease, its mechanism on progression, its effect on the left ventricle and the postoperative results.

[102] Mistiaen, W. P., Somers, P., Knaapen, M. W., & Kockx, M. M. (2006). Autophagy as mechanism for cell death in degenerative aortic valve disease: An underestimated phenomenon in cardiovascular diseases. Autophagy, 2(3), 221-223.

[103] Mitchell, G. F., Verwoert, G. C., Tarasov, K. V., Isaacs, A., Smith, A. V., Rietzschel, E. R., ... & O'shaughnessy, K. M. (2011). Common genetic variation in the 3-BCL11B gene desert is associated with carotid-femoral pulse wave velocity and excess cardiovascular disease risk: the AortaGen Consortium. Circulation: Cardiovascular Genetics, CIRCGENETICS-111.

[104] Morita, Y., Watanabe, S., Ju, Y., & Xu, B. (2013). Determination of optimal cyclic uniaxial stretches for stem cell-to-tenocyte differentiation under a wide range of mechanical stretch conditions by evaluating gene expression and protein synthesis levels. Acta of bioengineering and biomechanics, 15(3).

[105] Myoishi, M., Hao, H., Minamino, T., Watanabe, K., Nishihira, K., Hatakeyama, K., ... & Bochaton-Piallat, M. L. (2007). Increased endoplasmic reticulum stress in atherosclerotic plaques associated with acute coronary syndrome. Circulation, 116(11), 1226-1233.

[106] New Heart Valve: https://newheartvalve.com/hcp/about-aortic-stenosis/

[107] Noh, M. R., Kim, J. I., Han, S. J., Lee, T. J., & Park, K. M. (2015). C/EBP homologous protein (CHOP) gene deficiency attenuates renal ischemia/reperfusion injury in mice. Biochimica et Biophysica Acta (BBA)-Molecular Basis of Disease, 1852(9), 1895-1901.

[108] Ohoka, N., Yoshii, S., Hattori, T., Onozaki, K., & Hayashi, H. (2005). TRB3, a novel ER stress-inducible gene, is induced via ATF4–CHOP pathway and is involved in cell death. The EMBO journal, 24(6), 1243-1255.

[109] Osnabrugge, R. L., Mylotte, D., Head, S. J., Van Mieghem, N. M., Nkomo, V. T., LeReun, C. M., ... & Kappetein, A. P. (2013). Aortic stenosis in the elderly: disease prevalence and number of candidates for transcatheter aortic valve replacement: a meta-analysis and modeling study. Journal of the American College of Cardiology, 62(11), 1002-1012.

[110] Oyadomari, S., & Mori, M. (2004). Roles of CHOP/GADD153 in endoplasmic reticulum stress. Cell death and differentiation, 11(4), 381.

[111] Park, S. J., Jung, S. H., Jogeswar, G., Ryoo, H. M., Yook, J. I., Choi, H. S., ... & Lim, S. K. (2010). The transcription factor snail regulates osteogenic differentiation by repressing Runx2 expression. Bone, 46(6), 1498-1507.

[112] Park, K. W., Waki, H., Kim, W. K., Davies, B. S., Young, S. G., Parhami, F., & Tontonoz, P. (2009). The small molecule phenamil induces osteoblast differentiation and mineralization. Molecular and cellular biology, 29(14), 3905-3914.

[113] Patel, V., Carrion, K., Hollands, A., Hinton, A., Gallegos, T., Dyo, J., ... & Nigam, S. (2015). The stretch responsive microRNA miR-148a-3p is a novel repressor of IKBKB, NF-κB signaling, and inflammatory gene expression in human aortic valve cells. The FASEB Journal, 29(5), 1859-1868.

[114] Peng, Y. Q., Xiong, D., Lin, X., Cui, R. R., Xu, F., Zhong, J. Y., ... & Yuan, L. Q. (2017). Oestrogen Inhibits Arterial Calcification by Promoting Autophagy. Scientific Reports, 7.

[115] Puthalakath, H., O'Reilly, L. A., Gunn, P., Lee, L., Kelly, P. N., Huntington, N. D., ... & Gotoh, T. (2007). ER stress triggers apoptosis by activating BH3-only protein Bim. Cell, 129(7), 1337-1349.

[116] Quiat, D., & Olson, E. N. (2013). MicroRNAs in cardiovascular disease: from pathogenesis to prevention and treatment. The Journal of clinical investigation, 123(1), 11.

[117] Rajamannan, N. M., Evans, F. J., Aikawa, E., Grande-Allen, K. J., Demer, L. L., Heistad, D. D., ... & Schoen, F. J. (2011). Calcific aortic valve disease: not simply a degenerative process. Circulation, 124(16), 1783-1791.

[118] Rajamannan, N. M., Subramaniam, M., Rickard, D., Stock, S. R., Donovan, J., Springett, M., ... & Spelsberg, T. (2003). Human aortic valve calcification is associated with an osteoblast phenotype. Circulation, 107(17), 2181-2184.

[119] Rathan, S., Ankeny, C. J., Arjunon, S., Ferdous, Z., Kumar, S., Esmerats, J. F., ... & Jo, H. (2016). Identification of side-and shear-dependent microRNAs regulating porcine aortic valve pathogenesis. Scientific reports, 6.

[120] Rathan, S., Yap, C. H., Morris, E., Arjunon, S., Jo, H., & Yoganathan, A. P. (2011, June). Low and Unsteady Shear Stresses Upregulate Calcification Response of the

Aortic Valve Leaflets. In ASME 2011 Summer Bioengineering Conference (pp. 245-246). American Society of Mechanical Engineers.

[121] Roche, P. L., Nagalingam, R. S., Bagchi, R. A., Aroutiounova, N., Belisle, B. M., Wigle, J. T., & Czubryt, M. P. (2016). Role of scleraxis in mechanical stretch-mediated regulation of cardiac myofibroblast phenotype. American Journal of Physiology-Cell Physiology, 311(2), C297-C307.

[122] Romaine, S. P., Tomaszewski, M., Condorelli, G., & Samani, N. J. (2015). MicroRNAs in cardiovascular disease: an introduction for clinicians. Heart, heartjnl-2013.

[123] Ron, D., & Walter, P. (2007). Signal integration in the endoplasmic reticulum unfolded protein response. Nature reviews. Molecular cell biology, 8(7), 519.

[124] Rupaimoole, R., & Slack, F. J. (2017). MicroRNA therapeutics: towards a new era for the management of cancer and other diseases. Nature Reviews Drug Discovery, 16(3), 203-222.

[125] Sacks, M. S., & Yoganathan, A. P. (2007). Heart valve function: a biomechanical perspective. Philosophical Transactions of the Royal Society of London B: Biological Sciences, 362(1484), 1369-1391.

[126] Sahoo, S., Meijles, D. N., Al Ghouleh, I., Tandon, M., Cifuentes-Pagano, E., Sembrat, J., ... & Pagano, P. J. (2016). MEF2C-MYOCD and Leiomodin1 suppression by miRNA-214 promotes smooth muscle cell phenotype switching in pulmonary arterial hypertension. PloS one, 11(5), e0153780.

[127] Saito, A., Ochiai, K., Kondo, S., Tsumagari, K., Murakami, T., Cavener, D. R., & Imaizumi, K. (2011). Endoplasmic reticulum stress response mediated by the PERK-eIF2α-ATF4 pathway is involved in osteoblast differentiation induced by BMP2. Journal of biological chemistry, 286(6), 4809-4818.

[128] Shah, M. Y., Ferrajoli, A., Sood, A. K., Lopez-Berestein, G., & Calin, G. A. (2016). MicroRNA therapeutics in cancer—An emerging concept. EBioMedicine, 12, 34-42.

[129] Shapero, K., Wylie-Sears, J., Levine, R. A., Mayer, J. E., & Bischoff, J. (2015). Reciprocal interactions between mitral valve endothelial and interstitial cells reduce endothelial-to-mesenchymal transition and myofibroblastic activation. Journal of molecular and cellular cardiology, 80, 175-185.

[130] Shen, W., Zhou, J., Wang, C., Xu, G., Wu, Y., & Hu, Z. (2017). High mobility group box 1 induces calcification of aortic valve interstitial cells via toll-like receptor 4. Molecular Medicine Reports, 15(5), 2530-2536.

[131] Shi, K., Lu, J., Zhao, Y., Wang, L., Li, J., Qi, B., ... & Ma, C. (2013). MicroRNA-214 suppresses osteogenic differentiation of C2C12 myoblast cells by targeting Osterix. Bone, 55(2), 487-494.

[132] Shimizu, S., Eguchi, Y., Kosaka, H., Kamiike, W., Matsuda, H., & Tsujimoto, Y. (1995). Prevention of hypoxia-induced cell death by Bcl-2 and Bcl-xL. Nature, 374(6525), 811-813.

[133] Smith, C. R., Leon, M. B., Mack, M. J., Miller, D. C., Moses, J. W., Svensson, L. G., ... & Williams, M. (2011). Transcatheter versus surgical aortic-valve replacement in high-risk patients. New England Journal of Medicine, 364(23), 2187-2198.

[134] Somers, P., Knaapen, M., Kockx, M., Van Cauwelaert, P., Bortier, H., & Mistiaen, W. (2006). Histological evaluation of autophagic cell death in calcified aortic valve stenosis. J Heart Valve Dis, 15(1), 43-47.

[135] Song, R., Fullerton, D. A., Ao, L., Zhao, K. S., Reece, T. B., Cleveland, J. C., & Meng, X. (2017). Altered MicroRNA Expression Is Responsible for the Pro-Osteogenic Phenotype of Interstitial Cells in Calcified Human Aortic Valves. Journal of the American Heart Association, 6(4), e005364.

[136] Stevens, H. C., Deng, L., Grant, J. S., Pinel, K., Thomas, M., Morrell, N. W., ... & Denby, L. (2016). Regulation and function of miR-214 in pulmonary arterial hypertension. Pulmonary circulation, 6(1), 109-117.

[137] Sucosky, P., Padala, M., Elhammali, A., Balachandran, K., Jo, H., & Yoganathan, A. P. (2008). Design of an ex vivo culture system to investigate the effects of shear stress on cardiovascular tissue. Journal of biomechanical engineering, 130(3), 035001.

[138] Sun, W., Julie Li, Y. S., Huang, H. D., Shyy, J. Y., & Chien, S. (2010). microRNA: a master regulator of cellular processes for bioengineering systems. Annual review of biomedical engineering, 12, 1-27.

[139] Sun, L., Rajamannan, N. M., & Sucosky, P. (2011). Design and validation of a novel bioreactor to subject aortic valve leaflets to side-specific shear stress. Annals of biomedical engineering, 39(8), 2174-2185.

[140] Sun, L., Rajamannan, N. M., & Sucosky, P. (2013). Defining the role of fluid shear stress in the expression of early signaling markers for calcific aortic valve disease. PLoS One, 8(12), e84433.

[141] Taylor, P. M., Batten, P., Brand, N. J., Thomas, P. S., & Yacoub, M. H. (2003). The cardiac valve interstitial cell. The international journal of biochemistry & cell biology, 35(2), 113-118.

[142] Taylor, J. K., Zhang, Q. Q., Wyatt, J. R., & Dean, N. M. (1999). Induction of endogenous Bcl-xS through the control of Bcl-x pre-mRNA splicing by antisense oligonucleotides. Nature biotechnology, 17(11).

[143] Thubrikar, M. J. (1989). The aortic valve. CRC press.

[144] Thubrikar, M. J., Aouad, J., & Nolan, S. P. (1986). Comparison of the in vivo and in vitro mechanical properties of aortic valve leaflets. The Journal of Thoracic and Cardiovascular Surgery, 92(1), 29-36.

[145] Thubrikar, M., Bosher, L. P., & Nolan, S. P. (1979). The mechanism of opening of the aortic valve. The Journal of Thoracic and Cardiovascular Surgery, 77(6), 863-870.

[146] Thubrikar, M. J., Nolan, S. P., Aouad, J., & Deck, J. D. (1986). Stress sharing between the sinus and leaflets of canine aortic valve. The annals of thoracic surgery, 42(4), 434-440.

[147] Valentine, M. S., Herbert, J. A., Link, P. A., Gninzeko, F. J. K., Schneck, M. B., Shankar, K., ... & Heise, R. L. (2017). The Influence of Aging and Mechanical Stretch in Alveolar Epithelium ER Stress and Inflammation. bioRxiv, 157677.

[148] Valisno, J. A., Elavalakanar, P., Nicholson, C., Singh, K., Avram, D., Cohen, R. A., ... & Seta, F. (2017). Bcl11b is a Newly Identified Regulator of Vascular Smooth Muscle Phenotype and Arterial Stiffness. bioRxiv, 193110.

[149] Van Rooij, E., Sutherland, L. B., Liu, N., Williams, A. H., McAnally, J., Gerard, R. D., ... & Olson, E. N. (2006). A signature pattern of stress-responsive microRNAs that can evoke cardiac hypertrophy and heart failure. Proceedings of the National Academy of Sciences, 103(48), 18255-18260.

[150] Van Rooij, E., Sutherland, L. B., Thatcher, J. E., DiMaio, J. M., Naseem, R. H., Marshall, W. S., ... & Olson, E. N. (2008). Dysregulation of microRNAs after

myocardial infarction reveals a role of miR-29 in cardiac fibrosis. Proceedings of the National Academy of Sciences, 105(35), 13027-13032.

[151] Wakabayashi, Y., Watanabe, H., Inoue, J., Takeda, N., Sakata, J., Mishima, Y., ... & Aizawa, S. (2003). Bcl11b is required for differentiation and survival of [alpha][beta] T lymphocytes. Nature immunology, 4(6), 533.

[152] Walter, P., & Ron, D. (2011). The unfolded protein response: from stress pathway to homeostatic regulation. Science, 334(6059), 1081-1086.

[153] Wang, B., Cai, Z., Liu, B., Liu, Z., Zhou, X., Dong, N., & Li, F. (2017). RAGE deficiency alleviates aortic valve calcification in ApoE−/− mice via the inhibition of endoplasmic reticulum stress. Biochimica et Biophysica Acta (BBA)-Molecular Basis of Disease, 1863(3), 781-792.

[154] Wang, X., Guo, B., Li, Q., Peng, J., Yang, Z., Wang, A., ... & Cao, H. (2013). miR-214 targets ATF4 to inhibit bone formation. Nature medicine, 19(1), 93-100.

[155] Wang, M., & Kaufman, R. J. (2014). The impact of the endoplasmic reticulum protein-folding environment on cancer development. Nature reviews. Cancer, 14(9), 581.

[156] Wang, W., Lian, N., Li, L., Moss, H. E., Wang, W., Perrien, D. S., ... & Yang, X. (2009). Atf4 regulates chondrocyte proliferation and differentiation during endochondral ossification by activating Ihh transcription. Development, 136(24), 4143-4153.

[157] Wang, H., Shi, J., Li, B., Zhou, Q., Kong, X., & Bei, Y. (2017). MicroRNA Expression Signature in Human Calcific Aortic Valve Disease. BioMed research international, 2017.

[158] Warnock, J. N., Nanduri, B., Pregonero Gamez, C. A., Tang, J., Koback, D., Muir, W. M., & Burgess, S. C. (2011). Gene profiling of aortic valve interstitial cells under elevated pressure conditions: modulation of inflammatory gene networks. International journal of inflammation, 2011.

[159] Wiltz, D., Arevalos, C. A., Balaoing, L. R., Blancas, A. A., Sapp, M. C., Zhang, X., & Grande-Allen, K. J. (2013). Extracellular matrix organization, structure, and function. In Calcific aortic valve disease. InTech.

[160] Wu, J., Thabet, S. R., Kirabo, A., Trott, D. W., Saleh, M. A., Xiao, L., ... & Harrison, D. G. (2013). Inflammation and Mechanical Stretch Promote Aortic Stiffening in Hypertension Through Activation of p38 MAP Kinase. Circulation research, CIRCRESAHA-113.

[161] Xerri, L., Parc, P., Brousset, P., Schlaifer, D., Hassoun, J., Reed, J. C., ... & Birnbaum, D. (1996). Predominant expression of the long isoform of Bcl-x (Bcl-xL) in human lymphomas. British journal of haematology, 92(4), 900-906.

[162] Xiao, G., Jiang, D., Ge, C., Zhao, Z., Lai, Y., Boules, H., ... & Franceschi, R. T. (2005). Cooperative interactions between activating transcription factor 4 and Runx2/Cbfa1 stimulate osteoblast-specific osteocalcin gene expression. Journal of Biological Chemistry, 280(35), 30689-30696.

[163] Xu, C., Bailly-Maitre, B., & Reed, J. C. (2005). Endoplasmic reticulum stress: cell life and death decisions. Journal of Clinical Investigation, 115(10), 2656.

[164] Xu, H. X., Wang, Y., Zheng, D. D., Wang, T., Pan, M., Shi, J. H., ... & Li, X. F. (2017). Differential Expression of MicroRNAs in Calcific Aortic Stenosis. Clinical laboratory, 63(7), 1163.

[165] Yanagisawa, H., Miyashita, T., Nakano, Y., & Yamamoto, D. (2003). HSpin1, a transmembrane protein interacting with Bcl-2/Bcl-xL, induces a caspase-independent autophagic cell death. Cell death and differentiation, 10(7), 798.

[166] Yang, L., Ge, D., Cao, X., Ge, Y., Chen, H., Wang, W., & Zhang, H. (2016). miR-214 attenuates osteogenic differentiation of mesenchymal stem cells via targeting FGFR1. Cellular Physiology and Biochemistry, 38(2), 809-820.

[167] Yang, T., Gu, H., Chen, X., Fu, S., Wang, C., Xu, H., ... & Ni, Y. (2014). Cardiac hypertrophy and dysfunction induced by overexpression of miR-214 in vivo. journal of surgical research, 192(2), 317-325.

[168] Yang, X., & Karsenty, G. (2004). ATF4, the osteoblast accumulation of which is determined post-translationally, can induce osteoblast-specific gene expression in non-osteoblastic cells. Journal of Biological Chemistry, 279(45), 47109-47114.

[169] Yang, X., Qin, Y., Shao, S., Yu, Y., Zhang, C., Dong, H., ... & Dong, S. (2016). MicroRNA-214 inhibits left ventricular remodeling in an acute myocardial infarction

rat model by suppressing cellular apoptosis via the phosphatase and tensin homolog (PTEN). International heart journal, 57(2), 247-250.

[170] Yang, S. Y., Wei, F. L., Hu, L. H., & Wang, C. L. (2016). PERK-eIF2α-ATF4 pathway mediated by endoplasmic reticulum stress response is involved in osteodifferentiation of human periodontal ligament cells under cyclic mechanical force. Cellular signalling, 28(8), 880-886.

[171] Yao, Q., Song, R., Ao, L., Cleveland, J. C., Fullerton, D. A., & Meng, X. (2017). Neurotrophin 3 upregulates proliferation and collagen production in human aortic valve interstitial cells: a potential role in aortic valve sclerosis. American Journal of Physiology-Cell Physiology, 312(6), C697-C706.

[172] Yap, C. H., Saikrishnan, N., Tamilselvan, G., & Yoganathan, A. P. (2012). Experimental measurement of dynamic fluid shear stress on the aortic surface of the aortic valve leaflet. Biomechanics and modeling in mechanobiology, 11(1), 171-182.

[173] Yap, C. H., Saikrishnan, N., & Yoganathan, A. P. (2012). Experimental measurement of dynamic fluid shear stress on the ventricular surface of the aortic valve leaflet. Biomechanics and modeling in mechanobiology, 11(1), 231-244.

[174] Ye, J., Kumanova, M., Hart, L. S., Sloane, K., Zhang, H., De Panis, D. N., ... & Koumenis, C. (2010). The GCN2-ATF4 pathway is critical for tumour cell survival and proliferation in response to nutrient deprivation. The EMBO journal, 29(12), 2082-2096.

[175] Yu, S., Zhu, K., Lai, Y., Zhao, Z., Fan, J., Im, H. J., ... & Xiao, G. (2013). atf4 promotes β-catenin expression and osteoblastic differentiation of bone marrow mesenchymal stem cells. International journal of biological sciences, 9(3), 256

[176] Zeng, Q., Song, R., Fullerton, D. A., Ao, L., Zhai, Y., Li, S., ... & Xu, D. (2017). Interleukin-37 suppresses the osteogenic responses of human aortic valve interstitial cells in vitro and alleviates valve lesions in mice. Proceedings of the National Academy of Sciences, 114(7), 1631-1636.

[177] Zhang, C., Hong, F. F., Wang, C. C., Li, L., Chen, J. L., Liu, F., ... & Wang, J. F. (2017). TRIB3 inhibits proliferation and promotes osteogenesis in hBMSCs by regulating the ERK1/2 signaling pathway. Scientific Reports, 7(1), 10342.

[178] Zhang, X., Yu, S., Galson, D. L., Luo, M., Fan, J., Zhang, J., ... & Xiao, G. (2008). Activating transcription factor 4 is critical for proliferation and survival in primary bone marrow stromal cells and calvarial osteoblasts. Journal of cellular biochemistry, 105(3), 885-895.

[179] Zhang, X. W., Zhang, B. Y., Wang, S. W., Gong, D. J., Han, L., Xu, Z. Y., & Liu, X. H. (2014). Twist-related protein 1 negatively regulated osteoblastic transdifferentiation of human aortic valve interstitial cells by directly inhibiting runt-related transcription factor 2. The Journal of thoracic and cardiovascular surgery, 148(4), 1700-1708.

[180] Zhong, G., Chen, Y., Yang, L., Luo, Y., Liu, Y., Chen, Q., & Yao, J. (2016). Regulation of microRNA-214 on vascular smooth muscle cell proliferation and potential treatment effects in hypertension mouse. International Journal of Clinical and Experimental Pathology, 9(10), 10215-10223.

[181] Zhao, Y., Ponnusamy, M., Zhang, L., Zhang, Y., Liu, C., Yu, W., ... & Li, P. (2017). The role of miR-214 in cardiovascular diseases. European Journal of Pharmacology.

[182] Zhao, C., Sun, W., Zhang, P., Ling, S., Li, Y., Zhao, D., ... & Wang, C. (2015). miR-214 promotes osteoclastogenesis by targeting Pten/PI3k/Akt pathway. RNA biology, 12(3), 343-353.

[183] Zhou, C., Liu, Y., Li, X., Zou, J., & Zou, S. (2016). DNA N6-methyladenine demethylase ALKBH1 enhances osteogenic differentiation of human MSCs. Bone research, 4.

[184] Zhu, H., Chen, X., Chen, B., Chen, B., Song, W., Sun, D., & Zhao, Y. (2014). Activating transcription factor 4 promotes esophageal squamous cell carcinoma invasion and metastasis in mice and is associated with poor prognosis in human patients. PloS one, 9(7), e103882.

[185] Zhu, Y., Chen, H., Zhang, X., Zhang, L., Liu, Y., & Ren, C. (2016). Downregulation of MALAT1 Promotes Aortic Valve Calcification by Inhibiting TWIST1 Expression. Lipid and Cardiovascular Research, 2(2), 34-41.